Methodology for the Performance Evaluation of Ceiling Recessions for Vertical Floor Opening Protection

by

Steven P. Grant

A thesis
presented to the University of Waterloo
in fulfillment of the
thesis requirement for the degree of
Master of Applied Science
in
Mechanical Engineering

Waterloo, Ontario, Canada, 2013

I hereby declare that I am the sole author of this thesis. This is a true copy of the thesis, including any required final revisions, as accepted by my examiners.

I understand that my thesis may be made electronically available to the public.

ABSTRACT

Current Canadian Building Codes mandate prescribed design requirements for the protection of vertical floor openings by means of draft stops and closely spaced sprinklers. In the event that a design cannot meet the requirements, they also allow for the use of an alternative solution as long as the alternative solution can be proven to provide at least an equivalent level of performance as that prescribed in the Code. A commonly suggested alternative to the use of draft stops includes the construction of a recession at the perimeter of the floor opening; however, the performance of this design relative to that of an equivalent draft stop design has not been thoroughly evaluated.

In this research, the available methods for the evaluation of ceiling recession designs are reviewed in order to identify appropriate tools with which to conduct such an analysis. While both analytical analysis and experimental testing could be used, experimental testing of the design is not considered here as this option would not commonly be pursued by design teams due to restrictions on both project budget and design timelines. From the available analytical tools, the fire modeling software Fire Dynamics Simulator (FDS) is selected for evaluation of the ceiling recession design due primarily to the ability of FDS to address complex geometries with appropriate spatial resolution to investigate details of flow and thermal profiles at the ceiling level in a larger compartment.

Previous FDS studies are reviewed and an independent validation study is conducted in order to develop an analysis methodology which is appropriate for the evaluation of ceiling recession designs. A case study evaluation is conducted consisting of two dimensionally distinct ceiling recession configurations in the same compartment and two separate source fire heat release rates (HRR). Results are analyzed to evaluate the selected analysis methodology with respect to the characteristics of the simulated flow, and thermal detector response. Results show that the presence of an obstruction to the ceiling jet flow significantly improves thermal detector response where the source fire HRR is low. At higher source fire HRRs, the difference in activation time is found to be minimal amongst configurations of ceiling recession considered in the study.

Predictions of thermal detector response time for a selected ceiling recession design are compared to predictions made for code-prescribed draft stop configuration as would be necessary

for an alternative solution evaluation. Results indicate that ceiling recession designs provide a reduced level of performance at both low and high source fire HRRs when the thermal detector is placed at the recession ceiling level. In contrast, when the thermal detectors are located at distances greater than 80 mm below the upper ceiling, a design which is permitted by the Code, the performance of the ceiling recession appears better than that of the prescribed draft stop design. Results from the model for detectors placed at distances from the ceiling exceeding 40 mm, however, require further confirmation through experimental testing or additional modeling.

ACKNOWLEDGEMENTS

I would like to thank my supervisor, Dr. Elizabeth Weckman for her advice and support throughout this project. I would also like to thank my colleagues at Leber-Rubes Inc. for their technical assistance and advice in defining the scope and methods utilized in this research.

I would like to thank the management team at Leber-Rubes Inc. for providing me with the financial and technical resources required to complete this project as well as the generous allowance of time away from the office in the pursuit of this degree.

To my family and friends, thank you for your support and patience throughout this process. Most importantly I would like to thank Johanna for her constant encouragement and tireless support without which I would never have completed this thesis.

CONTENTS

LIST OF FIGURES

LIST OF TABLES

NOMENCLATURE

A	Area or surface area, (m^2)
b	Plume radius, (m)
c	Specific heat, (kJ/kg. °C)
D	Diameter of a fire source, (m)
D^*	Characteristic fire diameter
g	Gravitational acceleration, (m/s^2)
h	Convective heat transfer coefficient, (W/m^2K)
H	Height of the ceiling above the fire source, (m)
K_c	Fraction of convective heat release contained in smoke layer
L	Mean flame height above base of fire, (m)
m	Mass, (kg)
$\dot{m}$	Mass flow rate of a plume, (kg/s)
Q	Heat release rate, (kW)
Q*	Normalized rate of heat release
Q_{cond}	Conductive heat transfer, (kW)
Q_{conv}	Convective heat transfer, (kW)
Q_{rad}	Radiative heat transfer, (kW)
r	Radial distance from the centerline of the plume, (m)
RTI	Response time index, ($(ms)^{1/2}$)
t	Time, (s)
T	Temperature, (°C)
T*	Normalized temperature
U	Ceiling jet velocity, (m/s)
U*	Normalized ceiling jet velocity
z	Distance measured down from the upper ceiling, (m)
Z	Distance of layer interface above the real or substitute fire source, (m)

Greek Symbols

δ	CFD physical grid size, (m)
ρ	Density, (kg/m^3)
Δ	Change in a given property

Subscripts

act	Detector activation property
c	Convective
d	Detector property
g	Gas product property
I	Interface (layer) property
avg	Average value for a property
p	Plume property
∞	Ambient conditions property

1	Relates to the lower layer
2	Relates to the upper later
x	Cartesian "x" axis coordinate
y	Cartesian "y" axis coordinate
z	Cartesian "z" axis coordinate

1 INTRODUCTION

1.1 Vertical Floor Openings

Vertical floor openings, defined as those openings that penetrate a floor assembly and provide an opening between multiple storeys of a building, are an important feature in modern building design. They form important elements of the design of indoor atria, open stairways, escalators, and natural light wells. Unfortunately, while they may do much to enhance an overall design, their inclusion within a building can create hazardous conditions since they allow smoke from a fire to simultaneously fill multiple storeys. From a fire safety perspective, this can potentially lead to undesirable impacts including:

- increased probability of occupant injury due to exposure to hot and toxic products of combustion,
- delays in occupant evacuation due to poor visibility on several floors and queuing conditions at exits,
- delays in fire alarm system response due to venting of heat and smoke away from automatic detectors,
- increased property damage due to smoke and heat exposure, and
- delay in fire department response due to the presence of smoke on multiple floors.

To reduce the potential for such impacts, many Canadian building regulations, such as the 2006 Ontario Building Code, the 2010 National Building Code of Canada, and the 2006 Alberta Building Code, contain prescriptive design requirements for fire protection in vertical floor openings [1–3]. Depending on the size and configuration of an opening, Canadian Codes mandate the provision of draft stops to pool smoke and enhance the probability of detection of the fire on the floor of origin with thermal and/or smoke automatic detection at the opening perimeter [1–3]. A similar method of protection for vertical floor openings is also mandated by some international building regulations [4, 5].

1.2 Draft Stop Protection Method

Schematics of a draft stop, floor opening and thermal detector configurations are shown in Figure 1-1 and Figure 1-2. The draft stop, constructed of a noncombustible material and extending 457 mm (18 inches) or more down from the ceiling level [6], is positioned around the opening. The draft stop is intended to act as an obstruction to the horizontal movement of the ceiling jet, or plume of hot gases and smoke travelling along the ceiling away from the fire. By obstructing the movement of gases, the draft stop forces the formation of a thicker layer of hot gas at the ceiling above the fire and in the region upstream of the opening. This in turn is intended to ensure that adjacent detectors will be exposed to the conditions required for actuation. In most cases, sprinkler heads are installed around the perimeter of the floor opening [6, 7].

The intent of this is that in the event of a fire, the sprinklers will activate and cool the hot gases near the ceiling, reducing their buoyancy, and limiting migration of heated air and products of combustion upward through the opening.

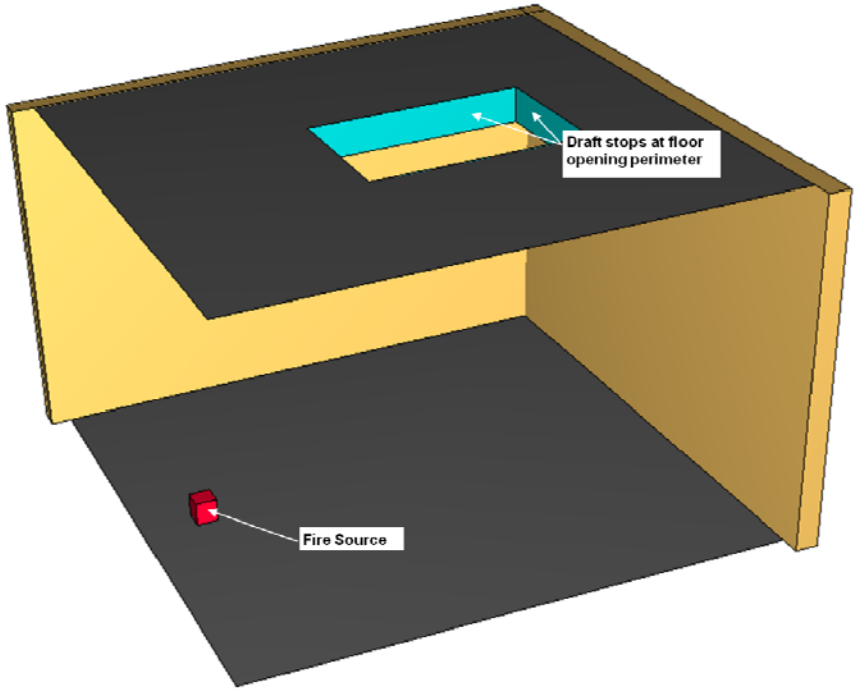

Figure 1-1: Standard draft stop configuration

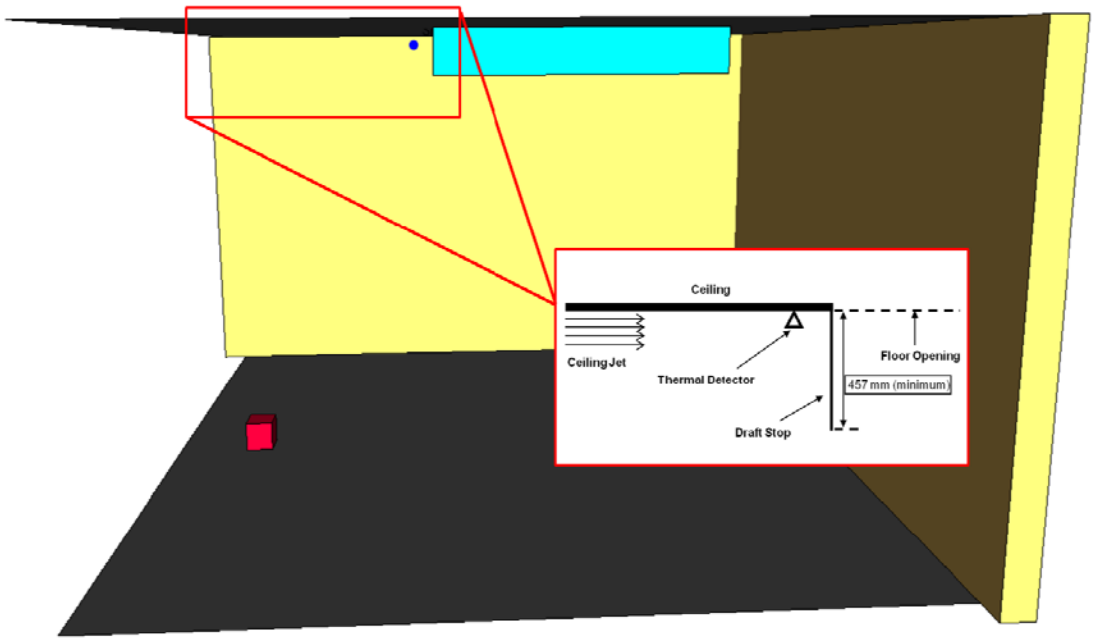

Figure 1-2: Intended function of draft stops

The installation of draft stops can be difficult, (or impossible) in some situations due to dimensional constraints within the building and/or conflicts with other prescriptive design requirements that are embodied in the Code [8, 9]. Conflicts are especially common during renovations of buildings since existing conditions can significantly constrain design flexibility. A common occurrence of this arises in the situation shown in Figure 1-3, where draft stops are mandated for a floor opening containing an open stair. Under most building regulations it is required to provide a minimum vertical clearance (headroom) between the stair treads and any obstruction above [1–5]. Since draft stops are required to extend a minimum of 457 mm below the ceiling level at the perimeter of the floor opening, in many cases the minimum headroom clearance requirement and the draft stop depth requirement cannot be achieved simultaneously. A strict interpretation of the Building Code in this situation would preclude the use of an open stair in the design.

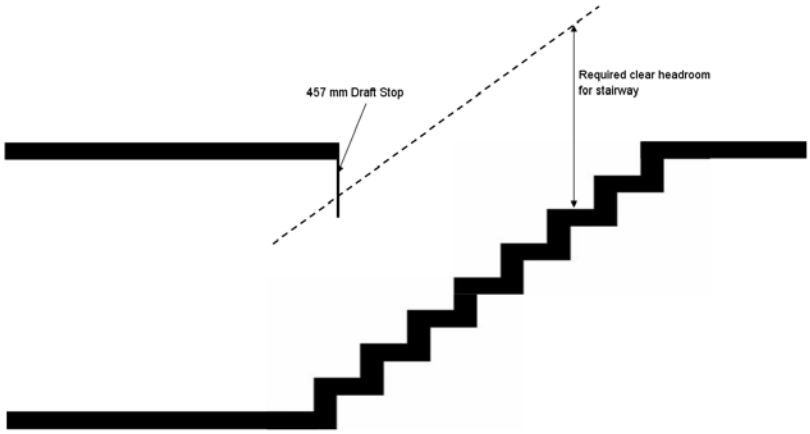

Figure 1-3: Headroom clearance conflict at stairway

Fortunately, Canadian Building Codes permit the development of alternative solutions where prescriptive code requirements cannot be met. These alternative designs are then evaluated as performance based design options, as discussed in more detail in the next section.

1.3 Alternative Solutions

Acceptable methods of compliance with the 2006 Ontario Building Code (OBC) are outlined in Division A, Part 1 Section 1.2 of that standard. Compliance with Division B of the Code must be achieved either by employing applicable acceptable solutions in Division B, or by using an alternative solution that will achieve at least the same level of performance as the applicable acceptable solutions with respect to the objectives and functional statements attributed to the applicable acceptable solution.

An alternative solution is defined in Division A, Part 1 Article 1.4.1.2 of the OBC as "a substitute for an acceptable solution". An acceptable solution is defined as "a requirement stated in Parts 3 to 12 of Division B". This framework for compliance is also found in the 2010 National Building Code of Canada.

Where an alternative solution is utilized in a design, before that design can be accepted, the designer is required to provide experimental or theoretical analysis which proves that the level of performance of the alternative solution will achieve, or exceed, the level of performance intended by the prescriptive requirements [1, 2]. This analysis often takes the form of a

comparison of values of the parameters critical to the prescriptive requirements with those achieved using the alternative solution. In all cases, alternative solutions must be reviewed and approved by the Authority Having Jurisdiction (AHJ), generally a municipal Building Department official or employee of another government agency.

One method by which the performance of a prescriptive solution can be compared to an alternative solution is via realistic experimental simulation of the scenario under study. Realistically, industry timelines and budget constraints often rule out the feasibility of experiment as a means of evaluating an alternative solution. This is especially the case where multiple design scenarios must be tested since the cost of even a single full scale experiment is high. In some cases, where experiment is the only evaluation option that will produce verified results, alternative solutions are not pursued by a design team due to the increased design costs and delays to the project schedule.

In lieu of experimentation, theoretical evaluations, such as those utilizing first principles, physical properties, and numerical correlations are often the preferred method by which to evaluate an alternative solution in industry. This is primarily attributed to the lower cost associated with this type of analysis and the speed with which it can be conducted. However, in many cases the application of theoretical principles to the evaluation of complex design scenarios is not straightforward. Significant simplifications of the real scenario and a wide array of assumptions are often required to modify the design scenario to a form for which the theoretical principles can be applied. Additionally, the impact of some important design parameters may need to be neglected in order to facilitate straightforward evaluation of the other parameters of interest.

An example of such trade-offs is embodied in the correlations often used to calculate the maximum temperature below a flat ceiling. The correlations were derived from a set of experiments that studied the maximum temperature below a flat unobstructed ceiling for a particular design fire [10]. However, most “real” fire scenarios do not fit this description due to the presence of compartment walls, ceiling obstructions, floor openings, air handling systems,

and doors and windows. Nonetheless this method is still considered an important tool for predictions of maximum temperature in the ceiling layer of enclosure fires.

To compensate for simplifications in the scenario or limitations in the method, a theoretical analysis often includes significant factors of safety to both the input parameters, and the selected failure criteria. This is intended to ensure that the conclusion can be considered independent of the impact of the sources of error. Unfortunately, this approach can potentially lead to overly conservative designs or to the rejection of potential designs where a theoretical analysis is the only available means of evaluating an alternative solution.

Due to the difficulties noted, there is a need in industry for new, well documented evaluation methods which can be used to more accurately assess particular classes of design scenarios proposed as alternative solutions, while maintaining project budgets and construction timelines. Favorable methods would provide reasonable accuracy in the analysis at low cost (in terms of both time required and cost of the analysis) while having the flexibility to evaluate multiple scenarios and design configurations under a given set of possible fire scenarios and protection measures.

The present research focuses on development of such a method for alternative solutions relating to the design of draft stops and protection of vertical floor openings. In this instance, one potential alternative concept which has been proposed involves recessing the draft stop into the ceiling slab and thereby creating a recession that is intended to trap heat and smoke and ensure the activation of detectors. This alternative is not generally accepted, however, and therefore requires further investigation. As a basis for this study, better definition of the design concept and existing theory related to its analysis are contained in the next several sections.

1.4 Ceiling Recession Protection Method

The ceiling recession protection method is illustrated schematically in Figure 1-4. This method involves creating a recession at the ceiling level at the perimeter of a vertical floor opening. The depth of the proposed recession is often varied depending on the vertical space available at the opening, as well as the proposed construction of the ceiling/floor assembly. The automatic

detection required by the Codes is then installed within the ceiling recession based on the spacing with respect to nearby obstructions and dimensional restrictions that are outlined in NFPA 13 for draft stops.

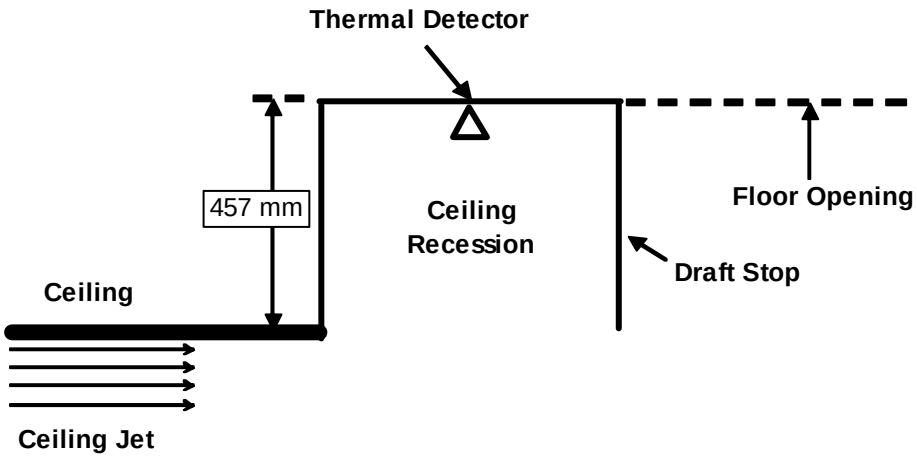

Figure 1-4: Example ceiling recession configuration with sprinklers

The intent of the alternative design illustrated in Figure 1-4 is functionally the same as the draft stop protection method. The recession is intended to trap ceiling jet gases within the ceiling recession to facilitate actuation of the detectors in that space.

The primary benefit of this design from an architectural standpoint is that no ceiling mounted obstructions have to be installed in the headroom available in the compartment. This mitigates many of the architectural issues encountered with the use of draft stops and provides architects with increased design flexibility for open stairs and vertical floor openings.

To date the performance of this category of alternative solutions for draft stop designs has not been subject to a detailed evaluation. Of primary concern to an AHJ is the impact of the proposed ceiling recession on the performance of adjacent thermal detectors (i.e. sprinklers). In addition, the effects of variation in the dimensions of the recession are not fully understood. This poses a difficulty for both designers and the AHJ since it is not clear that all proposed ceiling recession designs would perform equally or to the level of performance required of the

prescribed draft stop designs. Therefore, it is necessary to develop an industry appropriate method for the reliable evaluation of various designs in this category of alternative solutions.

1.5 Performance Evaluation

The intent of a draft stop is to ensure detection of heat from a fire and activation of closely spaced sprinklers adjacent to the vertical floor opening. The intent of the closely spaced sprinklers is to cool the gases within the hot layer in order to mitigate the risk that those gases might pose should they migrate to floor areas above. Based on this, any alternative solution to this method must provide a level of performance, with respect to these functions, at least equivalent to the draft stop method. Therefore, for the evaluation of any alternative protection method, two primary elements must be considered:

1. The effect of the configuration under study on the reaction time of the thermal detectors (sprinklers) and
2. the ability of the sprinklers in the proposed design, once activated, to cool and control the spread of hot gases from the floor of fire origin to floors above.

The focus of this thesis is on the development of methods by which to assess the first element: the impact of the alternative draft stop configuration on the reaction time of adjacent thermal detectors.

1.6 Research Objectives

The primary objectives of this research are:

1. To develop an appropriate methodology to evaluate the performance of thermal detectors within ceiling recessions for the evaluation of alternative solutions for the protection of vertical floor openings.
2. To evaluate the proposed methodology through the analysis of selected ceiling recession designs in order to determine the limits of its application to alternative solutions.

Evaluation of the response of thermal detectors for alternative vertical floor opening protection methods is the primary focus of this research. Therefore, the discharge pattern of sprinklers and performance of the design with respect to cooling of the ceiling jet gases is considered outside the scope of this thesis.

In the following chapters a general review of pertinent literature relating to the development of ceiling jets and the interactions of ceiling jets with compartment boundaries is provided. Additional discussion is provided regarding available tools appropriate for use in the evaluation of protection of vertical floor openings. From this, an evaluation method is selected for this research and evaluated in terms of its ability to accurately characterize compartment temperatures and velocities, which are critical parameters for vertical floor opening protection methods. Based on this evaluation, a methodology for the analysis of the performance of the ceiling recession protection method is developed. The final chapters of this thesis discuss the application of the methodology, conclusions drawn from the results of the analysis, and recommendations for future work based on this research.

2 LITERATURE REVIEW

In this chapter the literature pertinent to analysis of ceiling jets, draft stops, and thermal detector response is reviewed. First, the characteristics of buoyancy driven flows within a compartment are discussed in order to establish critical parameters that govern ceiling jet flows and their relation to thermal response times of detection systems. The impact of vertical floor openings on these critical parameters is then discussed and a qualitative evaluation of the ceiling recession method in comparison to the draft stop method is provided based on the theoretical principles outlined. Following this, theoretical principles, numerical correlations, and other analytical tools which can be used to characterize these critical parameters are discussed. The objective of this literature review is to determine an appropriate analysis method for the evaluation of vertical opening protection designs in the context of industry alternative solutions. Based on the information provided, an analysis method is selected and more detailed objectives for the evaluation of the alternative design are outlined.

2.1 Fire Plumes

Combustion of a horizontal fuel bed causes the formation of a fire plume above the heated source. Since the characteristics of the fire plume will directly determine the conditions which develop within an enclosure during a fire it is important to understand several key aspects of their behavior. Work by McCaffrey [11] showed that the fire plume above a 30 cm burner included three distinct regions illustrated in Figure 2-1. The three regions of a fire plume are described as follows:

1. Persistent flame region, near the burning source, characterized by an accelerating flow of burning gases.
2. Intermittent flame region located above the persistent flame region and characterized by intermittent flaming and a near-constant flow velocity.
3. Buoyant plume region located above the flaming regions and characterized by decreasing velocity and temperature of the plume gases with height caused by the entrainment of cooler ambient air.

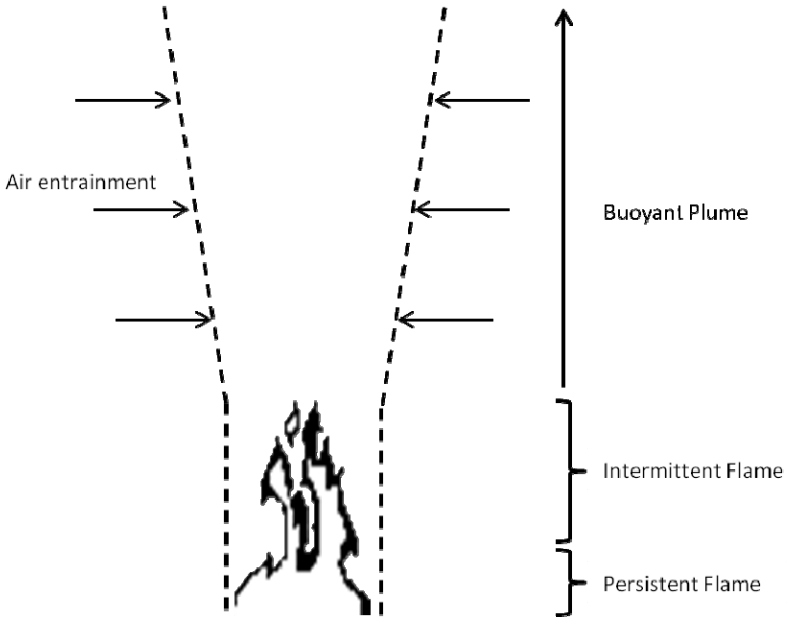

Figure 2-1: Fire plume showing McCaffery's three regions

In general, fire plumes can be discussed based on two classifications: weak plumes, and strong plumes. A fire plume is generally referred to as a weak plume when the density deficiency in the plume (i.e. the difference between the density of plume gases and the surrounding ambient air) is small. In this type of fire, the temperature of the plume gases, especially near the ceiling level, is not significantly different than the temperature of the surrounding air. This type of plume is common during the initial stages of fire plume development where the heat release rate is low, as well as for a range of fire sizes in enclosures with very high ceiling heights. In contrast, a fire plume is generally classified as "strong" when there is a large density deficiency between the plume gases and surrounding air. In this case, the temperature of the plume at the ceiling level is much higher than that of the ambient air.

Although the distinction between these two classifications of fire plumes is not clearly defined mathematically, it can be evaluated, in general, based on a comparison of the flame height of a fire and the ceiling height of the enclosure. Where the flame height of a fire approaches the enclosure ceiling height, a strong fire plume can be anticipated [10]. Whether classified as weak or strong, the characteristics of the fire plume will directly determine the conditions which develop within an enclosure during a fire.

2.2 Ceiling Jets

As a fire grows, the heated air and products of combustion that form the fire plume rise due to buoyancy [12]. Where the fire occurs in a compartment with a ceiling, the plume gases will impinge directly on the ceiling, turn, and continue to flow horizontally along the ceiling away from the fuel source as illustrated in Figure 2-2.

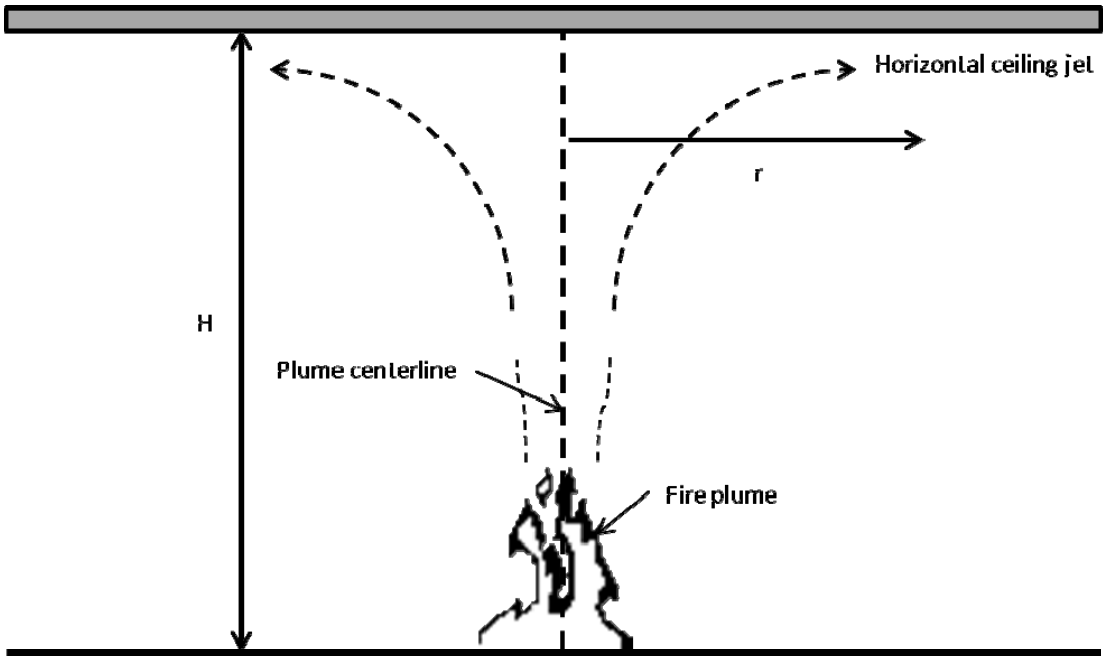

Figure 2-2: Formation of a ceiling jet caused by a fire plume below a ceiling

This buoyancy driven horizontal flow is defined as a ceiling jet [10]. The development of the ceiling jet within a compartment is highly sensitive to the geometry of the compartment (i.e. location of walls, ceiling height, openings, etc.) since obstructions to the ceiling jet flow will impact flow temperature, velocity, and the rate of air entrainment. The properties of the ceiling jet, specifically temperature and velocity, depend on the original strength of the fire plume and are particularly important in determining the response of ceiling mounted automatic detectors (sprinklers, heat detectors, smoke detectors) since these are generally installed with the intent that they will be immersed in the ceiling jet flow [6]. This is indeed usually the case since as the ceiling jet moves away from the heated plume, the depth of the flowing gases will increase due

to entrainment of cool room air. Since this entrainment acts to reduce the temperature and velocity of the ceiling jet with distance from the fire source, the position of the detector downstream of the fire is very important in terms of its response.

Experimental studies aimed at quantifying the characteristics of the ceiling jet flow have been conducted since the 1950s at various research institutions [13–21]. Based on the results of these studies, numerical correlations have been developed to estimate the maximum temperature and velocity of the ceiling jet with respect to the source fire heat release rate, compartment height, and the horizontal distance from the fire plume where the jet is unconfined (i.e. the jet does not encounter obstructions as it flows along the ceiling) [10].

In the case when a ceiling jet encounters obstructions, such as compartment walls, hot gases are restricted from flowing outward and a hotter gas layer will develop at the ceiling level. As this hot layer develops, the ceiling jet will become immersed in the hot layer which will alter the characteristics of air entrainment and change the distribution of temperature and velocity near the ceiling in comparison to that of an unconfined ceiling jet. In this situation, the ceiling jet is classified as a confined ceiling jet.

Where a hot layer forms within an enclosure, temperature values within the ceiling jet will be higher for a given fire heat release rate, compartment ceiling height, and radial distance from the fire plume when compared to an unconfined ceiling jet. This change is primarily attributed to the entrainment of warmer air at the lower ceiling jet boundary from the hot gas layer [22–24]. The magnitude of this effect varies depending on the fire size, the fire location relative to obstructions, and the fire growth rate. Confined ceiling jet studies conducted by Motevalli and Ricciuti noted ceiling jet temperature increases ranging from 25% to 50% at steady state for 0.75 kW and 2.0 kW fires respectively [22]. Additional work conducted by Vittori relating to the impact of beamed ceilings on sprinkler activation found temperature increases of 23% - 50% within the hot layer over a range of fire growth rates and fire locations, within the enclosure [25].

Mixing between a hot fluid moving over top of a cool fluid is an inefficient process [12]. Therefore, in compartments where there is little or no forced convection into or out of the

compartment, a discernible boundary known as the interface layer will develop between the hot gas layer forming at the ceiling and cooler ambient gases in the remainder of the compartment. As a fire continues to burn, plume gases will continue to feed the hot ceiling layer, which will increase in depth below the ceiling, and the location of the interface will descend toward the floor of the compartment. The temperature of the hot layer is not uniform throughout its depth, but instead the highest temperatures occur near the ceiling, and temperatures decrease to near ambient at the lower boundary of the layer [22, 26].

Whether described as a ceiling jet, a hot layer, or the upper hot layer of a compartment interface layer, the accurate representation of the formation and flow of gases along a compartment ceiling above the fire plume is critical in the evaluation of thermal detector response since detectors are positioned with the intent that they will be quickly immersed within this flow.

2.3 Impact of Vertical Openings

Where a ceiling contains an opening, hot gases will flow from the fire along the ceiling to the leading edge of the opening and then, due to buoyancy, rise through the opening.

A 'balcony spill plume' is the general term used for situations where smoke and hot gases travel horizontally under an obstruction, in this case the ceiling, and then turn vertically when the edge of the obstruction, termed the spill edge, is reached [27]. The characteristics of balcony spill plumes have been experimentally found to depend on the characteristics of the fire, the width of the spill plume, and the height of the ceiling above the fire. Studies of balcony spill plumes have largely been restricted to the determination of the mass flow rate of the plume. Multiple correlations have been derived to estimate this value [28–32].

Experiments conducted by Harrison [33] include a flat lower ceiling configuration where the ceiling jet formed by a 10 kW fire in a 0.5 m high space was permitted to flow unobstructed to the spill edge of the apparatus. Harrison observed that the spill plume resulting from this configuration projected horizontally beyond the test compartment before rising as a plume. He attributed this to the momentum in the ceiling jet at the spill edge carrying the gases past the edge before turning upward. The velocity of the ceiling jet at the spill edge is directly related to

the heat release rate of the fire (see Section 2.5.1), with higher velocity values being produced by larger heat release rate fires for the same geometric configuration.

Since in this situation the ceiling jet gases are not contained at the ceiling level of the compartment, the development of a hot gas layer within the original fire room can be hindered, or prevented entirely, by the presence of a vertical opening. If thermal detectors are then installed at a distance below the finished ceiling level, they may not be located directly within the depth of the ceiling jet. Since exposure to hot gases near the ceiling is required to ensure actuation of the device, for cases where a vertical opening hinders the formation of the hot layer, delays in detector response can occur. It is clear that additional protection measures must be considered for situations with vertical floor openings in order to mitigate the inherent risks associated with this design feature.

2.4 Qualitative Comparison of Draft Stops vs. Ceiling Recession

Based on the principles of fire plumes, ceiling jet behavior, and hot gas layer development, it can be surmised that the proposed ceiling recession protection method will create substantially different flow characteristics at the ceiling than would be expected with the draft stop protection method.

In the draft stop protection method the ceiling jet flow will develop as a confined ceiling jet caused by the obstruction of the flow at the draft stop. The characteristics of this type of flow have been extensively studied and a reasonable approximation of maximum temperature and velocity values within the ceiling jet can be determined.

In comparison, for the ceiling recession protection method, automatic detectors and draft stop are recessed above the level of the finished ceiling. Since no obstruction to the ceiling jet flow will exist at the ceiling level, flow characteristics similar to an unconfined ceiling jet can be expected upstream of the spill edge of the recession. Upon reaching the spill edge of the recess, the characteristics of the flow are initially expected to change to resemble a balcony spill plume. Once plume gases reach the upper surface of the recession, recirculation within the recession will further alter the flow characteristics. These changes in flow characteristics have the potential to

significantly change the temperature and velocity of the hot gases through additional air entrainment into the flow, and the formation of recirculation eddies within the recession.

Based on the above, to better define the appropriate physical processes governing a ceiling recession method for fire protection of a vertical opening, the reaction of the ceiling jet when encountering the recession, and the resulting changes to the ceiling jet flow, must be evaluated. From this, the potential impact to adjacent thermal detector response times can also be determined.

For this purpose, evaluation tools are required which have the ability to represent/quantify the characteristics of the ceiling jet flow, and resulting thermal detector response, under the conditions noted. Some available methods are reviewed in the next section.

2.5 Evaluation Tools

2.5.1 Ceiling Jet Correlations

2.5.1.1 Unconfined Weak Plume Driven Ceiling Jets

The properties of a ceiling jet below an unobstructed ceiling due to a weak fire plume have been extensively studied. Correlations have been developed to predict the maximum temperature and velocity in a ceiling jet by Alpert [15], Heskestad [19], Cooper [34], and Motevalli and Marks [35]. A comparative review of available ceiling jet correlations presented by Alpert [10] recommends the use of the nondimensional excess temperature correlation developed by Heskestad and the nondimensional velocity developed by Alpert for the prediction of steady ceiling jet flows beneath unobstructed ceilings. These correlations are adequately fit by the following expressions; key dimensional parameters are illustrated in Figure 2-2 above.

$$\Delta T_0^* = \left(0.225 + 0.27\frac{r}{H}\right)^{-4/3} \qquad \text{For } 0.2 \leq r/H < 4.0 \qquad [2\text{-}1]$$

$$\Delta T_0^* = 6.3 \qquad \text{For } r/H \leq 0.2 \qquad [2\text{-}2]$$

$$U_0^* = 1.06\left(\frac{r}{H}\right)^{-0.69} \qquad \text{For } 0.17 \leq r/H < 4.0 \qquad [2\text{-}3]$$

$$U_0^* = 3.61 \qquad \text{For } r/H \leq 0.17 \qquad [2\text{-}4]$$

These dimensionless expressions can be used in conjunction with the following correlations to determine maximum temperature and velocity values for the ceiling jet [10]:

$$\dot{Q}_0^* = \frac{\dot{Q}}{\rho_\infty c_p T_\infty g^{1/2} H^{5/2}} \qquad [2\text{-}5]$$

$$\Delta T_0^* = \frac{\Delta T / T_\infty}{\left(\dot{Q}_0^*\right)^{2/3}} \qquad [2\text{-}6]$$

$$U_0^* = \frac{U/\sqrt{gH}}{\left(\dot{Q}_0^*\right)^{1/3}} \qquad [2\text{-}7]$$

These correlations are considered sufficient for weak fire plumes located below unobstructed ceilings.

It should be noted that the correlations above provide an estimate of the maximum steady state temperature and velocity within the ceiling jet. Therefore, they cannot be used to estimate temperature and velocity during the growth phase of a fire, where the heat release rate is changing as a function of time. . They are also limited in that estimations of temperature and velocity as a function of distance below the ceiling cannot be obtained.

The limitations in these correlations could have significant implications where the correlations are used to estimate thermal detector response. First, thermal detectors are intended to detect a fire in its initial stages, prior to significant growth, such that suppression and control measures can be implemented. Therefore, prediction of the actuation of the detector during the growth phase of the fire is of primary importance in the design of these fire protection systems. Secondly, the correlations estimate the maximum theoretical temperature within the ceiling jet. However, as discussed above, the temperature within the ceiling jet is not uniform throughout its depth [22, 26]. Therefore, the use of these correlations will be subject to a greater degree of

error when the detector is not located at the same vertical position as that for which this maximum temperature was originally determined.

2.5.1.2 Confined Weak Plume Driven Ceiling Jets

Where a hot upper layer develops due to the presence of internal partitions, the ceiling jet can become fully submerged. Where Equations 2-1 to 2-7 are applied to the confined ceiling jet condition, maximum temperatures will be under-predicted, while the maximum velocity will be over-predicted due to the influence of the forming hot layer [22]. This change is primarily attributed to the fact that as the depth of the hot layer increases the ceiling jet will become immersed in the hot layer. When this occurs, entrainment at the lower boundary of the ceiling jet will draw in hot layer gases instead of cooler ambient enclosure air, resulting in higher temperatures.

Additional correlations have been developed which predict the temperature and velocity where the ceiling jet is submerged within the hot layer. A method developed by Evans utilizes the introduction of a substitute heat release rate (Q_2) and a substitute source distance below the ceiling (H_2) to account for this scenario during the growth phase of a fire as follows [36]:

$$\dot{Q}_2^* = \left(\frac{1+C_T\dot{Q}_1^{*2/3}}{\xi C_T} - \frac{1}{C_T}\right)^{3/2} \quad [2\text{-}8]$$

$$Z_2 = \left(\frac{\xi \dot{Q}_1^* C_T}{\dot{Q}_2^{*1/3}\left[(\xi-1)(\beta^2+1)+\xi C_T \dot{Q}_2^{*2/3}\right]}\right)^{2/5} Z_1 \quad [2\text{-}9]$$

$$\dot{Q}_2 = \dot{Q}_2^* \rho_\infty c_p T_\infty g^{1/2} Z^{5/2} \quad [2\text{-}10]$$

$$H_2 = H_1 - Z_1 + Z_2 \quad [2\text{-}11]$$

The temperature ratio, ξ, is defined as:

$$\xi = \frac{T_2}{T_\infty} \qquad [2\text{-}12]$$

The values of C_T and β are 9.115 and 0.913 respectively as determined by Zukoski et al. [37]. Once the substitute heat release rate is determined, the maximum temperature and velocity in the hot layer can be calculated utilizing the correlations for the unconfined case. This method was found to be accurate for full-scale fires by Evans [36], but the expressions under predicted the maximum ceiling jet temperatures in comparison to scaled laboratory experiments. Evans [36] postulates the difference between the full-scale and small-scale fires could be due to weaker turbulent mixing in the small-scale fires. Evans recommended that, where his correlations are to be applied to larger fires than used in his original work, existing correlations for maximum temperature which were derived from experiments based on larger fires would apply [36]. Further work conducted by Motevalli and Ricciuti [22] compared the results of the Evans method, using the maximum temperature correlation developed by Motevalli and Marks [38] and the correlation developed by Heskestad and Delichatsios [39] to small scale experiments conducted for the confined ceiling jet case. This comparison indicated a constant under-prediction of the maximum ceiling jet temperature regardless of the maximum temperature correlation used [22]. Motevalli and Ricciuti conclude, based on their study, that the source of error hypothesized by Evans (i.e. change in turbulent mixing) is incorrect and further evaluation is required.

Further work by Cooper developed correlations for situations where only a portion of the plume flow penetrated the hot upper layer [40]. Cooper's correlations were also compared to experimental data in the work conducted by Motevalli and Ricciuti with results similar to Evans method in that the temperature values were constantly under-predicted by Cooper's method [22].

2.5.1.3 Strong Plume Driven Ceiling Jet

The correlations above are appropriate for weak fires where the flame height of the fire is less than the compartment ceiling height. When the flame height approaches the ceiling height, the

characteristics of the ceiling jet are altered. The flame height for a given fire at atmospheric conditions can be estimated based on the correlation developed by Heskestad [41].

$$l = -1.02D + 0.235\dot{Q}^{2/5} \qquad [2\text{-}13]$$

Heskestad and Hamada [18] developed a correlation for excess temperature for the strong fire plume case by measuring ceiling jet temperatures for $0.3 \leq \frac{l}{H} \leq 3$.

$$\frac{\Delta T}{\Delta T_p} = 1.92\left(\frac{r}{b}\right)^{-1} - exp\left[1.61\left(1 - \frac{r}{b}\right)\right] \qquad for\ 1 \leq \frac{r}{b} \leq 40 \qquad [2\text{-}14]$$

where ΔT_p is the excess temperature on the plume centreline at the level of the ceiling calculated from Equation 2-4, and b is determined based on:

$$b = 0.42\left[\left(c_p\rho_\infty\right)^{4/5} T_\infty^{3/5} g^{2/5}\right]^{-1/2} \frac{T_p^{1/2}\dot{Q}_c^{2/5}}{\Delta T_p^{3/5}} \qquad [2\text{-}15]$$

As discussed for the weak plume correlations, the strong plume equations outlined above do not allow for variations in the fire plume ceiling jet with time or vertical distance. Therefore, these correlations can be used to estimate maximum values at steady state conditions, but cannot account for changes in the heat release rate of the fire during fire growth, or provide estimates of temperatures that might be expected for various distances below the ceiling.

2.5.1.4 Application of Correlations

The unconfined ceiling jet correlations were developed based on an experimental setup which closely resembles the geometry associated with the ceiling recession protection method. Since there is no obstruction to the ceiling jet flow below the ceiling level, Equations 2-1 to 2-7 would be appropriate to estimate the maximum values of temperature and velocity that might occur in the ceiling jet gases along the lower ceiling leading to the recession, where the jet is driven by a weak fire plume. However, the correlations above have not been evaluated against configurations where the elevation of the ceiling increases, and may not be appropriate for the

prediction of temperature or velocities within the recessed area of the ceiling. For this reason, available correlations are not appropriate for the evaluation of thermal detector response times in the situation where a ceiling recession is used to protect a vertical opening.

Similarly, the experimental setup used in the development of the confined ceiling jet correlations closely resembles the configuration encountered when draft stops are used for fire protection since the ceiling jet will be obstructed and a thicker hot layer will form. Therefore, it is anticipated that Equations 2-8 to 2-12 could be used to determine maximum temperature and velocity values in the ceiling layer and evaluate thermal detector response for this protection method for weak and strong plumes.

In general, the correlations developed for steady state temperature and velocity in the ceiling jet do not provide the level of spatial or temporal resolution required to directly evaluate the ceiling configurations of interest in this thesis. However, estimated values obtained using the correlations will be useful in the validation of results determined by other means.

2.5.1.5 Impact of Geometry on Ceiling Jet

For both the confined and unconfined cases, the maximum temperature and velocity values in the layer of hot gases along the ceiling are directly related to the radial distance from the plume centerline (r). In both cases, due to increasing entrainment of air as r increases, the values for the maximum temperature and velocity decrease. Therefore, the distance between a thermal detector and the centerline of the fire plume will directly affect the temperature and velocity of the ceiling jet gases found at the detector. It is of interest to determine whether this is significant with respect to the performance of thermal detectors in the ceiling recession protection method.

The radial distance between the plume centerline and a thermal detector would be equal for the ceiling recession method and the draft stop protection method due to required compliance with the sprinkler spacing provisions of NFPA 13. However, the distance the ceiling jet travels in order to reach the detector is larger for the ceiling recession method since the ceiling jet gases are required to travel upward into the recession. The ceiling jet might therefore entrain more air, resulting in gases with lower temperatures and velocities reaching a thermal detector in the

recession. It is important to determine whether this difference is significant, particularly when the heat release rate of the fire is low, since small reductions in temperature and velocity values may result in significant delays in detector activation.

2.5.1.6 Impact of Enclosure Boundaries

The formation of a hot gas layer within an enclosure due to the confinement of the ceiling jet by enclosure walls will significantly increase the temperature of the ceiling jet for a given r and Q. Ensuring the formation of a hot layer by restricting the exit of the ceiling jet flow at the floor opening is the basis of the draft stop protection method. On the other hand, the presence of a ceiling recession is intended instead to promote formation of a hot layer within the ceiling recession.

In order to evaluate the performance of ceiling recession designs, the formation of a ceiling hot layer when a draft stop is used should be evaluated against the formation of a hot layer for a ceiling recession design. To facilitate comparison, other elements which could impact the analysis, such as the distance from the fire plume and/or detector to adjacent enclosure walls, were removed where possible. This approach aims to ensure that differences in thermal detector activation time highlighted by the analysis are caused by the differences between the two designs, rather than because of the enclosure geometry.

2.5.1.7 Impact of Heat Transfer to the Ceiling

It is noted that the ceiling jet correlations discussed above do not contain variables which explicitly account for heat losses from the ceiling jet to the enclosure ceiling. Instead these effects are inherently included during development of the correlations from experimental data. The following section discusses the impact of heat transfer to the ceiling, and of the selected ceiling material, in order to determine potential impacts with respect to the analysis of the ceiling recession configurations of interest.

For weak fire plumes, heat losses to the ceiling, and consequent cooling of the ceiling jet, can be important in determining the response times of thermal detectors since initial ceiling jet temperatures and velocities are not very much in excess of ambient values. This is less

important for strong fire plumes where large temperature differences between the ceiling jet and ambient air, well in excess of those values required for thermal detector activation, are anticipated.

The rate of heat transfer from a fire plume to a ceiling can be discussed in terms of three regions: the free fire plume region, the turning region, and the downstream flow region.

In the free fire plume which is in the vertical space between the fire source and the ceiling, entrainment of ambient air cools the plume and causes radial expansion of the plume with height.

The second region, where the plume impinges on the ceiling and turns to follow the ceiling, is termed the turning region. Based on his experimental data, Alpert defined the radius of the turning region as being approximately equal to 0.18H, where H, in this case, is the ceiling height of the compartment measured from the top of the fuel source to bottom of the ceiling[12]. In this region plume gases travelling vertically impinge on the ceiling and are forced to flow horizontally outward to form the ceiling jet which continues to be fed by the flow of hot gases from the fire plume below.

Studies conducted by Yu and Faeth quantified the convective heat flux from a weak thermal plume to the ceiling within the turning region using small pool fire experiments with heat release rates ranging from 0.05 kW to 3.46 kW [42]. Based on these experiments a correlation was developed which quantifies the convective heat flux to the ceiling for given values of the heat release rate of the fire, the ceiling height, and the Rayleigh number of the weak plume. Further work conducted by Kokkala [43] verified the correlations developed by Yu and Faeth using up to 10 kW natural gas flames for flame heights up to 70% of the ceiling height (i.e. weak plumes).

For flame heights exceeding 70% of the ceiling height (i.e. strong plumes), Kokkala [43] determined that the correlations determined by Yu and Faeth for heat transfer within the turning region would significantly under predict the heat-transfer rate to the ceiling because of additional losses due to thermal radiation from the fire plume to the ceiling.

Outside of the turning region of the plume, i.e. in the hot gas layer travelling along the underside of the ceiling, the convective heat flux to the ceiling was found to decrease significantly as the distance from the plume centerline increased [42]. This trend was confirmed by further weak plume experiments conducted by Alpert [44], and Veldman et al. [45].

Based on the studies discussed here, it can be surmised that the rate of convective heat transfer from the plume to the ceiling will significantly impact the response of ceiling mounted thermal detectors for the case of detectors located close to the ceiling and a weak fire plume.

Since the temperature of a ceiling jet formed by a strong fire plume is likely to greatly exceed the activation temperature of most thermal detectors even at positions away from the centreline of the main fire plume, relatively minor heat losses to the ceiling are not likely to significantly impact thermal detector response times.

2.5.2 Thermal Detector Activation

Thermal detectors such as heat detectors or sprinklers rely for actuation upon exposure of a sensing element to an increase in temperature. Therefore, the heat transfer characteristics and thermophysical properties of the sensing element, the area of the sensing element, and the thermal and physical properties of the fluid to which the element is exposed are the primary factors affecting detector response. The total heat transfer to a sensing element can be expressed as an energy balance as follows:

$$Q = Q_{cond} + Q_{conv} + Q_{rad} \qquad [2\text{-}16]$$

Since detection normally occurs in the initial stages of a fire, when the heat release rate of the fire is low, radiative heat transfer to the sensing element (Q_{rad}) is normally considered negligible [46]. Additionally, the sensing element of a detector is generally immersed in flowing hot gases at the ceiling level such that convective effects will dominate heat transfer to the element. Similarly, in most detectors the sensing element is thermally isolated from the remainder of the detector assembly. Consequently, heat transfer to the sensing element by conduction can be considered negligible [46].

Therefore, the rate of convective heat transfer between the hot fluid and the sensing element is the primary process affecting detector response. Equation 2-16 above can be rewritten in terms of the rate of convective heat transfer to determine the total heat transfer (Q) required to cause actuation of the detector as follows:

$$Q = Q_{conv} = h_d A_d (T_g - T_d) \qquad [2\text{-}17]$$

The value of the convective heat transfer coefficient (h_d) is dependent on the fluid properties (thermal conductivity, density, and viscosity), the flow velocity, the thickness of the sensing element, and the location of the sensing element within the flow [47]. The surface area of the sensing element (A_d) is included since a larger surface area will increase the rate of convective heat transfer to the element. T_g and T_d represent the temperature of the hot gases and the ambient temperature of the sensing element (in C or K) respectively.

The characteristics of ceiling jets, hot layers, thermal detectors, and the temperature and velocity of the hot fluid are critical in determining the actuation time of a thermal detector. These properties can be used in conjunction with the thermo-physical properties of the sensing element to determine the actuation time of a thermal detector.

The sensing element of a thermal detector can be treated as a single mass with given thermal properties. In this case, the temperature change within the sensing element can be determined as follows:

$$\frac{dT_d}{dt} = \frac{Q}{m_d c_d} \qquad [2\text{-}18]$$

Where dT_d/dt is the change in temperature of the sensing element over time.

In order to characterize the convective heat transfer to a sensing element in a specific detector, Heskestad and Smith [48] proposed the use of a time constant, τ, which is a function of the mass, specific heat, convective heat transfer coefficient, and the area of the sensing element.

Further work conducted by Hollman [49] determined that the convective heat transfer coefficients for sprinklers and heat detector sensing elements were similar to those found for spheres and cylinders in cross flow. Therefore, the heat transfer coefficient for thermal detectors can be estimated as being proportional, based on the time constant, to the square root of the velocity of the gases passing the detector. Since the mass, thermal capacity, and area of the sensing element remain constant for a given detector design, the Response Time Index (RTI) determined for a given detector can be defined as:

$$RTI = \tau u_g^{1/2} \quad [2\text{-}19]$$

Utilizing these concepts, an equation for determining the actuation time of a detector was developed as follows [50]:

$$t_{act} = \frac{RTI}{\sqrt{u_g}} * \ln\left(\frac{T_g - T_\infty}{T_g - T_{act}}\right) \quad [2\text{-}20]$$

Equation 2-20 can be used to determine the activation time of a thermal detector provided the temperature of the gases to which the detector sensing element is exposed is known and constant. This analysis would hold when a fire is fully developed and burns at a constant heat release rate. Since detection generally happens during the growth stage of a fire Equation 2-20 will provide varying degrees of accuracy depending on the growth rate of the fire of interest. The accuracy increases when the fire grows quickly and levels off to a fully developed fire with approximately constant heat output.

Additional correlations with which to determine detector activation times have been developed by Beyler [51] utilizing the temperature and velocity-time correlations for a growing fire developed by Heskestad and Delichatsios [39]. These correlations require an integral solution based on an estimated growth rate for the design fire and are cited in NFPA 72 "National Fire Alarm and Signaling Code" as a means of estimating detector activation times as well as appropriate detector spacing [46].

Both Equation 2-20 and the correlations developed by Beyler require the use of ceiling jet temperature and velocity correlations to determine the required inputs. As discussed in Subsection 2.5.1 above, available ceiling jet correlations will not provide the level of detail necessary to evaluate the comparative performance of thermal detectors for different ceiling configurations.

2.5.3 Balcony Spill Plume Theory

The discussion above has been limited to temperatures and flow characteristics of the fire plume as it rises, impacts the ceiling, turns and flows along the unobstructed ceiling. Another aspect of the flow that should be considered, however, is the balcony spill plume which occurs at a vertical opening without an obstruction or draft stop, as well as at leading edge of the ceiling recession geometry proposed here. In this latter situation, the ceiling jet will flow, unobstructed, to the spill edge of the recession. The characteristics of balcony spill plumes have been experimentally found to depend on the characteristics of the fire, the width of the spill plume, and the height of the ceiling above the fire.

Spill plume correlations have not been developed which characterize the temperature or velocity of the plume upon reaching the edge of the obstruction. Therefore, the application of balcony spill plume theory to the ceiling recession geometry will not yield additional information for use in estimating thermal detector response times. However, further review of experimental observations for balcony spill plumes is of value to this research as it provides insight into the characteristics of the behavior of ceiling jet flows at vertical openings.

The velocity of the ceiling jet at the spill edge and resultant horizontal projection of the plume are significant with respect to the ceiling recession protection method since a large horizontal projection of the plume may cause a portion of the hot ceiling jet gases to bypass the ceiling recession where the recession is narrow. This could potentially reduce exposure of the thermal detector sensing element to the hot gases, resulting in a delay in detector response. Since such a delay is linked directly to life safety objectives in the code, large heat release rate fires must be considered as part of this research in order to determine the impact, if any, of the horizontal projection of the ceiling jet at the spill edge of a ceiling recession design.

2.5.4 Computer Models

In addition to an array of engineering correlations for estimating fire plume characteristics, there are a number of computational tools available to designers. These range from relatively simple algebraic models, to sophisticated Computational Fluid Dynamics (CFD) models. In general, computer models designed for the analysis of compartment fires can be grouped into one of the following categories:

- Algebraic Models
- Zone Models
- Field Models

The selection of an appropriate model to evaluate a given problem is a significant issue facing designers. Use of the most complex types of models can produce superior results in some cases, but often requires additional input information, and significantly more time in order to set up and evaluate a problem. In contrast, simpler models such as zone based models or algebraic models can produce similar results in some cases, but in a fraction of the time required for CFD analysis. Consequently, the ability to evaluate and select an appropriate model for a given problem is of particular importance within the fire protection and building design industry.

In the following subsections the general characteristics of each model group are discussed in the context of the present application. Following this, an evaluation of the scope of applicability of these models is provided with respect to the evaluation of hot layer development and therefore thermal detector response in the presence of vertical openings for the two protection configurations considered.

2.5.4.1 Algebraic Models

Algebraic Models consist of pre-programmed equations and correlations that describe overall fire dynamics. In general, these types of models permit users to input key data on their chosen fire scenario into a spreadsheet and obtain results based on the programmed equations such as the ceiling jet and hot layer correlations discussed above.

The primary advantage of algebraic models is that results are obtained quickly. Additionally, these types of models allow the user to quickly investigate the sensitivity of the result to changes in specific input parameters. These models are not well suited for analyses involving time-dependent fire growth and, in general, do not account for interactions of many of the chemical and physical processes involved in an enclosure fire [52].

The applicability of algebraic models in the evaluation of thermal detector response for the vertical opening protection methods under study is therefore similar to the scope determined for the correlations discussed above. Although the models may provide reasonable estimates of selected parameters, they will not allow one to account for finite changes in geometry or time dependent variables. Therefore, the use of algebraic models for the current evaluation of vertical opening protection methods is not considered reasonable given the complex geometries involved. However, similar to the manual calculation methods, the results of algebraic models do provide a means of conducting an order of magnitude validation of results obtained via other evaluation methods.

2.5.4.2 Zone Models

In contrast to algebraic models, zone models are formulated to solve a set of conservation equations associated with fire growth and development (i.e. conservation of mass, conservation of energy, conservation of species) on discrete control volumes within the enclosures of interest [52]. The enclosure volume is subdivided into multiple (normally two) zones and the conservation equations, written as a set of ordinary differential equations in time are solved to provide estimates for key enclosure parameters (i.e. temperature etc.).

A primary advantage to using a zone based model to estimate fire development is that time-dependent parameters can be estimated for a given fire scenario. Additionally, the computation time required to obtain results from a zone model is often relatively low (normally less than 1 minute) which permits quick analysis of multiple scenarios with varying inputs.

The primary disadvantage of a zone model is that the solutions to the conservation equations provide only a single value for each parameter within each zone. In other words, results are averaged over the domain and yield limited spatial information. In general, zone models cannot be applied to solve for fire and hot layer development in complex enclosure geometries. Nonetheless, some zone models have been configured to provide predictions of thermal detector response times within the hot layer of an enclosure [52]. These models are discussed in the following sections. A more comprehensive summary of available zone models can be found in Section 3, Chapter 7 of the 4th edition of the SFPE Handbook of Fire Protection Engineering [52].

LAVENT and DETACT-QS

Models such as Link Actuated VENTs (LAVENT) developed by David and Cooper [53], and DETector ACTUATION - Quasi Stead (DETACT-QS) developed by Evans [54] are examples of zone models designed specifically to predict the response of thermal detectors for a fire contained within a compartment. These models are widely used in industry and have been subjected to multiple studies in which model output was compared to experimental results with varying levels of agreement [22, 55, 56, 57].

Both models implement ceiling jet correlations in combination with theory for hot layer development and assumptions of hot layer temperature profiles to determine the overall temperature near the detector. Therefore, the applicability of these models is limited to geometric configurations which closely resemble the experiments used in the development of the correlations. In addition, both models are limited to analysis of hot layer flow contained within a single compartment and therefore, since no account can be made for the distinct characteristics of hot gas flow through or across an opening, the geometry associated with hot layer development in a ceiling recession cannot be defined.

Consolidated Model of Fire Growth and Smoke Transport (CFAST)

CFAST is a two zone fire model intended to simulate the distribution of smoke, fire gases, and heat throughout a given fire compartment as well as in several adjoining compartments [58]. It is commonly used in industry as it is publicly available software which was developed and is maintained by the National Institute of Standards and Technology (NIST). Through their development work, NIST has conducted a number of validation studies which are published for reference by model users [59]. CFAST solves a system of ordinary differential equations the describe conservation of mass, conservation of energy, the ideal gas law, and equations for density and internal energy [58]. Further, the model allows the user to define multiple compartments which are open to one another (both horizontally and vertically) in order to simulate conditions in rooms located away from a fire. CFAST utilizes the ceiling jet correlation developed by Cooper to define an additional zone within the fire compartment of the model that is distinct from the upper layer, and can therefore be used to predict temperatures and velocities within the ceiling jet [58]. The ceiling jet correlation is not applied in compartments adjacent to the fire compartment. It is noted that Cooper's ceiling jet algorithm was developed for the prediction of gas temperatures and velocities in the ceiling jet developed under a flat, unconfined ceiling above a fire source [59].

Temperatures obtained from the ceiling jet algorithm are utilized by the model to predict the actuation time of heat detectors where the fire is located within the compartment [60]. The thermal detector link temperature used to predict activation is modeled using the differential equation developed by Heskestad and Smith [48] as discussed in Section 2.2.2.

Validation work conducted by NIST comparing ceiling jet temperatures predicted by CFAST to experimental data found that reasonable accuracy (within experimental uncertainty) was provided for experiments in which a well defined ceiling jet developed below a flat ceiling [59]; however, no assessment was made of CFAST predictions as they related to ceiling jet velocities, thermal detector response times, or ceiling jets developed below confined ceilings.

CFAST may be appropriate for use in the evaluation of ceiling jet temperatures when the ceiling is flat. However, when there are ceiling obstructions, such as draft stops, or changes in ceiling elevation, such as ceiling recessions, the CFAST ceiling jet algorithm cannot be expected to provide accurate. For this work then, CFAST is not considered appropriate for the evaluation of hot layer development or thermal detector response for the ceiling configurations of interest.

2.5.4.3 Field Models

In general, field models developed for fire applications provide a solution to the constant density low Mach number approximation of the Navier-Stokes equations, a coupled set of partial differential equations for conservation of mass, energy, species, and momentum. The computational domain must be defined to match the geometry of interest and is then subdivided into a mesh of smaller cells with dimensions selected by the user. The set of coupled partial differential equations is solved iteratively for the variables of interest resulting in values of each variable, within each cell in the domain. Values within an individual cell are uniform and equal to the average value for that volume. A smaller cell size, in general, results in a higher degree of accuracy in the simulation but will also increase the computational requirements for a solution. When a field model is applied to an entire building, the computational domain can include millions of cells depending on the selected cell size. Therefore, computation times for a single full building simulation will be extremely large depending on the time of fire development to be simulated, and the number of variables to be determined.

One advantage of field models is that values for each variable within an individual cell can be determined distinctly as functions of time. Similarly, differences in values across adjacent cells can be monitored where a level of spatial resolution is necessary for the analysis. Additionally, since field models are formulated to estimate solutions of the Navier-Stokes equations, they do not rely as heavily upon use of experimental correlations in determining a solution. This can be vital where correlations based on experimental data do not exist for a scenario of interest; however, all field models do still require the use of submodels to represent certain key physical parameters such as turbulence and radiation.

The main disadvantage of field models is the simulation times necessary for the analysis of complex situations. As discussed previously, industry timelines often play a role in the decision to pursue an alternative solution. Therefore, it is plausible that, for some situations, the time required for a field model analysis will not be considered feasible within the timeframes of the project. Nonetheless, field models can be extremely useful to research alternative solution configurations outside of the design cycle as they facilitate more comprehensive analysis of various characteristics of the flows developed within a fire compartment in order to establish critical parameters that govern those flows under certain design conditions and configurations. It is in this latter context that they are reviewed here.

Field model development is an emerging field in fire dynamics research which has led to the development of multiple models by a number of institutions. Examples of commercially available field models which are specifically designed for the simulation of thermally driven flow include: Simulation of Fires in Enclosures (SOFIE), JASMINE, SMARTFIRE, CFX, FireFOAM, and Fire Dynamics Simulator (FDS).

Fire Dynamics Simulator (FDS)

FDS is a field model developed by NIST which often has been applied specifically for the evaluation of fire-related flows. The most current version of the model is 5.5.3 released in November 2010. The model can be described as follows [61]:

"FDS is a Computational Fluid Dynamics (CFD) model of fire-driven fluid flow. The model solves numerically a form of the Navier-Stokes equations appropriate for low-speed, thermally-driven flow with an emphasis on smoke and heat transport from fires. The partial derivatives of the conservation equations of mass, momentum and energy are approximated as finite differences, and the solution is updated in time on a three-dimensional, rectilinear grid. Thermal radiation is computed using a finite volume technique on the same grid as the flow solver. Lagrangian particles are used to simulate smoke movement, sprinkler discharge, and fuel sprays."

FDS is widely utilized in industry, since it is publicly available and is regularly updated. There is a growing body of work related to validation of FDS results carried out by the developers and industry users [62].

In order to set up an FDS simulation the enclosure geometries must be discretized into a rectilinear finite volume grid with a grid size chosen and defined by the user. Obstructions and measurement locations must be aligned with volumes on the grid, requiring slight modifications to the enclosure dimensions depending on the grid size selected. The impact of such geometric simplifications must be carefully considered by the user.

A set of partial differential equations describing the transport of smoke and hot gases, as well as mixing with the surrounding air is then formulated for the problem at hand, approximated by finite difference representations across each grid volume and in time, and solved for an estimate of temperature and velocity values at each location within the compartment [63]. Since the volumes extend all the way to the ceiling, the model does not rely upon the implementation of ceiling jet correlations to account for gas flows embedded within a larger solution volume, as would be the case for example with a zone model of a compartment fire. To represent flows in the immediate vicinity of the ceiling within FDS, however, it is necessary to model the velocity boundary layers at solid obstructions through the use of a submodel. This in itself can present a modeling challenge. For example, the default model for this in FDS Versions 5.4.0 and later was changed to the Werner-Wengle wall model for smooth walls to address inaccuracies observed in previous model solutions for which a velocity "half-slip" boundary condition at solid obstructions was assumed [61].

In predicting the fluid flow using the full Navier-Stokes PDEs, a turbulence submodel is required. In FDS, the Smagorinsky Large-Eddy Simulation (LES) turbulence model is used by default; however a Reynolds Averaged Navier-Stokes (RANS) or Direct Numerical Simulation (DNS) framework can also be adopted by the user. In the LES method, turbulence is modeled through simulation of the flow and mixing characteristic of turbulent eddies with length scales larger than the grid size chosen for a particular simulation. The impact of flow processes within

eddies of length scale smaller than the grid size are not considered, under the assumption that these will have minimal impact on the accuracy of the simulation.

Thermal detector actuation is determined based on a correlation proposed by Heskestad and Bill, a derivative form of the lumped capacitance based model in Equation 2-20, with an additional term to account for link cooling caused by the actuation of nearby sprinklers in situations where sprinklers rather than thermal detectors are modeled [61].

FDS has been the subject of multiple validation studies by both developers and industry users. These investigated the ability of FDS to predict parameters of interest (i.e. ceiling jet temperatures, velocities, thermal detector activation, and hot gas movement) as compared against experimental results. The model was originally designed for the analysis of industrial-scale fires and, in the view of the model development team, can be used reliably where a heat release rate is specified, and the principle aim of the modeler is to predict the transport of heat and exhaust products within the domain [61]. In these cases, the model has been found to predict flow temperatures and velocities to within 10% - 20% of experimental measurements depending on the resolution of the numerical grid [61].

The FDS Validation Guide provides a summary of selected validation studies that relate to its use for the simulation of ceiling jet and the actuation of detectors [62]. In general, the model provided good agreement with the experimental results for maximum temperature and actuation time of thermal detectors. The guide does not provide significant validation work with respect to the prediction of ceiling jet velocities or the characterization of a ceiling jet flow as it reaches the spill edge of a floor opening [62].

From an industry standpoint, FDS is an attractive tool due to its availability and the quantity of literature available that relates to model review and validation. Due to the formulation and optimization of the model for practical application, many simple industry level analyses can be processed using a single computer with affordable hardware. FDS is capable of addressing complex geometries, within the limitations of a rectilinear grid, and can provide time dependent predictions of key variables at spatially independent locations within the domain.

On the other hand, FDS is a complex model which, in order to be used properly, requires a significant level of understanding of the model formulation and an understanding of the physics and fluid flow implications for the scenario under study. For complex model geometries, model set up and modification are time intensive activities and may require significant review. From an industry standpoint, this level of understanding requires a significant time commitment in training the model user and continual updating of that user as FDS developers modify and update the inner workings of the model. This can be an expensive undertaking for industry, especially when the application of FDS for a given analysis is not appropriate for all cases.

SMARTFIRE

SMARTFIRE is a field model formulated for fire applications developed by the Fire Safety Engineering Group (FSEG) at the University of Greenwhich. The latest version of the model is v4.1 which was released in April 2008. The CFD solver evaluates the solution of the Navier Stokes equations for compressible flow and heat transfer including the two equation k-e turbulence model.

The model includes a number of features designed to aid users including a built in graphical scenario designer, the ability to directly import geometries from two dimensional Computer Aided Drafting (CAD) files, and an automatic mesh (grid) generator [64].

A time limited evaluation version of the model can be obtained for free through the developer's website [64]. Access to the full version of the model requires registration with the developer and annual payments for a commercial license of approximately £3000 UK.

SMARTFIRE has been subject to a number of validation studies by the developer and model users [65–67]. A verification and validation report has also been produced by the developer and is packaged with the software [68].

From an industry standpoint, SMARTFIRE is an attractive tool due to the availability of validation material and support of the model by the developers and its ability to address both simple and complex geometries. Built in model features, such as direct input of CAD drawings and the automatic mesh generator, are also beneficial as they reduce the amount of time required to set up simulations. The primary drawback to this model from an industry standpoint is the cost of the annual commercial license.

FireFOAM

FireFOAM is a fire development and suppression specific field model currently under development by FM Global based on the OpenFOAM CFD toolbox. FireFOAM utilizes the principles of Large -Eddy Simulation (LES) to simulate buoyancy-driven turbulent flows, non-premixed combustion, thermal radiation, solid fuel pyrolysis, Lagrangian droplet tracking, and surface film flow [69].

FireFOAM utilizes arbitrary unstructured meshes for application of finite volume CFD calculation methods. This is an extremely attractive feature as it does not require that irregular or complex model geometries be modified to fit a defined grid regime.

Since the model is based on the OpenFOAM CFD package, the software is free to download and use through the OpenFOAM Foundation.

From an industry standpoint, FireFOAM is still in the early stages of its development and, at this time, limited validation studies for the model are available. A series of presentations related to the model development, including discussion of some validation studies, is available through the website for the annual FM Global Fire Modeling Workshop [69]. Of particular interest to the present research, validation work presented by Wang [70] found that FireFOAM provided a reasonable representation of the thermal plume. Additional work by Maragkos et. al. [71] found that FireFOAM adequately represented the flow of a buoyant plume.

2.6 Selection of Analysis Tool

In the present analysis, a method which is appropriate for use within industry is desired. Primary considerations in choosing a tool to be used in industry evaluations of design alternatives include trade-offs such as the cost and time commitments required for the evaluation versus the level of accuracy provided, recognizing that the accuracy of prediction must be appropriate for comparison amongst several alternative designs. In addition, the accuracy must be such that potential errors in the simulations can be assessed and, as necessary, mitigated through the application of appropriate factors of safety to the final design.

Based on the available literature, it is clear that the development of the ceiling jet, hot layer, and the subsequent activation of thermal detectors is heavily dependent on the geometry of the enclosure being analyzed. Therefore, ideally the method would be versatile enough to be applied for analysis of a range of floor opening and enclosure configurations such that actual conditions within a building can be analyzed.

Available correlations for ceiling jets, hot layer development, and thermal detector actuation have been shown to provide reasonable agreement with corresponding experiments on a time and spatially averaged basis. However, in general these correlations are limited to the ceiling configurations for which they were developed and calculated values have shown significant divergence from experimental results where they were applied to other enclosure configurations. Therefore, these correlations do not provide the level of detail, or accuracy, for use as the sole basis for an analysis of alternative ceiling configurations. They could, on the other hand, be utilized for performing order of magnitude validation of other analysis approaches.

Most algebraic computer models implement selected correlations and therefore, these models are considered limited in application to the same degree as available correlations.

Zone models represent a more advanced means of modeling fire and hot layer development within a compartment since they allow for compartment specific factors, such as mechanical ventilation, to be incorporated into the analysis. This provides an increased level of flexibility over available correlations; however, a fundamental assumption in zone models is that of uniform properties throughout the hot layer, and therefore there is no spatial resolution within the

hot layer. Some models, such as CFAST, allow the user to implement additional ceiling jet correlations within the hot layer for the purposes of estimating thermal detector response. This approach is again limited to situations that fall within the range of applicability of the selected correlations. Therefore, the impact on the ceiling jet of the ceiling configurations of interest in this work are not well represented using available zone models.

Due to the limitations of available correlations, algebraic models, and zone models discussed above, a field model was selected as the most appropriate method with which to conduct the evaluation of ceiling recession thermal detector performance. Due to their availability to industry, FDS and FireFOAM were considered primary candidates for the present research.

Validation work conducted by Drean et. al. and presented at the 2012 FM Global Open Source CFD Fire Modeling Workshop [72] compared the results of FireFOAM and FDS to experimental results and correlations for properties of diffusion flames. The study considered a 10 cm diameter ethylene burner with a heat release rate of 25 kW. Where the centerline velocity of the diffusion flame as a function of distance from the fire source was considered, significant oscillations were seen in simulations of the intermittent and plume regions FireFOAM's LES formulation. These are shown in Figure 2-3.

A similar trend with respect to oscillations in the intermittent and plume regions of the diffusion flame was observed in FireFOAM results for the centerline temperature. Radial velocity values predicted in the plume region in this study found that FireFOAM tended to over predict the values in comparison to the experimental values. In comparison, FDS was found to underestimate these values.

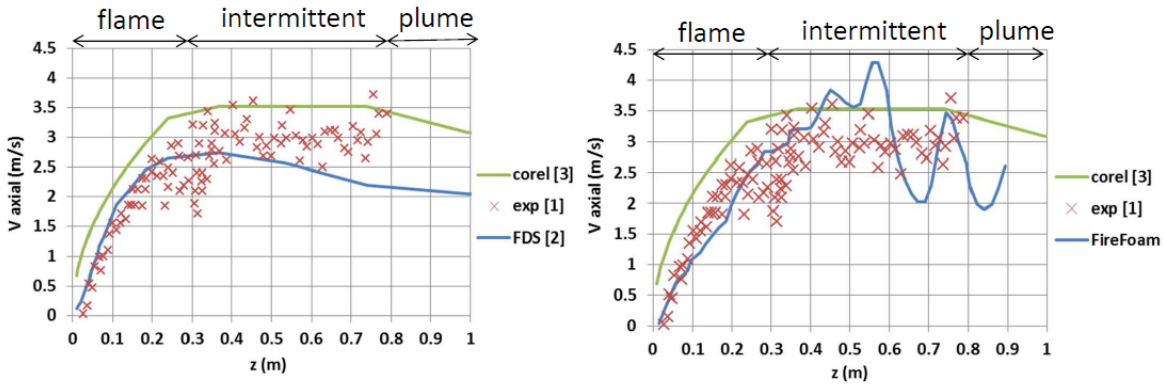

Figure 2-3: Comparison of simulated and experimental results for centerline velocity [72]

Predicted temperature and velocity in the fire plume will directly determine the downstream temperature and velocity values of interest in this research. As determined by Drean et. al. [72], there is significant differences in predicted results between FDS and FireFOAM for plume temperature and velocity which could impact the evaluation of interest here. In general, FireFOAM has not been subjected to the same level of validation work as FDS as it is a relatively new field model.

Based on the discussion in this section, FDS was selected for the performance evaluation of the ceiling recession thermal detectors in consideration of the following:

1. Complex geometries can be accommodated provided the proper grid size is selected.
2. The impact of selected design parameters can be evaluated through the modification of model inputs and comparative analyses.
3. FDS has been subjected to a significant amount of validation work by the developers and model users. These studies can be utilized by model users to evaluate the model's applicability to a given application. This level of supporting documentation is not currently available for FireFOAM.
4. Validation studies conducted by NIST and others have indicated that the model provides good general agreement with ceiling jet temperatures and device actuation for selected experiments.

In support of this latter point, a more thorough review of literature related to the application of FDS to these problems is contained in the following chapter. This review describes the limits of applicability of FDS for the present application, and highlights methodologies that were applied in this thesis.

3 EVALUATION OF FDS

The use of FDS for prediction of the critical attributes of ceiling jet flows is further discussed in this section. Strengths and limitations of its use are highlighted and a discussion of potential errors is presented.

A generalized discussion of the expected flow characteristics of the ceiling jet for the draft stop and ceiling recession protection methods was provided in Section 2.4. Based on the expected flow characteristics, the ability of FDS to predict ceiling jet and hot gas layer temperatures and velocities must be evaluated for three primary geometric configurations:

1. Confined ceiling jets (draft stop method flow)
2. Unconfined ceiling jets (ceiling recession method flow up to spill edge)
3. Balcony spill plumes (ceiling recession method flow at spill edge)

Furthermore, the ability of the model to predict thermal detector response must be assessed for each case.

A selection of validation work undertaken by the model developers (NIST) and other industry stakeholders is summarized in the FDS Validation Guide [62]. The guide provides results of FDS simulations in comparison to experimental data to aid users of FDS in evaluation of the applicability of FDS to a given analysis. A key advantage of the Validation Guide is that the cases discussed in the guide are reassessed with each minor release (update) of FDS. The repeated evaluation of the validation cases ensures that the changes in a new version of FDS do not negatively impact previous results [62]. This provides users of FDS with a set of experiments and comparative FDS simulation results which are relevant to the current release of the model. Additional comparisons are available in the form of industry investigations and academic research.

In the following sections, a summary of work relevant to the use of FDS for the evaluation of vertical floor opening protection methods is provided. In the final section, an overall discussion is provided summarizing the applicability of FDS for the evaluations required in this thesis.

3.1 Grid Sensitivity

An important parameter for any CFD analysis is the selection of an appropriate grid size for the scenario under consideration. The accuracy of a CFD prediction will generally be improved as the selected grid size is decreased but smaller grid sizes will significantly increase computational requirements. Therefore, the selection of an appropriate grid size is a process which involves balancing model accuracy with the required computation time.

The FDS User's Guide [73] provides guidance regarding the selection of a grid size by defining the characteristic fire diameter (D^*) as:

$$D^* = \left[\frac{\dot{Q}}{(\rho_\infty T_\infty g^{1/2})}\right]^{2/5} \qquad [3\text{-}1]$$

This quantity is related to the physical diameter of the source fire (D) by:

$$Q^* = (D^*/D)^{5/2} \qquad [3\text{-}2]$$

Q* represents the combined effect of the effective diameter of the fire and the size (heat release rate) of the fire. The ratio of D^* to the selected grid size (δ), essentially the number of grid cells located across the characteristic diameter of the fire (different from the physical diameter of the fire), can be used as one indicator in the choice of an appropriate grid size for a given fire simulation. For example, in simulations involving buoyant plumes, as D^*/δ increases, the accuracy of the numerical model predictions has been shown to improve [73]. Further, it has been observed that the model tends to produce good agreement with empirical plume correlations when the grid cell size in the vicinity of the fire is given by $D^*/\delta = 10$ [74]. Within the context of the current research, the choice of D^*/δ has two important implications.

First, since compartment temperatures and velocities are primarily driven by the interaction of the fire plume with the compartment, the accurate representation of the plume is critical in determining thermal detector response times within the ceiling recession. Therefore, D^*/δ is used as a guideline in the selection of an appropriate grid size for the analysis.

Second, experimental testing of the ceiling recession configurations will not be conducted as part of the current research, precluding comparison of the model versus experimental measurements. This is a common situation in the use of models for the evaluation of alternative solutions since experimental data for configurations similar to the scenario of interest is rarely available for comparison. Where measurements are not available for estimating model accuracy, the ratio of D^*/δ applied in previous validation studies can be used as a guideline for the selection of an appropriate grid size. The value of D^*/δ will be most appropriate when the studies involve similar fire sizes and compartment geometries as those of interest and, of course, are used in FDS predictions of the compartment parameters of interest (i.e. ceiling jet temperature, velocity, etc.). It should be made clear, however, that the application of this approach does not reduce the importance of conducting a separate grid sensitivity analysis within the parameters of interest for each new situation.

The primary parameters of interest in the current research are the ceiling jet temperature, velocity, and the flow of hot layer gases when encountering ceiling level obstructions such as draft stops and ceiling recessions. Therefore, where previous validation studies have analyzed the ability of FDS to predict these values under similar conditions as those under study here, and have found the model to be in good agreement with experimental results, the D^{*}/δ ratios applied in those studies were viewed as minimum values for the present analysis. Although it cannot be inferred that the level of accuracy obtained in past validation studies will be mirrored in the present analysis even when similar values of D^*/δ are applied, using these values as minimum limit values should provide a reasonable starting point for the analysis. From there, an appropriate grid sensitivity study will also be undertaken.

3.2 Previous FDS Validation Work - Compartment Temperature and Velocity

The following subsections summarize work previously conducted by others where FDS predictions were compared to experimental results. The review focuses on the prediction of temperature and velocity of ceiling jets, the development of the hot gas layer, and the interaction of the hot gas layer with compartment obstructions. The intent is to develop an understanding of the applicability of the FDS for prediction of these parameters in the ceiling recession configuration relevant in this thesis.

It is important to note that many of the validation studies reviewed were conducted using earlier versions of FDS. As previously discussed, for those studies contained in the Validation Guide, the results can still be considered applicable to the current version of FDS. Many other validation studies related to the present research are not contained within the Validation Guide and utilize older versions of the model [8, 33, 75, 76, 77, 78]. Although the results of these cannot in all cases be considered directly applicable to the current version of the model, they provide valuable information with regards to the capabilities of FDS as it pertains to the present research and are therefore included here.

3.2.1 NIST/NRC Test Series

Hamins et al. conducted a set of experiments that focused on measurements of ceiling jet temperature, hot gas layer temperature, and thermal detector activation [79]. Since the experiments were intended for comparison with FDS predictions, the study is included in the current edition of the FDS Validation Guide [62]. Fifteen experiments were conducted in the 21.7 m by 7.1 m by 3.8 m high compartment illustrated in Figure 3-1. Walls and ceiling of the compartment were covered with two layers, each 0.0125 m thick, of marinate boards. The compartment floor was covered with one layer of gypsum board on top of a layer of plywood.

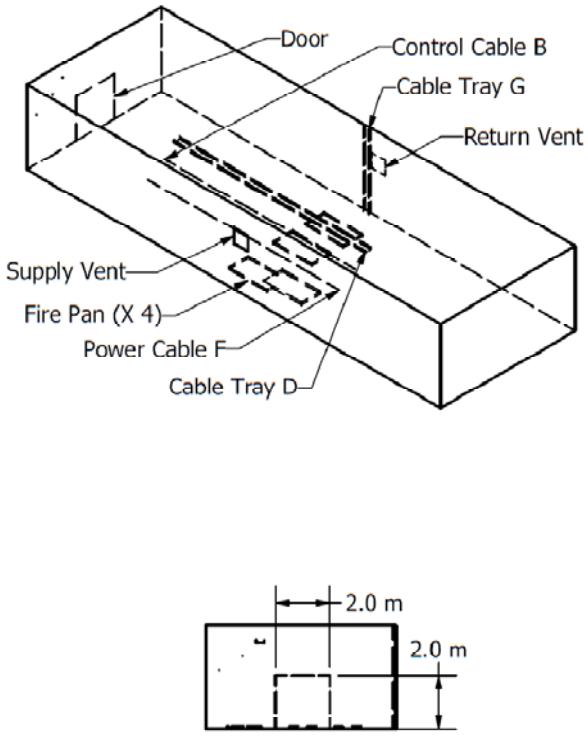

Figure 3-1: Experimental compartment as per [62]

Ventilation to the experimental compartment was provided both naturally, via a door opening measuring 2 m by 2 m, and mechanically through an air injection and extraction system. Ventilation condition was one of the test parameters varied in the study.

For 14 of the 15 tests, liquid heptane was used as the fuel, while toluene was used for the remaining experiment. In all cases, a single nozzle was used to spray liquid fuels onto a 1 m by 2 m fire pan with a depth of 0.1 m. Heat release rates for the tests were determined using oxygen consumption calorimetry. The target heat release rate for all tests was 1000 kW with the exception of Tests 1 and 7 (target 350 kW) and tests 13 and 16 (target 2000 kW). For all tests, the fuel flow was ramped up to achieve the target maximum heat release rates within approximately 3 minutes. A detailed evaluation of the measurement uncertainty in the experimental steady state heat release rate was conducted by the authors for one ventilation condition and was estimated to be 17%.

Seven thermocouple trees were located within the test compartment each consisting of 10 thermocouples spaced 350 mm apart starting 350 mm from the floor and ending 300 mm from the underside of the ceiling. All thermocouples were Type K, constructed of 24 gauge wires. Thermocouple tree #7, located 6 m away from the source fire was selected by the authors as the measurement plane for the FDS validation study. This tree was selected because it was sufficiently far from the fire source that the uncertainty in the experimental measurements caused by radiation heat transfer to the thermocouple beads was expected to be lower at this location. Uncertainty limits for measured hot gas layer temperatures are estimated by the authors for this location and summarized in [79]. The largest uncertainty range for the temperature measurements was estimated to be -7 °C to +17 °C. No velocity measurements were made in this study.

The FDS model was set up to match the parameters of the experimental compartment in all respects [73]. Heat release rates were specified based on the measured values from the experiments. The grid cell dimensions used for this evaluation were approximately 0.18 m by 0.11 m by 0.12 m high for all experiments. Based on the maximum cell dimension (0.18 m) and the maximum heat release rates of the experiments (350 kW, 1000 kW, and 2000 kW) the corresponding values of D^*/δ were 3.6, 5.2 and 7.3, all below the optimal value of 10 suggested in Section 3.1 above. This grid size could potentially impact the predicted temperatures since the fire plume may not be well resolved at this grid resolution, especially in the 350 kW and 1000 kW tests where the ratio of D^*/δ is significantly below 10. An independent grid sensitivity analysis was not published as part of this study.

Closely tied to the heat release rate inputs in an FDS model formulation is specification of the radiation losses. These are calculated through the use of a radiative fraction, generally understood to be the fraction of the total available heat energy that is lost through thermal radiation [61]. In general, a lower value for the radiative fraction will result in higher predicted values of compartment temperature since the fraction of energy lost from the fire plume due to radiation is reduced. Although extremely difficult to determine experimentally, for many combustibles the radiative fraction is thought to be between 0.3 and 0.4, therefore the default

value for this parameter in FDS is 0.35 which is considered appropriate for many sooty hydrocarbon fires [73].

In this FDS validation study, higher radiative fractions of 0.44 and 0.40 were utilized as these were considered more representative of heptane and toluene fires respectively [73]. Estimates for radiative fraction values for well-ventilated fires are provided in Table 3-4.16 in Section 3, Chapter 4 of the 4th edition of the SFPE Handbook [80] as 0.31 and 0.42 for heptane and toluene respectively. Although the values presented in this study may have been appropriate for the specific fuel utilized, this cannot be validated based on the information provided. The selection of radiative fraction could be a potential source of error for the prediction.

The evaluation of ceiling jet temperature predictions was based on comparison of measured and predicted values for temperature at the uppermost thermocouple (300 mm from the ceiling) on tree #7. Figure 3-2 below compares the measured ceiling jet temperature to the FDS predictions for tests 2 and 10, two of the closed door tests taken from [62]. Figure 3-3 provides the ceiling jet comparison for test 3, an open door test. Comparisons for all tests are available in the FDS Validation Guide [73].

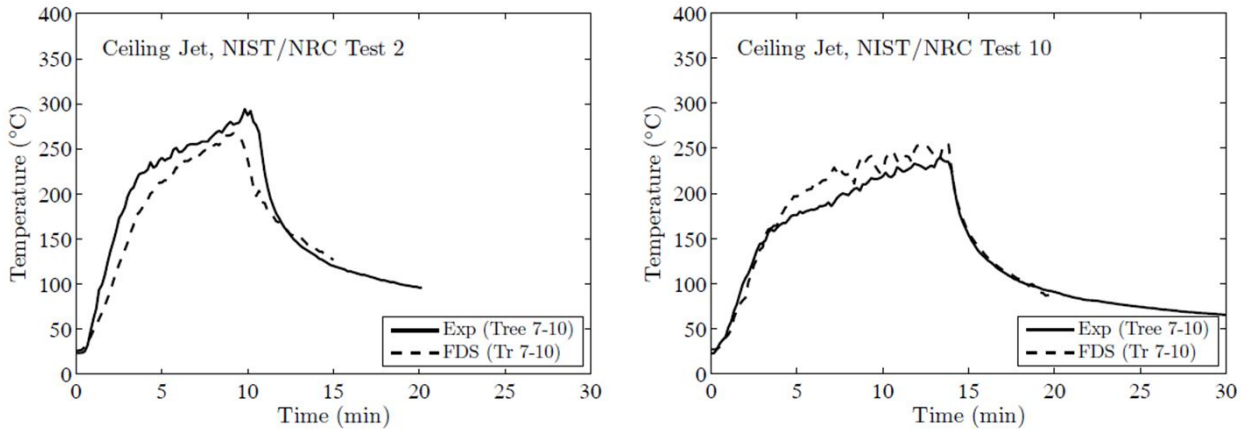

Figure 3-2: Ceiling jet temperature comparison for closed door tests 2 and 10 [73]

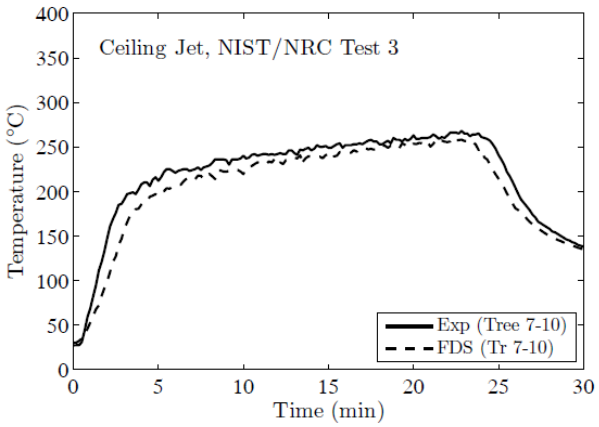

Figure 3-3: Ceiling jet temperature comparison for open door test 3 [73]

The results illustrated in Figures 3-2 and 3-3 were selected as they are representative of the worst case with respect to differences between the experimental data and predicted values for the ceiling jet temperature. All other tests for both the closed and open door ventilation conditions showed equal or better agreement than the results presented above.

It is clear from Figure 3-2 and 3-3 that the FDS predictions provide good general agreement with the trends observed in the experimental results. This would be expected since the input heat release rate used in the model was that obtained experimentally. In general, the accuracy of the model was improved in the open door tests. This result suggests that FDS may provide improved results when modeling situations where the fire is well ventilated, again not an unexpected result, since the behavior of well ventilated fires is generally better predicted [73]. It is noted that for all open door test cases, and using the high value for radiative fraction, the temperature values predicted by FDS were consistently equal to or below the experimental results.

Predicted results for temperatures at the uppermost thermocouple on rake 7 for the selected closed door tests (Figure 3-2) show opposite trends with respect to the measured temperatures of the ceiling jet. For test 2, FDS predictions are consistently below experimental values, with the exception of a portion of time during the decay phase of the fire. In test 10, ceiling jet temperatures are over predicted in the steady state burning region. It is noted that in test 10 the mechanical ventilation system within the compartment was turned on, whereas in test 2 this

system was not running. Therefore, variation in ventilation conditions in the compartment may have contributed to this difference in the results for these tests.

It is important to note that the radiation fraction for this work was changed by the authors from the FDS default value (0.35) to values they thought more representative of the fuels used. By increasing the radiative fraction, the amount of energy lost in the simulation due to radiation was increased which would result in lower temperatures in the compartment. Had this value not been changed by the authors, it can be expected that the simulated temperatures would have been shifted upward which may have improved the result for Tests 2 and 3, but reduced the accuracy of test 10. As is often the case, the impact on the results of the value chosen for radiative fraction was not investigated by the authors.

This study suggests that FDS predictions can provide good agreement with measured values of ceiling jet temperature for confined ceiling jets. Although the ceiling configuration utilized here does not resemble the ceiling recession configurations of interest in the present research, the results indicate that FDS can be employed to model a fire plume and thus predict ceiling jet temperature values in agreement with experiments.

This study also highlights the importance of several input parameters on FDS predictions. The first is the choice of radiative fraction and its impact on predicted upper layer temperature values. The second relates to overall fire ventilation conditions in terms of simulating a particular fire scenario, as demonstrated by the differences noted in the predicted results for the open door (well-ventilated) and closed door (under ventilated) tests. Although a specific discussion of the impact of fire ventilation is not provided by the authors, the results suggest that well ventilated fires are better resolved by the model.

3.2.2 Pope and Bailey Large Scale Post-Flashover Fire Tests

Pope and Bailey utilized FDS version 4 and two other empirical models to simulate eight large-scale post flashover tests conducted at the Building Research Establishment (BRE) test facility as part of the Natural Fire Safety Concept (NFSC) program [75]. Experiments were carried out by Lennon et al. [81] in a 3 m high compartment with a floor area of 12 m^2, using wood and

wood/plastic combinations as the fuel. Values of time dependent compartment temperatures measured under various ventilation and compartment insulation conditions were used as the basis for comparison with the empirical model results and FDS simulations of the same fire scenarios.

Fuel cribs formed from 50 mm by 50 mm by 1 m length softwood members, kiln-dried to 14% moisture content, were used for the fuel load in the experiments. For Tests 3, 5, 7 and 8, 20% (by mass) of the timber members were replaced with polypropylene members of similar dimension to generate fires with higher heat release rates. The fuel load consisted of 49 cribs, spaced evenly throughout the compartment such that the fuel load density for all tests was 40 kg of wood per square meter [81].

Temperatures were measured once per minute at 64 points in the compartment via thermocouples positioned at 16 locations, and 4 heights at each location for the duration of the fire test. No measurements of velocity or thermal detector activation were made in the study. Figure 3-4 provides an illustration of the original test compartment and temperature instrumentation as provided in [75].

Temperature values recorded during 5 of the 8 experiments were used as the basis for the FDS evaluation. Data from Test 1 was not considered since the original experiment was stopped prematurely due to spalling of the pre-cast concrete planks that formed the roof of the test enclosure. Experimental data from Tests 2 and 8 were omitted due to the poor quality of the input data from those experiments.

For the FDS evaluation the compartment dimensions and ventilation openings were modeled to match those in the experimental tests. Compartment boundaries were modeled as thermally thick materials with ambient thermal properties matching the values assumed by Lennon et al [75]. Despite its importance on the results, the value of radiation fraction utilized for the FDS simulations was not provided by the authors.

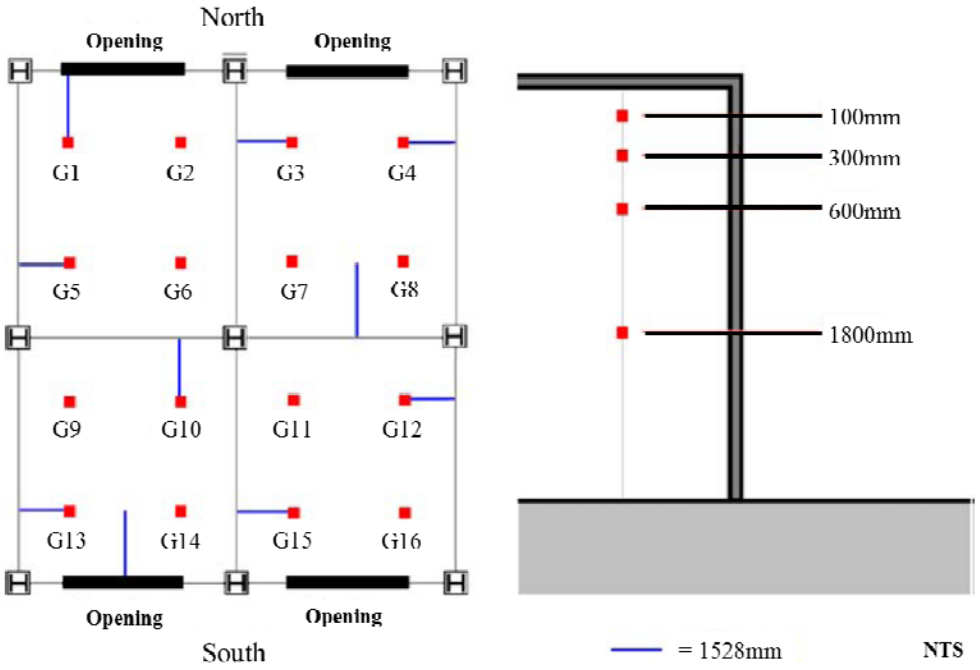

Figure 3-4: Experimental compartment setup for BRE NFSC tests [75]

Final FDS simulations were run for two different grid cell sizes (0.2 m^3 and 0.4 m^3), based on the results of a sensitivity analysis conducted by the authors [75]. These mesh scales were necessary to limit the computational time required to simulate the full domain, for the entire measurement time in the tests (120 min).

The input heat release rate was based on mass loss measurements taken during the experiments, such that the burning rate of the fuel was not predicted by the model. The average fuel load was determined based on averaged data taken from seven fuel packages instrumented for mass loss measurements in the experiment [75]. A six degree polynomial line of best fit was applied to the measured average mass loss rate curve across the experiment time (7200 seconds) and the time differential of the resulting curve taken to formulate a plot of average burning rate of the cribs with time. The burning rate was supplied to FDS with values for the heat of combustion for the fuel. For wood crib fuel packages (Tests 4, and 6), a heat of combustion of 17.5 MJ/kg was used based on the value obtained for the tested wood and published in the original experiment [75]. Mixed fuel packages (Tests 3, 5, and 7) consisted of 80% wood (by mass) and 20% polypropylene plastic and were assigned a heat of combustion based on a weighted average of

the reported calorific values for each material [75]. This weighted average assumption could lead to errors in the FDS input since data was not available regarding the fractions of each fuel burning with time in the experiments; however, the assumption was deemed an acceptable approximation within the limitations of the study by the authors [75].

For all FDS simulations, the source fire was modeled as a simple burner (i.e. the geometry of the crib was not created in the model) with a specified heat release rate. Compartment temperatures were then predicted and spatially averaged throughout the compartment for each increment in time. It was found that FDS consistently under-predicted the average gas temperature in the compartment, by between 11% and 33% in comparison to the experiment, for the 0.4 m^3 mesh for the five experimental data sets considered. Similarly, average compartment temperatures were under-predicted for the 0.2 m^3 mesh cases, by between 3% and 21% from the measured temperatures for the five test cases considered. Interestingly, for both grid sizes, the highest differences correspond to tests that utilized 100% wood cribs as the fuel source (tests 4 and 6). For the 0.2 m^3 grid size, the differences for Tests 4 and 6 were found to be 21% and 16% respectively where measured temperatures were compared to simulated results, whereas temperature differences for the other tests were below 8% from the measured values. Further discussion regarding this discrepancy was not provided by the authors, but the distinct differences in agreement between measured data and FDS predictions for the two fuel sources, points to the impact of the prescribed heat release rate of the fire on the FDS results.

An evaluation of D^* for the FDS models was not provided in [75] but it was noted by the authors that grid independence was not achieved in the plume region. The burning rate data provided [81], can be used in conjunction with the assumed calorific values for the fuel to estimate a maximum heat release based on the assumption of complete combustion. These values were used to estimate D^* for the selected grid sizes for these tests and evaluate the ratio of D^*/δ for each case as summarized in Table 3-1.

Table 3-1: Summary of D*/ δ estimates for Tests 4 and 6

Test #	Approximate Maximum HRR (kW)	D^*/δ	
		0.4 m^3 Grid	0.2 m^3 Grid
3	1004	2.5	5.0
4	875	2.4	4.7
5	1664	3.0	6.1
6	1225	2.7	5.4
7	1230	2.7	5.4
7	1230	2.7	5.4

The values in Table 3-1confirm that the recommended ratio of D^*/δ (10) was not achieved. Within the context of the current research, D^*/δ values exceeding those of the 0.2 m^3 grid size studies should be used in order to mitigate the risk of model error in the analysis of the ceiling recession configurations.

Under-prediction of compartment temperatures was particularly pronounced when predicted values of temperature for individual thermocouples were analyzed instead of the average compartment temperatures. This is expected since values averaged over 64 measurement locations could dampen out significant deviations from experimental data that might occur at any given position within the compartment. This is of particular interest and potential impact in the context of the current research since the performance of individual detectors in various ceiling recession geometries is to be analyzed.

A relevant example of this is highlighted in Figure 3-5 and Figure 3-6 from [75] which illustrate the results of Test 5 for the compartment average temperatures and the temperatures recorded at a single measurement location. In Figure 3-5 and Figure 3-6, the solid line indicates the value measured in the experiment.

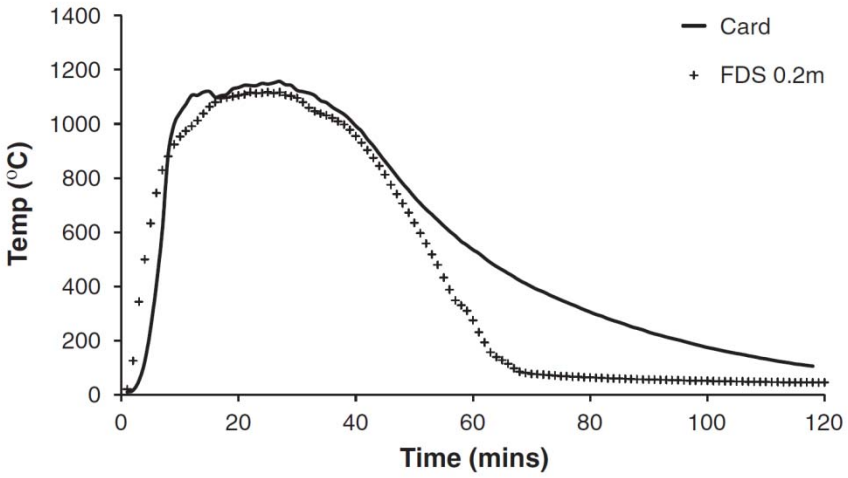

Figure 3-5: Test 5 average compartment temperatures [75]

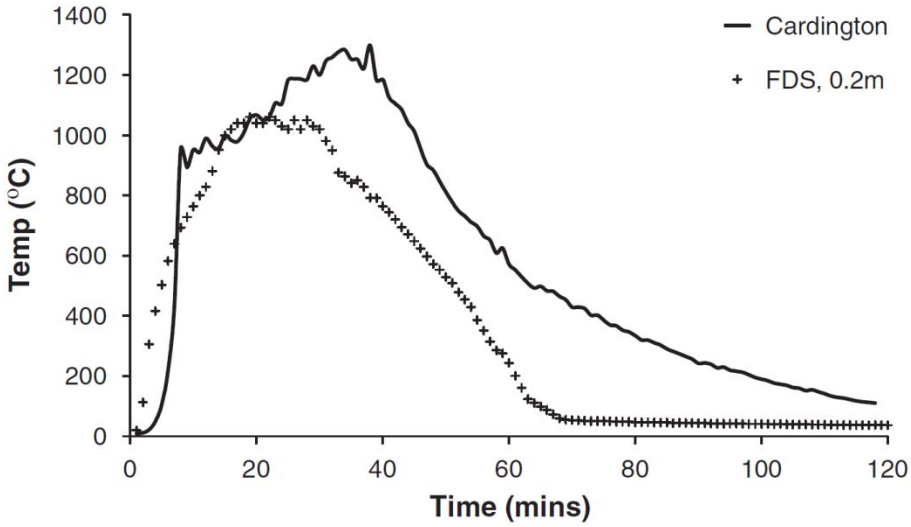

Figure 3-6: Test 5 temperatures at position G2, 1800 mm [75]

Although there are clear deviations between measured and predicted values of temperature with time in Figure 3-5, sole use of the information contained in Figure 3-5 would tend to support the use of FDS to predict compartment temperatures during the growth phase of the fire for the scenario under consideration since the curves are well fit. However, examination of Figure 3-6 shows that great care must be taken in drawing this type of conclusion for a single measurement location since there were clearly significant deviations between measured and predicted values at position G2 in the tests. Most notable in Figure 3-6 is the significant difference in the magnitude and position (with respect to time) of peak temperature at measurement location G2.

On the other hand, it is encouraging to note that even where the temperature values predicted using FDS differ substantially from the experimental values for a selected measurement location, overall trends in measured temperature with time are followed. This suggests that elements of the compartment flow, such as the movement of hot gases away from the fire plume, are still reasonably well represented in the modeled results.

3.2.3 Work by Smardz

In 2006, Smardz compared temperature and velocity values predicted using FDS Version 4.07 to experiments conducted in a 1/3 scale ISO room model equipped with a balcony and smoke reservoir [76]. FDS predictions were compared to a series of six experiments conducted using two different fuel sources. The objective of this work was to evaluate the use of FDS for simulation of the conditions within the main enclosure, and within the generated balcony spill plume, for different strengths of fire. The impacts of various model inputs, such as grid size, were also investigated.

The scaled experimental compartment, shown in cross section in Figure 3-7 from [76], measured 1.2 m by 1.2 m by 0.82 m high. Ventilation was provided through an opening 270 mm wide, with an adjustable height between 500 mm and 550 mm, located on one wall of the enclosure. A 350 mm deep balcony attachment was located outside of the compartment for four of the six experiments.

Six insulated 1.5 mm type-K thermocouples, spaced 120 mm apart vertically and with the uppermost at 120 mm below the compartment ceiling, were placed in one corner of the room, 120 mm from adjacent walls and used to measure compartment temperatures.

The velocity of hot gases exiting the compartment through the opening was measured via one bi-directional velocity probe located at the upper boundary of the opening, 120 mm outside of the compartment. The probe had been calibrated crudely, so velocity values were subject to an error of approximately ±20%.

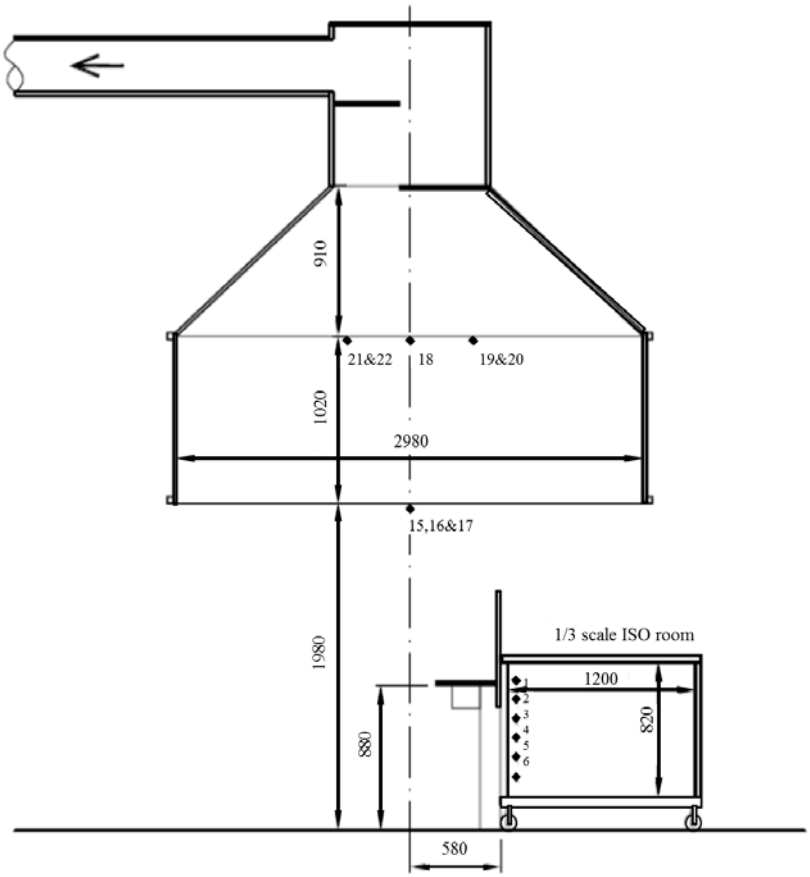

Figure 3-7: Experimental compartment setup as per [76]

Two fuel sources were considered. Experiments 1-4 were conducted using diesel oil, while experiments 5-6 used ethanol. Heat release rate curves were generated by oxygen consumption calorimetry for each experiment. The maximum heat release rates for experiments 1-4 ranged from 61 kW to 86 kW, and 40 kW to 49 kW for experiments 5-6.

Experiments 2 and 5 were selected from the experimental results for comparison to FDS. Experiment 2 involved a diesel oil fire with a maximum heat release rate of 86 kW and included the balcony attachment at the opening to the compartment. Experiment 5 was a 49 kW ethanol pool fire with no balcony attachment at the compartment opening.

FDS models were run using various grid sizes in order to determine the impact of grid volume size on the model results.

For the compartment temperature and velocity studies, the heat release rate of the source fire was supplied to the model based on the experimental measurements.

Material properties were supplied to the model to match the thermal properties of the experimental enclosure.

Examination of the FDS input code for this work indicates that the FDS default value for the radiative fraction (0.35) was applied for the analysis.

Experimental and simulated compartment temperature results were compared using the average temperature rise of the upper layer, which was defined by the author as the average value of temperature measured by the three uppermost thermocouples within the compartment. The basis of the comparison was an evaluation of prediction error determined in relation to the measured values as follows:

$$\left|Prediction\ Err = \frac{FDS\ Value - Exp\ Value}{Exp\ Value} * 100\%\right| \quad [3\text{-}3]$$

In general, FDS tended to over-predict average upper layer compartment temperatures except in the decay phase of the fire, where FDS predications fell below the measured values. The accuracy of predicted average temperature for the model simulation was found to be heavily dependent on the grid size selected. Table 3-2 below summarizes the maximum calculated prediction error for upper layer compartment temperature for each experiment and two grid sizes [76].

Table 3-2: Summary of grid size and prediction error for average compartment temperature

	Experiment 2		Experiment 5	
Max. Grid cell dimension (m)	0.08	0.04	0.08	0.04
Max. HRR (kW)	86		49	
D^*/δ	4.5	9	3.6	7.3
Prediction Error	41%	14%	51%	50%

It is clear from the results of Table 3-2 that a significant improvement in model accuracy, from 41% prediction error down to 14%, was realized with the reduction in the grid size for Experiment 2. However, this same improvement was not observed for Experiment 5, which showed no significant improvement in accuracy. Smardz hypothesizes that this may be due to insufficient grid resolution for this scenario, and that an increase in the ratio of D^*/δ may have provided an improved result.

Interestingly, compartment temperatures were over predicted for both experiments in the work by Smardz. This is the opposite trend to that found by Pope and Bailey in their work, where FDS consistently under predicted compartment temperatures. It is important to note, however, that the experimental compartments for these experiments were significantly different particularly in size, the number of measurement locations, and source fire heat release rate. Therefore, a direct comparison of these results is not possible. There are also many potential areas within FDS for the cause of this discrepancy; examples include the selected radiation fraction, grid size, and the resolution of radiation heat transfer from compartment boundaries, all of which would significantly influence the predicted results. It is also possible that this trend reversal was caused by the different parameter of interest in each study. In Pope and Bailey [75] the average compartment temperature was used for the comparison, which included temperature predictions throughout the compartment. Since the study by Smardz [76] considered only the average upper layer temperature (i.e. temperature measurements from the lower portions of the compartment were not included in the average). It is also possible that FDS over predicted the

near ceiling temperatures in the Pope and Bailey study, but this was damped out when results were averaged throughout the compartment. It is also noted that, the height of the FDS compartment studied by Smardz was 20 mm less than the height of the experimental compartment. This would tend to cause an over prediction of temperature by FDS.

Flow velocities within the compartment were not compared in detail by Smardz [76], but it was noted that FDS predictions of velocity exhibited significant deviations from experimental values. Since it was not clear to what extent this error was due to the predictive capability of FDS versus poor calibration of the bi-directional probes in the experiment, or to differences between the actual and modeled positions of the probes, an evaluation of the percent error for velocity was not provided.

Overall the work by Smardz [76] reinforces the importance of grid size selection for model accuracy in the prediction of compartment temperatures, as was previously discussed in other validation studies [73, 75]. Additionally, Smardz's work highlights the impact that variations in compartment configurations (fuel type, dimensional differences, etc.) can have on model accuracy, as evidenced by the significant prediction error that was observed in the FDS study of experiment #5.

3.2.4 Summary of Results

The results of three FDS validation studies focusing on compartment temperature and velocity were reviewed for application to the analysis of the ceiling recession configuration of primary interest here.

The studies by NIST [73], Pope and Bailey [75], and Smardz [76] all highlight the importance of the ratio of D^*/δ when evaluating temperatures within a fire compartment.

The studies also indicate that a constant FDS model bias with respect to predicted compartment temperatures cannot be assumed; instead, the accuracy of the FDS predictions is highly dependent on the details of the compartment, the simulation grid size, the fuel type, and the model inputs such as radiation fraction.

The importance of ventilation conditions within the fire compartment were also highlighted, specifically in the work by NIST [73] where it was shown that the model provides increased accuracy for compartment temperatures where the fire is well ventilated.

Validation work focusing on compartment velocities is limited due in part to the difficulty in accurately measuring this parameter in experimental fire tests, as evidenced in the work by Smardz [76].

3.3 Previous FDS Validation Work - Flow Characterization at Obstructions

As discussed in Section 2.1.4 and 2.2.3, the movement of hot layer gases at the spill edge forming a balcony spill plume may exhibit similar characteristics to the ceiling jet flow expected in the ceiling recession configurations of interest in this work. Of particular interest is the ability of FDS to characterize the flow of hot layer gases at the spill edge of the recession and at other obstructions such as draft stops. Therefore, previous FDS validation studies for balcony spill plumes which compare the model predictions for velocity and temperature at the spill edge and at ceiling level obstructions are reviewed in this section.

3.3.1 Harrison Spill Plume Study

Harrison utilized FDS version 3.0 to investigate factors affecting air entrainment into balcony spill plumes [33]. Results of the model were compared to experimental results obtained from testing conducted on a 1/10 scale model of the selected scenario.

The experimental compartment, illustrated in Figure 3-8 from [33], was 1 m by 1 m by 0.5 m high and contained a variable size (both in height and width) opening centered on one compartment wall. Compartment walls were constructed of 20 mm thick Kaowool ceramic fibre insulation (CFI) boards attached to a steel frame. The CFI boards were covered at the compartment exterior with a 2 mm thick steel substrate to protect the compartment from mechanical damage.

A balcony obstruction was placed outside of the compartment at the opening and channeling screens were attached to the balcony in order to prevent hot gases from dispersing laterally at the compartment opening. The balcony and channeling screens were constructed of 10 mm thick CFI board. The entire test compartment was located below an exhaust hood simulating the upper ceiling level of an atrium.

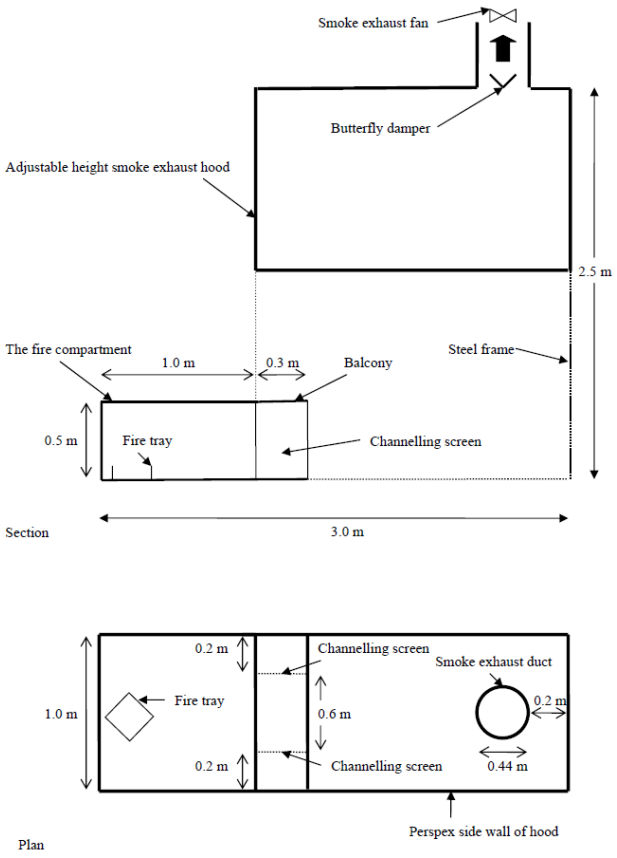

Figure 3-8: Example of experimental test setup for Harrison spill plume study [33]

The fire source was a denatured ethanol (IMS) designed to provide a heat release rate of approximately 10 kW. Fuel was continually fed into the fire tray within the compartment via a fuel reservoir and flow meter controlled by a needle valve. To maintain a constant fuel flow rate, the reservoir was equipped with a constant pressure head device. The fuel tray measured 0.25 m by 0.25 m by 0.015 m high. The heat release rate of the fire was calculated for the experiments based on the measured fuel flow rate and the heat of combustion of the fuel. A commercial smoke generator was used to inject visible smoke into the fire compartment in order to observe

flow characteristics. Ventilation conditions were altered by modifying the width of the opening to the compartment and the depth of the "down stand" which was located 0.3 m upstream of the spill edge. It is noted that the down stand consisted of a variable height obstruction mounted at the ceiling level, similar to a typical draft stop.

Although the focus of Harrison's work was on the use of FDS to model the mass flow rate of air entrainment into the balcony spill plume, of particular interest to the current research are the temperature and velocity profiles at the spill edge that were evaluated as part of the study.

Gas temperatures were measured below the spill edge using a thermocouple tree, consisting of 18 - 0.5 mm diameter chromel/alumel (K-Type) thermocouples, centrally located directly below the spill edge. Thermocouples were located with 20 mm vertical spacing between 10 mm and 250 mm below the ceiling level. From 250 mm to 500 mm below the ceiling, thermocouples were spaced at 50 mm intervals.

Gas velocities were measured at 10 mm intervals below the spill edge using a pitot-static tube and a thermocouple at each measurement location. Gas velocities were calculated from the measured pressure differential and temperature based on the following:

$$U = \sqrt{\frac{2\Delta PT}{\rho_1 T_1}} \qquad [3\text{-}4]$$

Model predictions of temperature and velocity profiles at the spill edge were compared to experimental results.

The FDS model was set up to match the parameters of the experimental tests as well as configurations of the compartment which were not considered experimentally. Compartment walls, channeling screens, and the balcony were assigned physical and thermal properties based on the reported values for the materials utilized in the experimental compartment. It is noted however that the 2 mm thick steel substrate surrounding the exterior of the compartment walls was not included in the simulations.

The fuel source was modeled as a 0.17 m by 0.17 m by 0.015 m high fuel tray set to provide a steady state heat release rate in agreement with the experimental tests. Details regarding the method used to ramp up the heat release rate within the simulation were not provided by the authors; however, since the results of interest are reported based on steady state conditions the fire ramp up time will not impact the results.

A total of 25 simulations were conducted as part of Harrison's work which evaluated the impact of changes to the opening size (height and width), down stand depth, and balcony breadth on the predicted rate of air entrainment. Of the 25 simulated configurations, 4 were tested experimentally. Table 3-3 below summarizes the compartment parameters of the simulated configurations which were also tested experimentally.

Table 3-3: Summary of simulated compartment parameters compared to experiments

Simulation #	Down Stand Depth (m)	Opening Height (m)	Opening Width (m)	Balcony Breadth (m)
1	0.10	0.40	1.0	0.3
4	0.10	0.40	0.4	0.3
5	0.10	0.40	0.2	0.3
9	0.20	0.30	1.0	0.3

For each of the simulations noted above, the steady state heat release rate for the corresponding experiment was 10.30 kW.

A grid sensitivity analysis was conducted by the author by systematically reducing the selected cell size and comparing the result. Details regarding this analysis are not provided; however, it resulted in selection of a grid size of 20 mm in each direction for all simulations such that the ratio of D^*/δ for all simulations was 8.0. The radiation fraction utilized for the simulations was not provided by Harrison.

Figure 3-9 and Figure 3-10 compare the simulated temperature profile to the experimental results for two selected compartment configurations as provided in [33].

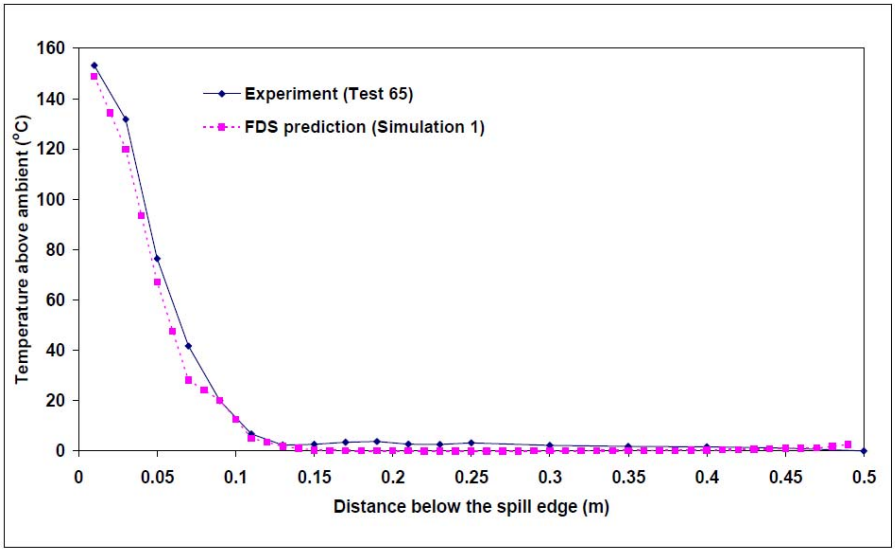

Figure 3-9: Comparison of temperature at the spill edge for simulation 1 [33]

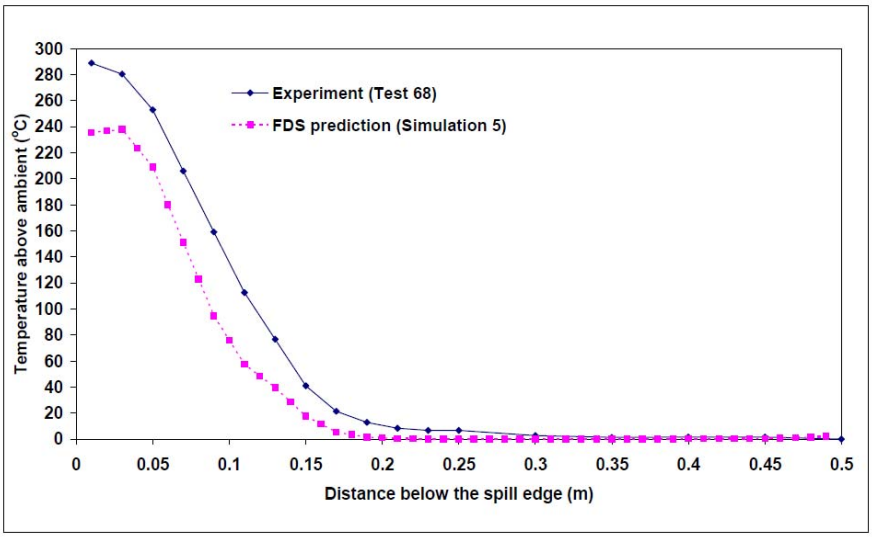

Figure 3-10: Comparison of temperature at the spill edge for simulation 5 [33]

Good agreement is observed between the experimental temperature values and the values predicted by FDS for simulation 1 in Figure 3-9. However, the accuracy of the model decreases

for simulation 5 indicated by a consistent under prediction of the temperature shown in Figure 3-10.

Harrison indicates that the discrepancy in predicted and measured results may be due to increased model error caused by heat loss to compartment boundaries [33]. Since the steel substrate which covered the exterior of the walls in the experimental compartment was not modeled in the FDS simulation, the rate of heat loss to the compartment boundaries in the model may have been higher than that in the experiments. Although this would impact all simulated values, it may be more pronounced in results from simulation 5 since this scenario involved a reduced compartment opening (0.2 m wide vs. 1.0 m wide in simulation 1) which causes an overall increase in compartment temperatures for this simulation.

Although this under prediction was attributed to the simulation of the compartment boundaries in [33], there are many other factors which could also play a role. The size of the ventilation opening in the compartment was reduced for experiment 5 which may have caused the source fire to be under ventilated. As was previously discussed in the work by in the work by NIST [73] under ventilated fires are, in general, subject to a greater degree of prediction error in FDS.

The radiation fraction applied to the analysis is another potential source of error for this study. As was previously noted, the radiation fraction applied to this study was not specified by the Harrison [33]. However, the fuel used for the experiment was denatured ethanol, which has an approximate radiative fraction of 12% [80]. Therefore, if the default value in FDS (0.35) was applied to the analysis the predicted values can be expected to be less than those measured in the experiment since the simulation would specify that a higher percentage of the overall heat energy of the fire was lost to radiation.

Figure 3-11 and Figure 3-12 compare experimental and predicted values for gas velocity below the spill edge as provided in [33].

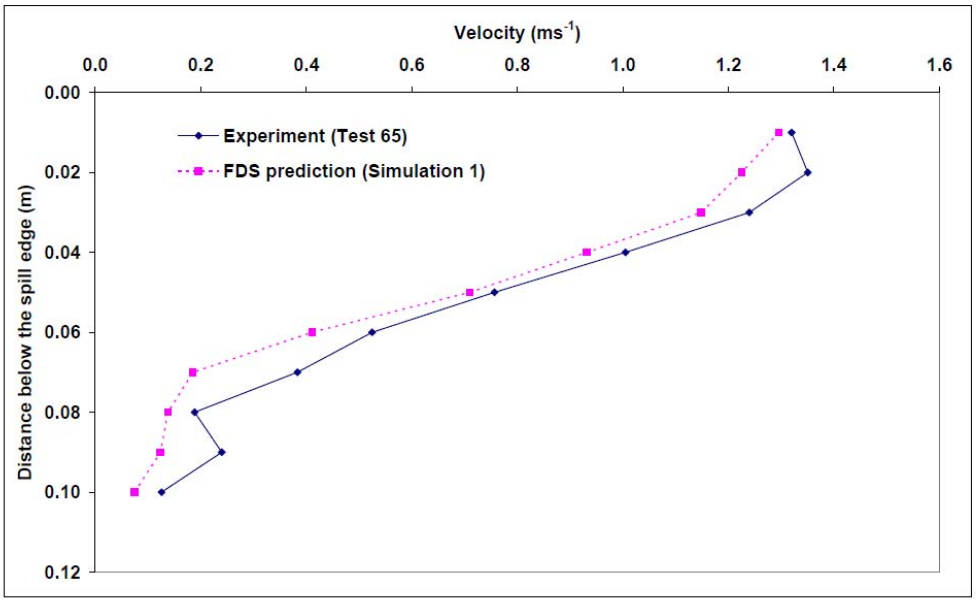

Figure 3-11: Comparison of velocity at the spill edge for simulation 1 [33]

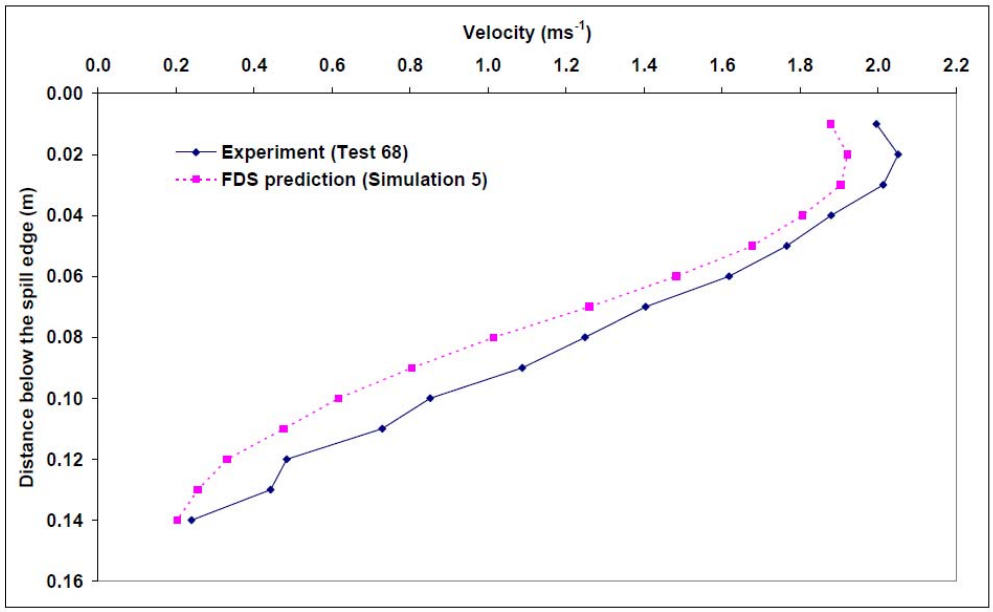

Figure 3-12: Comparison of velocity at the spill edge for simulation 5 [33]

In general the velocity profiles at the spill edge were in good agreement with the experimental results with FDS slightly under predicting the velocity in comparison to the experiment. Similar to the situation for temperature profiles, the difference between experimental and simulated

values is increased in simulation 5 in comparison to the results of simulation 1. Harrison attributes this difference to the increased heat loss to the compartment boundaries in the simulation, which would result in a higher rate of thermal decay in the ceiling jet leading to a lower ceiling jet velocity [33].

Within the scope of the current research, the results of this study highlight two important characteristics of FDS with respect to its use in the evaluation of ceiling recession configurations.

First, the values predicted by FDS for temperature and velocity at various heights below the spill edge were found to be in good general agreement with the experimental data. This trend held true for various compartment configurations which included the flow of hot gases over a down stand, a compartment feature identical to a draft stop (but with a smaller depth). This result suggests that FDS is capable of predicting the flow characteristics of the hot gases where the gases encounter obstructions. Although this study did not include a ceiling recession as part of the compartment geometry, it is encouraging that predicted results were comparable to experimentally measured values when flow over the down stand was considered.

Second, this study involved the comparison of simulated results for various compartment configurations, where the parameters of the opening size, balcony size, and downstand depth were modified. These dimensional changes are of the same order of magnitude (hundreds of millimeters) as the dimensional differences proposed in the configurations of interest in this research. In this context, the results of this study indicate that the impact of these types of dimensional changes will be resolved by FDS and that the impact of the changes in velocity and temperature profiles as a result of such geometric changes can therefore be studied. This result further supports the use of FDS for the evaluation of ceiling recession configurations.

3.4 Previous FDS Validation Work - Thermal Detector Activation

3.4.1 UL/NFPRF Sprinkler, Vent, and Draft Curtain Study

A series of 34 heptane spray burner experiments conducted in 1997 at Underwriters Laboratories was modeled using FDS to predict the activation time, and number of activated thermal detectors, located within a ceiling jet [82]. The goal of the study was to assess the ability of FDS to predict the thermal detector response time and the number of thermal detectors actuated within the compartment for comparison with results of the experiment. This study is included in the current edition of the FDS Validation Guide [62], so although the original modeling, conducted with Industrial Fire Simulator (IFS) and the experiments were conducted some time ago, the results of the simulations can be considered applicable to the current version of FDS.

Velocities in the ceiling jet were not specifically measured as a part of this study.

The compartment consisted of a 37 m by 37 m space equipped with a 30.5 m by 30.5 m adjustable height ceiling which was set at 7.6 m above the ground for the experiments. The ceiling was constructed of UL fire-rated Armstrong Ceramaguard (Item 602B) ceiling tiles with thermal properties reported by the manufacturer [62].The experiments were categorized into two test series based on heat release rate. Series I consisted of 22 experiments with a source fire heat release rate of 4.4 MW; Series II consisted of 12 experiments with a 10 MW fire source.

For all but one of the Series I tests, the source fire was ramped up to the maximum heat release rate of 4.4 MW following a t-squared growth curve set to reach steady-state in 75 seconds. For one of the tests (Test I-16) the growth curve was such that steady-state was achieved in 150 seconds. For the Series II tests, the fire was ramped up to 10 MW in 75 seconds, also following the t-squared growth profile. In all tests, the specified growth curve was followed until the maximum heat release rate was achieved or until the first sprinkler activated. Once either of these events occurred, the heat release rate of the fire at that point in time was maintained for the remainder of the test.

Source fires were evaluated at six selected locations within the compartment, labeled positions A through F, as identified in Figure 3-13 which provides a schematic of the test compartment for test series II as provided by [82]. The distance between the centerline of the fire plume and the nearest detector varied for different burner positions, but at no point was the burner located directly below a sprinkler head.

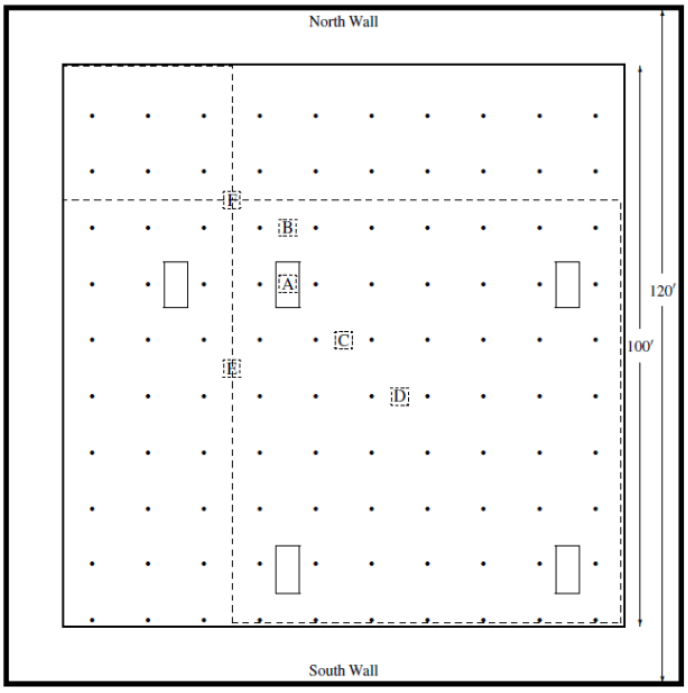

Figure 3-13: UL/NFPRF test compartment - test series II [82]

For 16 of the 22 Series I tests and all of the Series II tests, 1.2 mm thick and 1.8 m deep sheet metal draft curtains (draft stops) were suspended from the ceiling to enclose an area of approximately 450 m^2. For other tests the draft curtains were removed to evaluate the impact of these obstructions on sprinkler response time and the number of actuations within the compartment.

The underside of the ceiling was equipped with Central ELO-231 (Extra Large Orifice) upright sprinkler heads on 3 m spacing forming a grid consisting of 49 sprinkler heads. The sprinklers were noted to have an activation temperature of 74°C and an RTI value of 148 $(m*s)^{1/2}$. All sprinklers were positioned 0.08 m below the ceiling.

UL listed, double leaf, fire vents with steel covers were installed in the adjustable height ceiling of the compartment and recessed approximately 0.3 m into the ceiling. The vents were designed to open manually or automatically via a fusible link.

Although no values of uncertainty were reported with regard to the total number of actuated sprinklers, replicate experimental tests conducted for three Series I tests indicate that the experimental results are repeatable with respect to the number of sprinkler head activations, although individual activation times were found to vary.

The FDS computational domain was set up to match the dimensional parameters of the experimental test facility. The compartment ceiling was modeled as a thermally thick obstruction with thermal properties matching those of the ceiling material used in the experiments. The floor of the compartment was assumed to be adiabatic for the simulation.

The source fire was modeled as a heptane spray burner consisting of a 1 m by 1 m square located 0.6 m off the floor and positioned in agreement with the experimental tests. The heat release rate of the fire was ramped up following the curves specified for the experiments and to then maintain steady state conditions upon the activation of the first sprinkler head, or else to achieve the specified maximum heat release rate. Information regarding the radiative fraction used in the simulation was not provided.

The computational domain for all tests was modeled using a grid size of 0.3 m by 0.3 m in width with the vertical dimensions of the cells varying from 0.15 m near the ceiling to 0.3 m in the lower regions of the compartment. Based on this, the ratio of D^*/δ (assuming δ is equal to the largest grid dimension of 0.3 m) was 4.5 for the 4,400 kW case, and 6.2 for the 10,000 kW case. The purpose of varying the vertical dimension of the cells was to cluster more cells near the ceiling to determine if this would provide better predictions of thermal detector actuation and therefore improved agreement with the experimental data. It was noted by the authors that calculations performed with the denser grids did not significantly alter the results of the model.

Figure 3-14 provides a comparison of the predicted and measured sprinkler activations as provided in [62]:

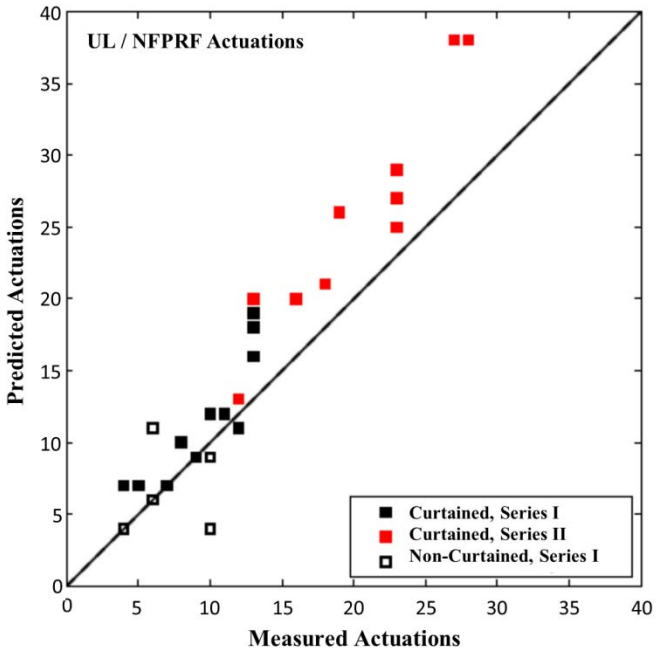

Figure 3-14: Comparison of predicted and actual sprinkler activations [62]

From the results of this study, two trends relevant to the current research are noted. First, the model tended to over predict the number of actuations occurring within the compartment, as indicated by a majority of data points being located above the match line. This suggests that the model was over predicting temperature and/or velocity values within the ceiling jet, resulting in the prediction of more sprinkler actuations than observed.

Second, the accuracy of the model with respect to the number of predicted actuations does not appear to be significantly affected by the presence of draft curtains at the ceiling level. Indicated by the open squares in Figure 3-14, the non-curtained simulations show a similar degree of divergence from the actual value in comparison to the results for the curtained scenarios. This suggests that the presence of an obstruction to the ceiling jet flow, causing the formation of a confined ceiling jet and hot gas layer, does not significantly impact the accuracy of the model in simulating thermal detector actuations. This result is of significant importance to the current

research since both classifications of ceiling jet flow (i.e. confined and unconfined ceiling jets) are expected to be found in the analysis of various ceiling recession configurations.

Unfortunately, results of this study, as discussed in the FDS Validation Guide, provides an assessment only of model accuracy based on the total number of actuations observed, and does not address the predicted response time of the sprinklers in comparison to the experimental values, a parameter which is of critical importance to the current research since the impact of the selected ceiling configurations on the detector response time were used as a measure of performance for the alternative designs.

Review of the original report by McGrattan et, al., which is based on the results produced by the original IFS simulations, provides a more detailed assessment of model accuracy with respect to sprinkler response times for the Series I tests. These are outlined below, although since they are not discussed in the current FDS Validation Guide, their applicability to the current version of FDS cannot be assessed. McGrattan et. al. noted that sprinkler activation times within the first ring (i.e. closest set of sprinklers to the fire) were predicted by IFS within approximately 15% of the experimental values, and 25% for the second ring [62]. Based on a visual review of the graphs provided in Appendix A of [62], these values appear to represent the maximum divergence between the predicted and experimental activation times at each sprinkler location.

Near-ceiling gas temperatures measured 0.08 m below the ceiling were predicted to within approximately 15% of the experimental values up to the point of sprinkler activation. As noted by the authors, predicted values were not expected to agree with experiment upon activation of the sprinklers since discharged water would wet the thermocouple leads and impact the measurement. In contrast, thermocouples in the simulation would continue to measure gas temperature since thermocouples are not modeled as physical obstructions within the domain.

This study suggests that FDS has the capability to address thermal detector response for both the confined and unconfined ceiling jet for various source fire heat release rates.

Further, validation studies discussed previously regarding the ability of the model to predict ceiling jet temperatures, a key parameter in determining thermal detector response times, note that good agreement with experimental values can be anticipated. This suggests that the error values noted for the original IFS study might be applicable to the current model although little validation work has been done in relation to predicted velocities which will also be a key parameter in determining thermal detector response characteristics.

Finally, this study further highlights the importance of input variable selection and sensitivity analysis for critical parameters in FDS, especially where model results are to be used for assessment of situations in which there is limited experimental data from which comparisons and evaluations of the prediction accuracy can be made.

3.4.2 Work by Hurley and Munguia

FDS version 4.0.6 was used to evaluate gas temperatures in the fire plume and ceiling jet, and thermal detector response under exposure to a heptane spray fire under a flat unobstructed ceiling [77].

The results of the model were compared to data from a series of full-scale tests conducted in a 36.6 m by 36.6 m enclosure under six selected ceiling heights ranging from 3.0 m to 12.2 m. The ceiling was constructed of 0.6 m by 1.2 m by 16 mm thick UL fire rated ceiling tiles. Of particular interest to the current research are the results of this study for the H=3.0 m and H=4.6 m cases which represent ceiling heights where open stairs requiring draft stop protection are common in buildings.

The heptane spray burner was located under the centre of the variable height ceiling and elevated 0.6 m above the floor of the compartment. The heat release rate of the test was controlled manually by altering the heptane flow rate in order to produce a ‘medium’ t-squared growth curve. For the 3.0 m and 4.6 m ceiling height tests fire growth was stopped when heat release rates of 1055 kW and 2100 kW were reached respectively. For other tests the heptane flow rate was increased throughout the duration of the test.

Instrumentation in the compartment consisted of thermocouple arrays located 100 mm below the ceiling level at radial distances from the fire plume centerline of 0.0 m, 2.2 m, 6.5 m, and 10.8 m, selected to represent a common sprinkler spacing arrangement. Each array consisted of four thermocouples, a type K inconel sheathed thermocouple and three thermocouples soldered to a 25 mm brass disk to simulate a heat detector. The disks were 25.4 mm in diameter and had thicknesses of 0.41 mm, 3.18 mm, and 6.54 mm. These disks were determined to have RTI values of 32, 164, and 287 $m*s^{1/2}$ when tested in accordance with UL 1767. Temperature data were recorded from each thermocouple at 1 second intervals throughout the test.

A detailed experimental uncertainty analysis, provided by the author, identifies and evaluates three primary sources of uncertainty: (1) thermocouple temperature measurements (±2.2°C based on manufactures data), (2) fuel flow measurements (±20 kW based on the uncertainty of the flow meter measurements converted to a corresponding heat release rate), and (3) repeatability uncertainty (estimated by calculating the standard deviation of temperatures measured in replicate tests). These uncertainties were combined using the root-sum-of squares technique for the purposes of comparison to predicted values.

A portion of the experimental geometry was created in FDS based on the dimensions of the enclosure used in the tests. The full experimental domain was not modeled in order to reduce the required model run time. This was justified based on the size of the test facility in comparison to the fire size with the conclusion that a large volume of the space would neither influence, nor be influenced by the fire. A multi-mesh approach was utilized to construct the computational domain. One mesh consisting of a 10 m by 10 m space with a ceiling height equal to the experimental tests was defined and centered about the fire source. Adjacent to this, a second mesh was defined to simulate the ceiling jet area were the detectors were located. This mesh consisted of a 10 m by 10 m space with the vertical dimension of the mesh limited to 50% of the total height of the ceiling measured from the ceiling level down. For both meshes the grid size selected was approximately 0.1 m^3. A grid sensitivity analysis in which the cell size was reduced to 0.066 m^3 in both meshes was conducted. It was concluded that grid independence was achieved for the selected cases in the ceiling jet region (i.e. at the radial distances of 2.2 m,

6.5 m, and 10.8 m) but not in the plume centerline region and limited discussion was therefore provided regarding the plume centerline temperature values.

For the 3.0 m and 4.6 m ceiling height cases the maximum heat release rate values (1055 kW and 2100 kW) and the selected grid size (0.1 m^3) correspond to D^*/δ values of 10.2 and 13.4 respectively. It should be noted that based on the selected grid size for this study, the recommended value for D^*/δ is exceeded which, in theory, would improve the accuracy of the simulation.

The floor of the computational domain was modeled as an inert surface. Thermal properties of the ceiling in the model were based on reported values for the UL fire rated ceiling tiles utilized in the experiment. Open boundary conditions were applied to the domain boundaries to permit fire gases to escape the domain in order to simulate the movement of gases at the edge of the lowered ceiling in the experiment.

The fire was modeled as a 1 m by 1 m by 0.6 m burner with the top surface assigned surface properties corresponding to the heat release rate of the experimental burner. A ramp function was used to provide a fire growth profile matching that of the experiment. The combustion reaction for the simulation was set to 'heptane' based on database values which were provided with FDS version 4 (note that these values are no longer provided by the developers). The radiative fraction for the model was set to the FDS default value of 0.35.

Thermocouples and heat detectors were located within the computational domain at locations matching those in the experimental setup (i.e. at radial distance as specified located 100 mm below the ceiling). Heat detectors were assigned an activation temperature of 1000°C in order to ensure a complete record of temperature values were provided by FDS. All other parameters for the thermocouples and heat detectors were set to the FDS default values.

As previously noted, the performance of FDS with respect to ceiling jet temperatures and detector activation for the 3.0 m and 4.6 m ceiling height cases are of particular interest to the current research. At a ceiling height of 3.0 m FDS predictions of the gas and detector

temperatures outside of the plume centerline were consistently higher than the measured values as illustrated in Figure 3-15 as provided in [77].

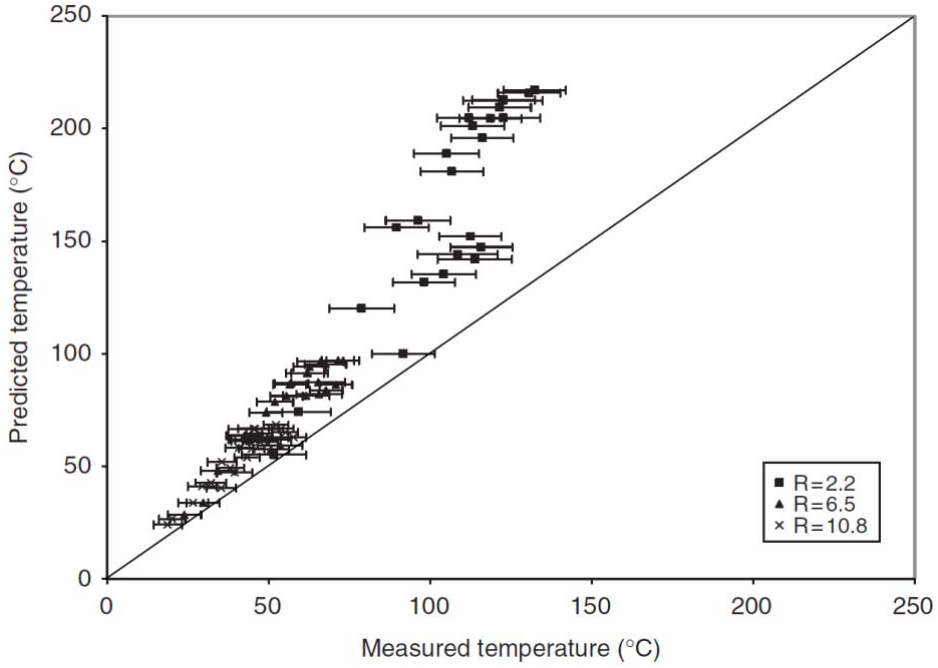

Figure 3-15: Comparison of predicted and measured temperatures for H=3.0 [77]

This over prediction is most prevalent at the r=2.2 m measurement location which suggests that this location is more greatly affected by the selected grid size than locations further from the centerline. At radial measurement locations of 6.5 and 10.8 m the predicted temperature more closely resembles the experimental data but for the most part are still not within the bounds of experimental uncertainty reported by the author.

For an enclosure ceiling height of 4.6 m, predicted temperature values for both the ceiling jet and the thermal detector temperatures are illustrated in Figure 3-16 as provided in [77].

For this ceiling height, the consistent over-prediction of temperature values observed in the 3.0 m ceiling height case is not present, and temperatures are actually under-predicted for some measurement locations. In general, the predicted values for this scenario were within the range of uncertainty determined by the author for measurement locations outside of the plume region.

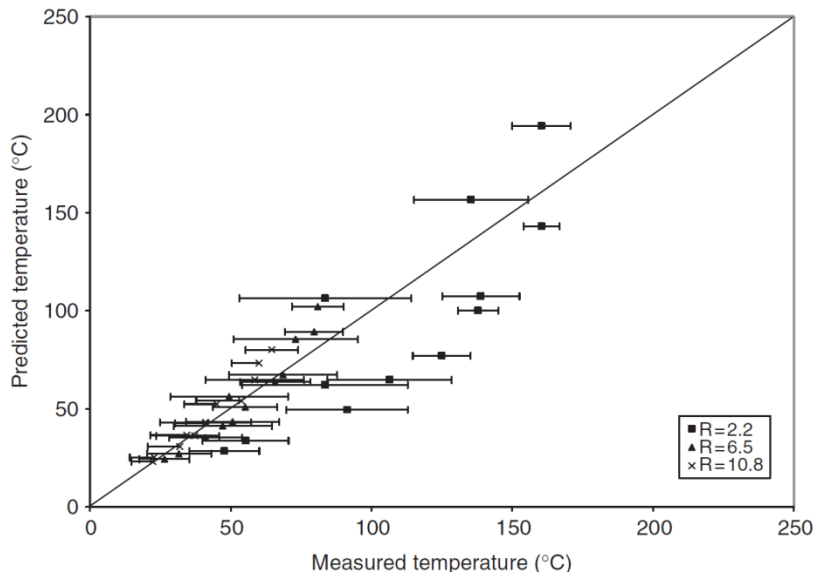

Figure 3-16: Comparison of predicted and measured temperatures for H=4.6 [77]

Overall the study found that outside of the plume centerline, predictions of ceiling jet temperature increase and thermal detector temperature rise were within a factor of 1.9 (including all studied scenarios collectively) of the experimentally measured values.

Within the context of the current research for vertical floor opening protection using a ceiling recession, this study indicates that FDS has the ability to provide reasonable predictions of temperature near the ceiling (in this case 100 mm from the ceiling) for compartment heights and measurement locations similar to those of interest in this thesis. Additionally, of interest from these results is the method utilized for the representation of the computational domain, where only a portion of the domain is modeled with open vent conditions applied to the vertical boundaries. The results indicate that utilizing this method does not appear to significantly impact temperature predictions at the ceiling level. This is an important result since a similar method for modeling the computational domain was required for the evaluation of the recession geometries in the current research, where isolating the impact of the dimensional changes at the ceiling level is considered crucial.

3.4.3 Work by Husted and Holmstedt

Husted and Holmstedt [78] undertook a computational study on the impact of draft curtains (draft stops) on sprinkler activation, comparing the results from three different computer models of a fire in a compartment layout similar to an entertainment centre in Denmark. The study compared the results of two CFD models (FDS version 4.07 and CFX 4.4) and one zone model (Argos). The results were not compared to experimental results.

The compartment consisted of a two level enclosure linked with an open stair and floor opening. The ceiling height in the lower level was 2.5 m with the exception of a raised portion at the stairway measuring 3 m by 6 m and with a ceiling height of 2.9 m. A draft curtain 0.4 m deep was located at the perimeter of the opening at the edge of the raised ceiling area. A source fire 1 m by 1 m in diameter was positioned at the centre of the raised portion of the ceiling. The fire was programmed to grow according to a medium t^2 growth curve to a maximum heat release rate of 5000 kW. Twelve "sprinklers", modeled as heat detectors with activation temperatures of 68°C and an RTI of 38 $(m*s)^{1/2}$, were positioned 50 mm below the 2.9 m high ceiling with 0.7 m horizontal spacing at locations characterized by their r/H position. The centre of the source fire was located 0.7 m horizontally from the closest heat detector. It is noted that heat detectors were used in the analysis so that sprinkler activation in the model would not impact the source fire or compartment temperatures.

The FDS simulation was conducted utilizing a 100 mm by 100 mm by 100 mm grid cell size. Grid sensitivity analysis was conducted by reducing the cell size in the z direction (height) by 50% to 50 mm. This modification did not result in a significant change in the calculated sprinkler activation times. It is important to note however that by not changing the size of the grid in the other two dimensions, the authors did not provide increased resolution in the directions governing smoke and heat transport below the ceiling, which may impact the results. Therefore, it cannot be concluded that grid independence was achieved in this study. Based on the largest grid cell dimension, the maximum heat release rate of the source fire, and Equation 3-1 the ratio of D^*/δ applied to this analysis was 18.9. This value of D^*/δ is much higher than any other study considered thus far which should, in theory, provide increased accuracy for the simulation.

FDS predicted an average reduction in sprinkler activation time with the draft stop in place of between 4-6%. This result was in qualitative agreement with the experimental results reported by McGrattan et. al. [62] which determined a 5-15% faster response time in their large-scale sprinkler tests that evaluated the impact of draft curtains on sprinkler activation. This suggests that FDS provides a reasonable prediction of thermal detector response for ceiling configurations involving confined and unconfined ceiling jets and thereby supports the use of FDS for the evaluation of thermal detector response for the ceiling recession configurations of interest in this thesis.

3.5 Other FDS Studies

3.5.1 AFSA – Impact of Draft Stops on Sprinkler Activation

The American Fire Sprinkler Association (AFSA) utilized FDS in a study of the impact of 18 inch draft stops at the perimeter of floor openings on sprinkler activation times using FDS Version 3 [8]. The results were not compared to other models or experimental results. Instead, the goal of the study was to model the impact of 18" draft stops, as mandated by NFPA 13, on the activation time of adjacent sprinklers given the advent and availability of quick-response sprinklers.

Three source fire conditions were considered representing medium, fast, and ultra-fast t^2 fires. The selected grid cell size was 0.098 m by 0.102 m by 0.097 m high which was noted as a balance between accuracy and computation time though no comparative results were provided. Other significant details regarding the model setup, such as the selected radiative fraction, are not provided in the study report. Predicted ceiling jet temperature and velocity values were not specifically examined as part of this study.

The results verified the expected result that the presence of the 18 inch draft stops provided a slight improvement with respect to the response time of the adjacent sprinklers when compared to the same fire scenario with no draft stops installed. The study also found that the use of quick-response heads without draft stops may provide an equivalent level of performance with respect to thermal detector response times. It is important to note that the results of this study were presented by the authors in terms of the relative level of performance for each fire scenario

considered and not as actual values for detector response. Nonetheless, the study highlights the potential of using of FDS for comparative analyses between different ceiling configurations as a means of obtaining relative results for thermal detector response times. This method would be especially useful where reliable experimental data for validation of the accuracy of specific results is not available to the user. Instead, the performance of the selected scenarios can be presented in terms of their results and trends in behaviour relative to one another in order to identify a "best" design and facilitate design decisions.

Within the context of this research, this comparative method could be directly applied to both the assessment of the selected ceiling recession geometries, as well as trends related to the performance evaluation of the ceiling recession method in comparison to the draft stop method. This method is applicable to this research since actual response time values, comparable to experimental results, are not necessarily required in order to assess trends in behaviour and therefore estimate the impact of the selected configurations on likely thermal detector response times.

In applying this approach, however, it is important to clarify that the predicted thermal detector actuation time, for a given fire scenario, may not be accurate.

3.6 Summary of Past Validation Work

3.6.1 General

Table 3-4 below provides a summary of the variables studied and the key parameters used in the validation studies considered above.

Table 3-4: Parameter summary of past validation studies

Study	Focus Parameter(s)	Fuel Source	Max HRR (kW)	Grid Size (m)	D^*/δ	Radiative Fraction
NIST/NRC [62]	Hot gas layer temperature	Heptane and Toluene	350 - 2000	0.18	3.6 - 7.3	0.4 - 0.44
Pope and Bailey [75]	Hot gas layer temperature	Wood / plastic test cribs	875 - 1664	0.2	4.7 - 6.1	N/A
Smardz [76]	Hot gas layer temperature	Diesel oil and ethanol	49 - 86	0.04	7.3 - 9	0.35
Harrison [33]	Spill edge temperature and velocity	Denatured ethanol (IMS)	10.3	0.02	8	N/A
UL/NFPRF [62]	Thermal Detector Activation	Heptane	4400 - 10000	0.3	4.5 - 6.2	N/A
Hurley and Munguia [77]	Thermal Detector Activation	Heptane	1055 - 2100	0.1	10.2 - 13.4	0.35
Husted and Holmstedt [78]	Impact of draft stops on sprinkler activation	N/A	5000	0.1	18.9	0.35
AFSA [8]	Impact of draft stops on sprinkler activation	N/A	N/A	~0.1	N/A	N/A

Review of validation work in which the results of FDS simulations were compared to measurements highlighted a number of key modeling concepts and results related to the current research.

For all previous work considered, and indeed in any computational modeling exercise, the importance of selecting a grid size appropriate for the analysis cannot be emphasized enough. The ratio of D^*/δ was introduced as a potential means of gauging the appropriateness of a selected grid. Further, it was shown that consideration of this ratio may be of additional benefit where experimental data is not available, since D^*/δ values used to obtain accurate results in previous studies for similar configurations have been shown to be useful as maximum grid sizes for additional work. However, as can be observed in Table 3-4 a wide range of D^*/δ ratios have been shown to provide reasonable results in comparison to experiment. Therefore, no single value, or range of values, for this ratio could be identified as optimal for the current analysis, and a grid sensitivity study was required in order to determine if grid independence was achieved.

3.6.2 Compartment Temperature

Past work which compared FDS predictions of ceiling jet temperature to experimental data show that the model can provide reasonable estimates of ceiling jet temperature, and hot gas layer temperature, for a variety of compartment configurations and ventilation conditions [62, 75, 76]. In the work by NIST and NRC [62], the ceiling jet temperature for one selected measurement point in a large volume compartment (21.7 m by 7.1 m by 3.8 m) was shown to be slightly over or under predicted depending on the ventilation conditions in the compartment, which were controlled by a door, and a mechanical ventilation system. Further work by Pope and Bailey [75] and Smardz [76] conducted in smaller experimental compartments provided similar results. In these latter studies, average hot gas layer temperatures were found to be in good agreement with experimental results provided an appropriate grid size was selected for the analysis.

Further work conducted by Hurley and Munguia [77] found that ceiling temperatures 100 mm below a ceiling were generally over predicted by FDS Version 4.0.6. The accuracy of the prediction was found to improve as the radial distance from the fire plume increased from 2.2 m to 10 m. This result may have significant implications for the current research since, based on the sprinkler spacing requirements of NFPA 13, the radial distance of interest for the actuation of ceiling recession sprinklers would be approximately 2.2 m (see Section 6.2.1 of this thesis for further details).

These results are further supported by the work of Husted and Holmstedt [78] who found that FDS provided good agreement with Alpert's ceiling jet correlations implemented in the zone model Argos.

It is important to note that the accuracy of the FDS models was not consistent for all cases in these studies. Pope and Bailey found a significant decrease in error when the source fuel was modified from wood cribs, to combination wood/plastic cribs, suggesting that the model was sensitive to the selected burning characteristics of the fuel, or the method used for determining the heat release rate from the experiments. Pope and Bailey also noted that the accuracy of the model was substantially less where only a single measurement point was considered instead of an average of many measurements throughout the domain of interest. Smardz also found significant differences in prediction error between two experiments when compared to FDS predictions. Again, numerous aspects of the two experiments were different including the types of fuel, maximum heat release rates, and compartment configuration; therefore, a single cause for the discrepancy cannot be determined.

The findings of validation studies discussed in this section suggests that FDS will provide reasonable prediction of ceiling jet and compartment temperatures, but that the model is highly sensitive to a range of model inputs including grid size, ventilation conditions, heat release rate, and fuel properties. Therefore, in the current research it was critical to maintain constant model inputs in the ceiling recession comparisons, and vary only the geometrical configuration in terms of recession dimensions. In this way, a more direct comparison is possible from the model results.

3.6.3 Velocity

Limited detailed data is available regarding validation work related to the ceiling jet velocity values predicted by the model. This may be partially due to difficulties in obtaining reliable experimental velocity data for fire tests, as was experienced by Smardz in his work [76]. Recent experimental work by Torero and Carvel supports this theory, as their work notes a need for further research into the area of developing accurate experimental velocity measurement techniques [83]. Balcony spill plume work conducted by Harrison [33] found that the steady-

state gas velocity profiles below the spill edge were slightly under predicted by FDS in comparison to experimental measurements for two different compartment configurations. This result suggests that FDS will provide a reasonable estimate of gas velocities in a compartment. However, since this result is based on a single validation study, further validation of FDS for hot gas layer velocity should be considered.

Validation studies focused on thermal detector activation also suggest that FDS provides reasonable representations of hot gas velocity in a compartment. As noted in Equation 2-20 the activation time of thermal detectors is reliant upon the gas velocity to the order of $1/\sqrt{u_g}$. While the activation time of a thermal detector is more heavily influenced by the temperature of the hot layer gases than the fluid velocity, the good results seen in sprinkler activation studies, such as those conducted by McGrattan et al. [62] and Hurley and Munguia [77], suggest that the velocity at the detector may also be well represented by the model. .

3.6.4 Flow Characterization at Obstructions

To the knowledge of the author, no validation studies have been conducted to date which examines hot layer development or thermal detector activation for the ceiling recession configurations discussed as the focus of this research. Similarly, detailed experimental work involving ceiling jet flow characteristics in ceiling recessions, such as skylights, is not currently available. Work conducted utilizing FDS to analyze balcony spill plumes, such as the work by Smardz [76] and Harrison [33], supports the ability of FDS to predict the initial stages of this flow (i.e. as the jet initially reaches the spill edge). Although not the focus of his work, the comparative study conducted by Harrison using FDS also suggests that the model was able to represent the upstream temperature of the ceiling jet flow at the compartment opening for various draft stop (downstand) depths once steady state conditions were reached, a situation which generally occurs long after thermal detector actuation in a real fire scenario. Within the context of the present research, however, these results support the use of FDS for the evaluation of ceiling recession configurations since the model was able to predict flow characteristics of the ceiling jet when encountering obstructions such as draft stops (downstands).

3.6.5 Thermal Detector Actuation

The use of FDS for the evaluation of interest in this research is further supported by the validation work conducted by McGrattan et al. [62], and Hurley and Munguia [77] concerning the actuation of thermal detectors. In both studies FDS predictions were found to be in general agreement with measurements. In the work by McGrattan et al. [62], the number of sprinkler activations within the compartment predicted by FDS were higher than observed in the experimental testing, suggesting an over prediction of gas temperatures and/or velocities. This trend was also observed by Hurley and Munguia [77] but was found to be dependent on the radial distance between the plume centreline and the detector position.

In general, these results suggest that FDS will provide a reasonable prediction of thermal detector response times, which is the key focus of the current research.

4 Validation study - Comparison with Motevalli and Ricciuti

4.1 Introduction

As was discussed in Chapter 3, FDS validation data specific to compartment velocities is limited. Therefore, in order to further assess the predictive capability of FDS version 5.5.3 for upper layer temperature and velocity, an independent validation study was conducted as part of this research. The primary objectives of this study were:

1. To evaluate the use of FDS version 5.5.3 for the prediction of the hot gas layer temperature for a ceiling recession configuration similar to that proposed in this research and thereby determine if the results of the model are as good as, or better than results of previous validation studies.
2. To provide a comparison of FDS simulations to experimental ceiling jet velocity data where current validation work is lacking.
3. To establish a grid size appropriate for the ceiling recession analysis.

To the knowledge of the author, detailed experimental data for hot ceiling jet flows into recessions are not currently available. Therefore, the experiments conducted by Motevalli and Ricciuti [22] related to confined ceiling jets were selected as the basis of comparison for this validation study.

Motevalli and Ricciuti conducted experiments in a 1.89 m by 1.89 m by 1 m high fire test apparatus illustrated in Figure 4-1. The experiments investigated ceiling jet temperature and velocities generated by a centrally located 2 kW source fire. Draft stops 0.5 m high were installed around the perimeter of the test ceiling in order to create a confined ceiling jet. Temperature and velocity measurements were taken at two radial locations within the compartment and at heights ranging from 2 mm to 100 mm below the ceiling level.

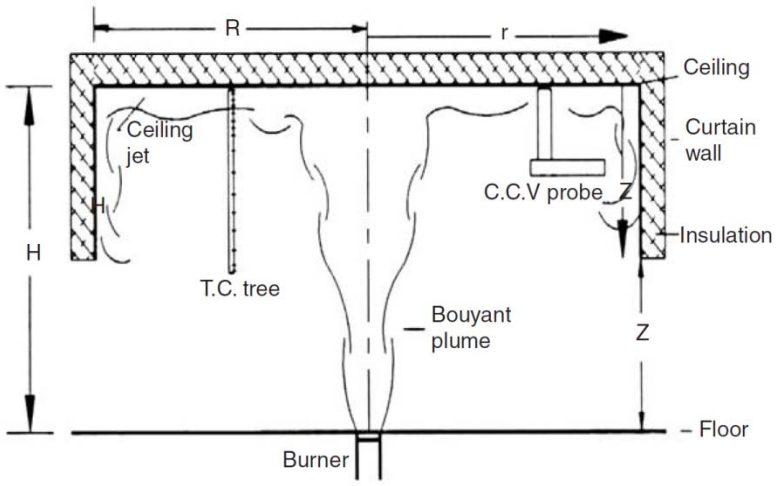

Figure 4-1: Experimental setup for Motevalli and Ricciuti experiments [22]

Results of these experiments are appropriate for the current validation study primarily due to the detailed data that is available for both hot gas layer temperatures and velocities near the ceiling. The test compartment is representative of a standard draft stop configuration at a vertical floor opening. Therefore, comparisons between FDS predictions and this data were representative of the level of accuracy that could be expected in an evaluation of the performance of thermal detectors adjacent to draft stops using FDS.

Unfortunately, Motevalli and Ricciuti do not provide estimates of experimental uncertainty in their data. Therefore, the overall accuracy of the FDS results cannot be estimated. However, general uncertainly values have been estimated based on other experimental work utilizing similar measurement techniques. These estimates are discussed in detail below.

For the purposes here, the experimental data is taken as the benchmark against which to compare results of the FDS simulations since measured temperature and velocity data previously have been compared to existing correlations implemented in the fire model LAVENT by Motevalli and Ricciuti. In that comparison, trends in velocity and temperature followed the expected pattern; however, the LAVENT temperature values (°C) were consistently less than experimental values by 20-30%, while velocity values were over predicted by up to 50%.

4.2 Description of Experimental Setup

The apparatus used in [22] consisted of a ceiling with dimensions of 1.89 m by 1.89 m, suspended 1.0 m above the burning surface and all housed in a larger test room. Dimensions of the room in which the apparatus was located were not provided. The ceiling was constructed of 1.27 cm thick fiberboard with a measured emissivity of 0.9. The backside of the ceiling was insulated with 8.26 cm of standard R-11 fiberglass insulation. Draft curtains having a depth of 0.5 m were installed at the perimeter of the ceiling to promote the formation of a confined ceiling jet. These were constructed of corrugated cardboard and insulated with the R-11 fiberglass insulation.

The fires, with heat release rates of 0.75 kW and 2.0 kW, were generated using a premixed methane/air mixture at stoichiometric conditions in a 2.7 cm diameter burner located at the floor level (1.0 m below the ceiling). Heat release rates were calculated using a heating value for methane of 49.997 MJ/kg and an air/fuel ratio of 9.52 [22]. Mass flow rate of the fuel was metered through a calibrated flow meter in order to achieve the desired heat release rates.

Temperature and velocity measurements were taken at r/H = 0.26 and 0.75 over a period of 40 minutes. In Motevalli and Ricciuti [22], temperature and velocity values are provided at times of 0.08, 1, 2, 3, 5, 10, 15, 20, 25 minutes during the experiment. Temperature and velocity measurements were taken simultaneously with an array of sensors using the Cross Correlation Velocimetry (CCV) technique. This method uses the temperature of the fluid as a tracer and obtains the velocity of the fluid particles via cross-correlation of the temperature-time records of a thermocouple pair. Sensor pairs were stacked vertically on the CCV probe such that readings could be obtained for any distance below the ceiling level. The top of the CCV probe was located such that detailed measurements could be obtained for distances ranging from 0.5 cm to 10.93 cm below the ceiling. The CCV technique was verified using laser Doppler velocimetry in separate work by Motevalli, Marks, and McCaffrey [84]. An estimate of error for this measurement method was not provided by Motevalli and Ricciuti. It was also noted by Motevalli and Ricciuti that velocity measurements for the 0.75 kW fire were unreliable due to the low velocities in the thermal plume generated by the weak source.

Upper layer temperatures were measured at a horizontal distance of r/H=0.26 using a 2nd probe consisting of 16 thermocouples located at positions from 0.2 cm to 52 cm below the ceiling in a vertical rake. Voltage signals from the thermocouples were amplified using a 16-channel amplifier before being relayed to a HP6942A multiprogrammer data acquisition system. Voltages from both sets of probes were transferred to a computer intermittently at a rate of 33 kHz where they were processed to produce velocity and temperature values.

4.2.1 Estimation of Experimental Uncertainty

Since an estimation of experimental uncertainty was not provided by Motevalli and Ricciuti and it is intended to use the experimental data as a means of evaluating the accuracy of the present FDS predictions, an estimation of experimental uncertainty is required. For this purpose, the experimental uncertainty arising from the following is considered:

- source fire heat release rate error due to fuel flow control to burner
- velocity measurement error due to CCV methodology
- temperature measurement error due to CCV methodology

The heat release rate of the experiment was controlled by moderating the fuel flow to the burner using a flow meter. Motevalli and Riahi [57] estimated the error in the heat release rate as ±5%, based on the original experiments conducted by Motevalli and Ricciuti [22]. This represents a range of heat release rate between 1.9 kW to 2.1 kW for the experiments. Given that the impact of this variability in heat release rate would be small in terms of the resulting temperature and velocity values at the ceiling (i.e. < 1°C and < 0.1 m/s based on estimates made using the confined ceiling jet correlations discussed in Chapter 2), this source of uncertainty can be neglected for the purposes of this study.

Temperature and velocity measurements were obtained using a CCV probe. The uncertainty in CCV measurements depends on the sampling rate, the flow velocity, and the intensity of thermal fluctuations [57]. These parameters were not provided by the Motevalli and Ricciuti; however, in work conducted by Motevalli and Riahi [57] it is noted that, for the range of ceiling jet flow velocities encountered in the work by Motevalli and Ricciuti, the uncertainty of the CCV

measurements (assumed to apply to both temperature and velocity here) varies by up to 10%. This value is in general agreement with the ±5% level of uncertainty estimated in the work of Motevalli, Marks, and McCaffrey [84], which compared the use of the CCV technique to other measurement methods in controlled PVC pipe flow bench scale tests. However, later work by Rockwell [85] regarding the use of CCV for measurements in turbulent fire-induced flows found that CCV velocity measurements could vary by up to 30% when compared with other measurement techniques. The primary cause of higher error was found to be misalignment of the thermocouples in relation to the direction of the bulk flow [85]. Correction factors to bring the accuracy to within approximately 5% are outlined in Rockwell's work, but require detailed information regarding the experimental setup, such as the probe offset angle and sampling frequency, in order to be applied [85]. Motevalli and Ricciuti did not conduct a detailed verification of the CCV probe set up or measurement results and did not specify if correction factors, such as those outlined by Rockwell [85] were applied to the experimental results [22]. As such, the level of uncertainty for these measurements cannot be accurately predicted. Therefore, for the purposes of this analysis, an uncertainly value of 10% has been applied to the experimental data based on the work conducted by Motevalli and Riahi [57]. However, the discussion above highlights the fact that the measurement of flow velocity in experimental fire compartments is difficult which may suggest why this type of data is scarce for fire driven flows.

Upper layer temperatures were measured utilizing a second thermocouple probe consisting of 16 Type K thermocouples. Again details regarding the construction of these thermocouple probes were not provided by the author so that experimental uncertainty for these measurements cannot be determined. However, Hurley and Munguia utilized Type K inconel sheathed thermocouples for their experimental work and estimated a minimum level of measurement uncertainty of ±2.2°C based on manufacturers data [77]. Therefore, for the purposes of this analysis, this uncertainty value has been applied to the experimental data from Motevalli and Ricciuti.

Figure 4-2 provides a comparison of the experimental temperature data obtained by [22] using the two measurement techniques noted above, including assumed uncertainty values at r/H=0.26 and z=40 mm.

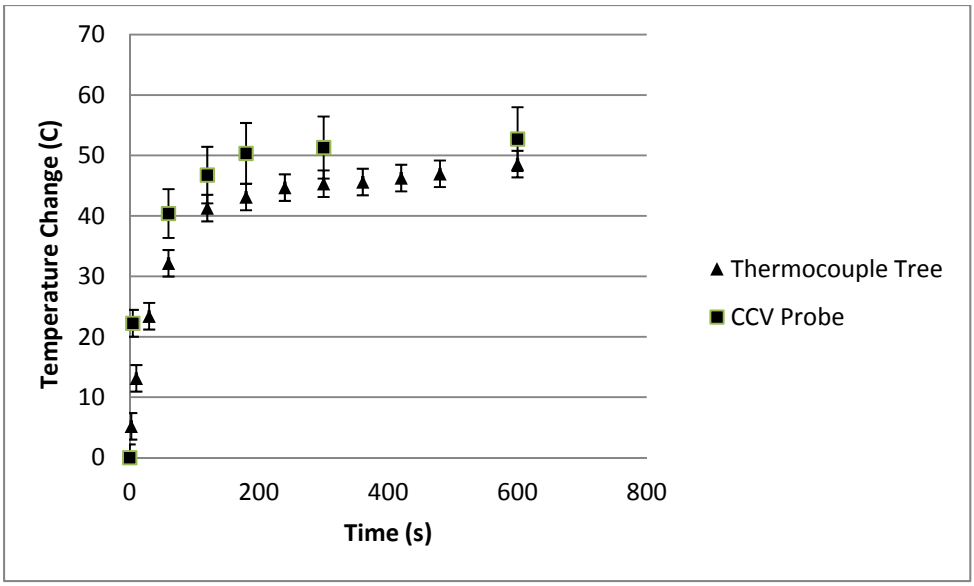

Figure 4-2: Temperature Change from Ambient at r/H=0.26, z=40 mm including Thermocouple Tree Data

Figure 4-2 indicates that the CCV temperature measurements were consistently above the values recorded by thermocouple tree. As indicated in Figure 4-1, while both probes were located at equal r/H values the locations of the two measurement probes were different. Although in theory the ceiling jet would have identical temperature and velocity values at these locations, in practice it is unlikely that the flow characteristics at these locations were identical. The difference in probe locations may have resulted in differences in the measured temperature values. However, this comparison suggests that the uncertainty values selected for both measurement techniques are appropriate for the purposes of this study since the thermocouple values fall within the uncertainty assumed for the CCV data.

A second method of velocity measurement was not utilized in the experiment. Therefore, the CCV probe velocity data cannot be compared to another source as a means of further analyzing the uncertainty of those measurements.

It is acknowledged that additional uncertainties undoubtedly impacted the experimental results due to other sources, such as the fluctuating nature of the fire and smoke layer at some measurement positions, location of instruments within the compartment, or the use of three different experiments in obtaining results. Since the degree of uncertainty from these sources

cannot be estimated reliably with the information available, they are not considered further for the purposes of this analysis.

4.3 Computational Model Setup

For the purposes of this study, the 2 kW fire scenario was selected since velocity data for the 0.75 kW scenario were noted as being unreliable by the authors. Further, results from the experiment at the measurement location of r/H=0.26 were selected for comparison to the FDS predictions, with temperature readings from measurement, z=20 mm at r/H=0.75, also considered. Measurements from r/H=0.26 were considered to facilitate evaluation of predicted temperature and velocity values near the fire plume where previous validation work [77] had indicated that FDS predictions were less accurate. Experimental temperature and velocity data were provided by the authors at times of 5, 60, 120, 180, 300, 600, 900, 1200, and 1560 seconds after fire ignition. However, since the focus of this research is centered on thermal detector actuation, which generally occurs during the growth phase of a fire prior to the onset of steady state conditions, the present model was set up to run for only 600 seconds in order to reduce required computation times.

The compartment was modeled as an enclosure of dimensions 1.88 m by 1.88 m by 1.0 m high. The slight modifications from the actual experimental compartment were required to accommodate the grid size selected for the model. Thermal properties specified for fiberboard from the LAVENT analysis provided by the authors were used for the FDS simulation. Thermal properties for the insulation material used in the experiment were not provided by the authors. Therefore, thermal properties for the insulation were based on default values for insulation provided in Pyrosim, a third party tool for the creation of FDS input files (see Table 4-1 below). Since thermal properties were not provided for the cardboard draft curtains, these surfaces were assigned the same thermal properties as the ceiling in the present simulation. All input thermal properties are summarized in Table 4-1.

Table 4-1: Thermal properties of materials for FDS simulation

Material	Emissivity	Specific Heat (J/kg*K)	Thermal Conductivity (W/m*K)	Density (kg/m^3)
Fiberboard	0.9	1485	0.0485	272
Insulation	0.9	963	0.00462	84.9

The 2.7 cm diameter round burner used in the experiments cannot be modeled using the rectilinear geometries required by FDS. Therefore, a 0.04 m by 0.04 m square burner was defined, with its centre aligned to the location of the center of the experimental burner. The primary combustion reaction in the simulation was set to that of methane. The heat release rate of the source fire was defined by assigning a heat release rate per unit area of 1250 kW/m^2 to the 0.0016 m^2 burner in order to produce a maximum steady state heat release rate of 2 kW. A fire growth time of 1 second was utilized for the simulations.

The specified fire growth time may cause discrepancies between the experimental data and the model early in the simulation since the experimental source would have achieved the target 2 kW heat release rate in less than one second. However, due to the numerical methods implemented by FDS, the model will tend to over predict the heat release rate briefly, and then oscillate to the defined steady state value when no growth time is provided.

Thermocouples were defined based on the default FDS parameters:

Bead Diameter	1 mm
Bead density	8908 kg/m^3
Bead Specific Heat	0.44 kJ/kg*K
Emissivity	0.85

A total of 3 thermocouples were located at r/H=0.26 from the plume centreline at vertical heights below the ceiling of z= 20, 40 and 100 mm. Velocity measurements were also recorded at these locations using the gas phase measurement devices defined in FDS. An additional thermocouple positioned at r/H=0.75 from the plume centreline and at a distance of 20 mm below the ceiling

was included in the model. These measurement locations were selected in order to evaluate temperature and velocity at various heights below the ceiling while conforming to the requirement of FDS that measurement positions conform to the selected grid (see Section 4.4 below).

Figure 4-3 provides a rendering and plan view of the computational domain used for the study.

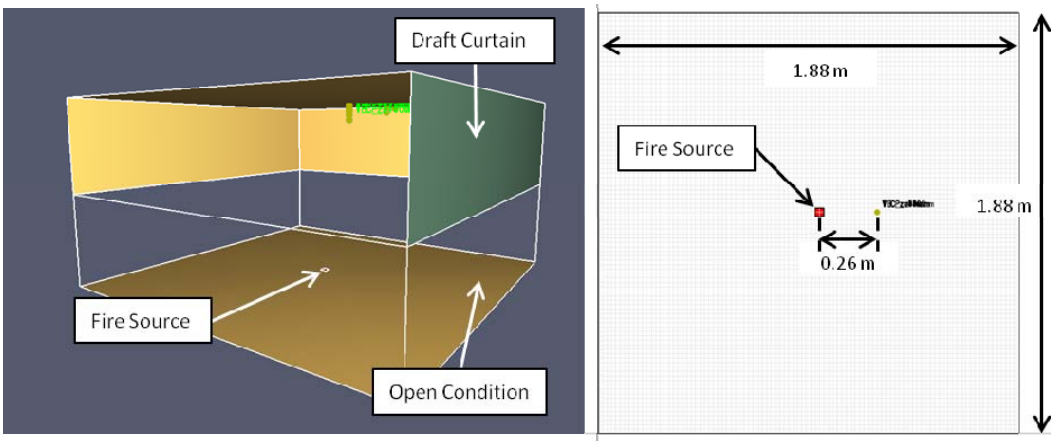

Figure 4-3: Computational Model Setup

As introduced in Section 3.2 of this thesis, FDS computes the amount of heat energy lost to the compartment due to radiation using the radiative fraction which has a default value of 0.35. The default value is considered appropriate for most sooty hydrocarbon fires. However, the work by Motevalli and Ricciuti studied here involved the use of a 2 kW premixed methane fire which would not produce significant amounts of soot. The radiative component of the combustion efficiency can be estimated based on the ratio of the total heat of combustion of a fuel (ΔH_c) and the radiative heat of combustion (ΔH_{rad}). Estimates for these values for well-ventilated fires are provided in Table 3-4.16 in Section 3, Chapter 4 of the 4th edition of the SFPE Handbook [80]. For methane, the following values are given:

ΔH_c	50.1 kJ/g
ΔH_{rad}	7.0 kJ/g

Therefore, the resulting radiative fraction for a well ventilated methane fire is estimated to be 0.1397. Based on this, a radiation fraction of 0.14 was applied to the simulation.

All other dimensional and thermophysical parameters utilized in the experiment were applied to the computational model.

4.4 Grid Selection

It has been suggested that the ratio of D^*/δ may provide a reasonable guideline for the selection of an appropriate grid size [74] [73]. As discussed previously, work by Davis et. al. [74] suggests that ratios of $D^*/\delta = 10$ will provide reasonable agreement with temperature values in most scenarios. However, validation studies discussed above have also indicated that D^*/δ ratios of less than 10 can also provide reasonable temperature results [33, 62, 75, 76, 82].

The value of D^* for the selected experiment can be determined from Equation 3-1, based on the known heat release rate, and the following assumed values for ambient air properties [22]:

Q	2 kW
ρ	1.1 kg/m^3
C_p	1004 J/kg K
T_∞	293.15 K
g	9.81 m/s^2

Substituting these values into Equation 3-1 yields a D^* of 0.082789. Therefore, in order to achieve a $D^*/\delta = 10$, a minimum cell size of approximately 0.008 m would be required. Applying this cell size over the computational domain required to recreate the geometry of the experiment (1.88 m by 1.88 m by 1.0 m) would result in approximately 6,903,125 cells in the model. This number of volumes would result in an extremely long required simulation time and, based on the results of some studies discussed in Chapter 3, may not be required in order to achieve accurate results.

In order to obtain preliminary results, an initial cell size of 0.02 m^3 was selected for the present analysis based on a review of the cell sizes and resultant values of a D^*/δ that have been used in previous validation studies, as summarized in Table 3-4. Use of this cell size results in a total of 441,800 cells and a value of $D^*/\delta = 4.14$. To evaluate grid sensitivity of the results, a second model run was conducted using a cell size of 0.01 m^3 resulting in 3,534,400 cells and a value of $D^*/\delta = 8.28$. In both cases, a single mesh was constructed across the entire computational domain in order to eliminate the risk that boundaries between mesh sections might impact the results.

4.5 Results

Experimental temperature and velocity results measured using the CCV probe are compared to corresponding values predicted here using FDS. The CCV probe data is selected as the basis for the comparison since both temperature and velocity values were measured at a single location in those experiments.

4.5.1 Temperature

The degree of error in the FDS simulation for a given grid size versus the experimentally measured data is quantified based on the prediction error as defined in Equation 3-3. Table 4-2 summarizes the minimum, maximum, and average values of prediction error in temperature for each selected measurement location.

Table 4-2: Summary of percent error in predicted versus measured temperatures (°C) at select locations for 0.02 m^3 grid size and Q=2 kW

	r/H = 0.26			r/H = 0.75
	z=20 mm	**z=40 mm**	**z=100 mm**	**z=20 mm**
Min (%)	15.95	0.01	2.22	14.99
Max (%)	16.89	4.60	11.61	29.84
Avg (%)	16.46	1.90	9.43	23.41

The error values reported in Table 4-2 above do not include the predicted values of temperature over the first 5 seconds of the simulation. Error values within this timeframe were substantially higher (>80% in some cases) than those seen for the remainder of the simulation. This suggests

that the method by which the initial growth in heat release rate of fire was defined in the model may have introduced error into the results, as discussed in Section 4.3.

In Figure 4-4 and Figure 4-5 experimentally measured values of the change in temperature relative to ambient are compared to predicted values for both r/H locations at z=20 mm below the ceiling. The overall trends in development of temperature with time are well represented for locations close to the ceiling (z = 20mm) evidenced by the similarity in the shape of the curve produced by the model in comparison to the experimental data. However, actual values of temperature (°C) are over predicted by an average of approximately 17% at r/H=0.26 (Figure 4-3) in comparison to measured values. The accuracy decreases and prediction error increases to approximately 23% (average), as r/H increases to 0.75 (Figure 4-4).

For both measurement locations, the results of the FDS model lie outside of the bounds of experimental uncertainly previously established for the measurements. One potential cause for this discrepancy is the assumed properties of the ceiling materials utilized for the simulation. Recall that the thermal properties for the ceiling insulation material, and the cardboard draft curtains were not provided by the author of the experiment. Therefore, for the purposes of this simulation values for these materials were estimated. The thermal properties of the ceiling materials will impact the rate of heat transfer between the ceiling jet and the ceiling in the simulation, and this will directly impact the simulated temperature, especially at locations near the ceiling. Another possible source of error is the selected grid size, which was previously highlighted to be larger than recommended values. Further discussion on this is provided in Section 4.5.2 below.

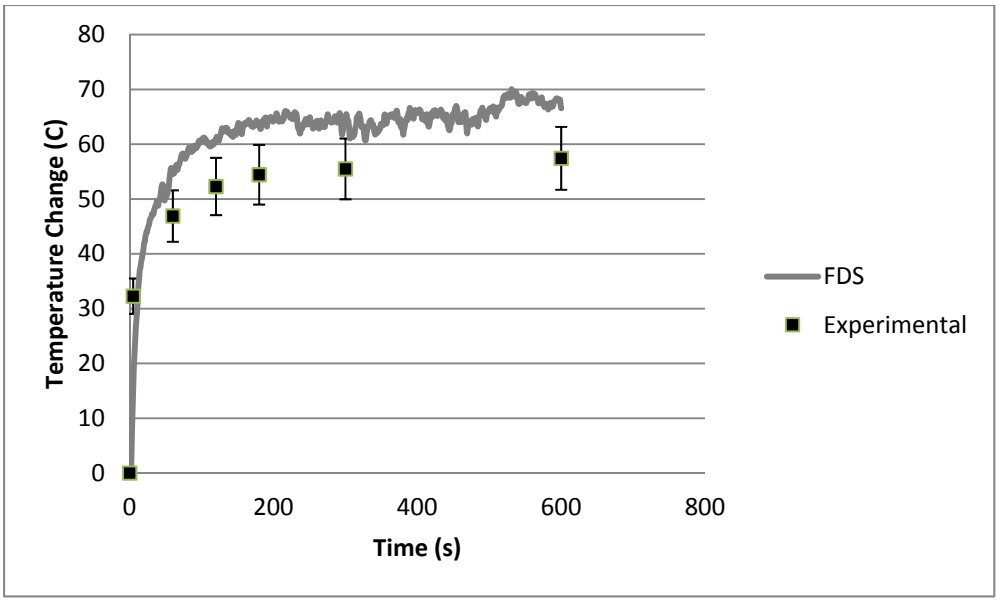

Figure 4-4: Temperature Change from Ambient at r/H=0.26, z=20 mm

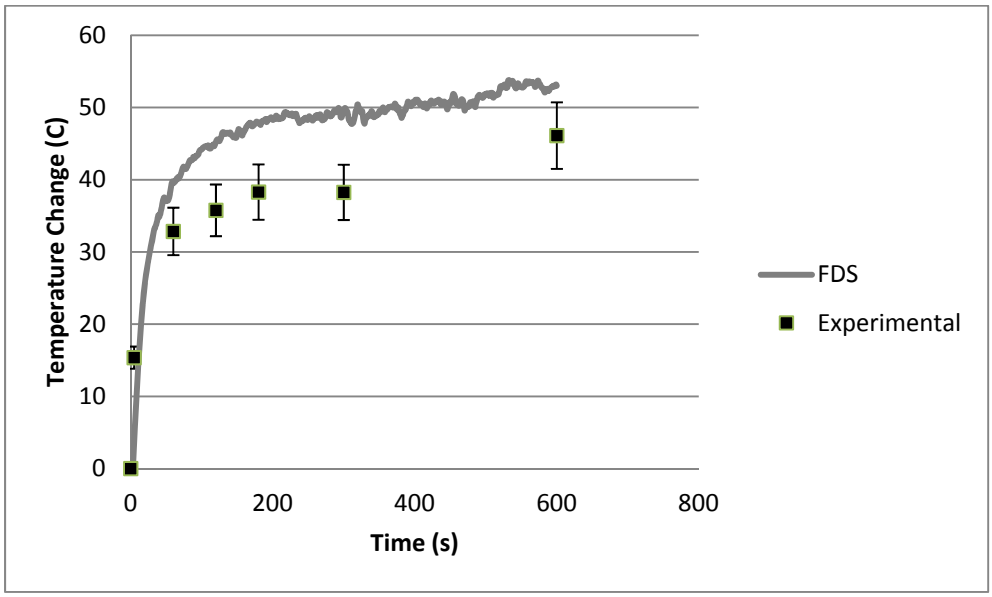

Figure 4-5: Temperature Change from Ambient at r/H=0.75, z=20 mm

Figure 4-6 and Figure 4-7 include comparisons of CCV probe temperature data with model predictions for r/H=0.26, at locations z=40 mm and 100 mm, respectively, below the ceiling.

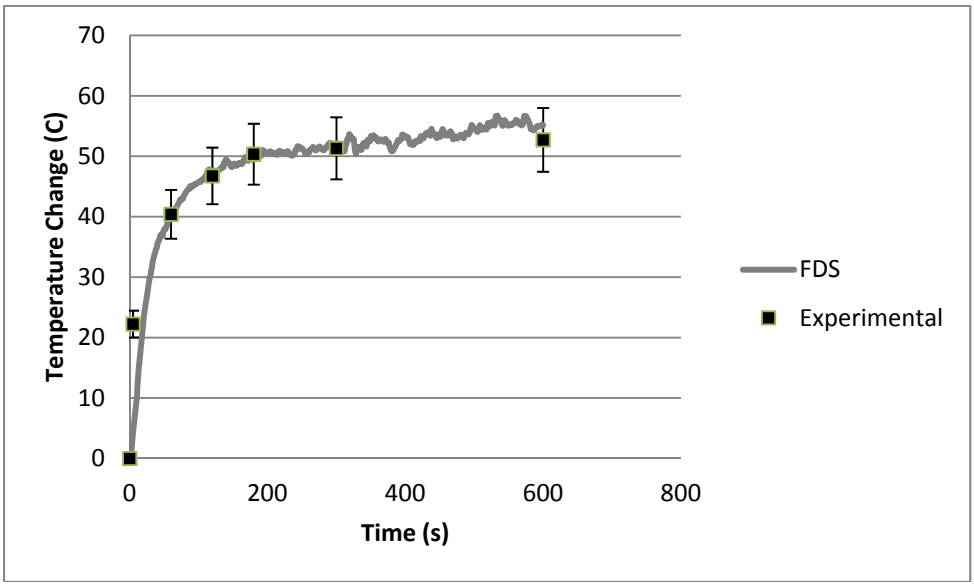

Figure 4-6: Temperature Change from Ambient at r/H=0.26, z=40 mm

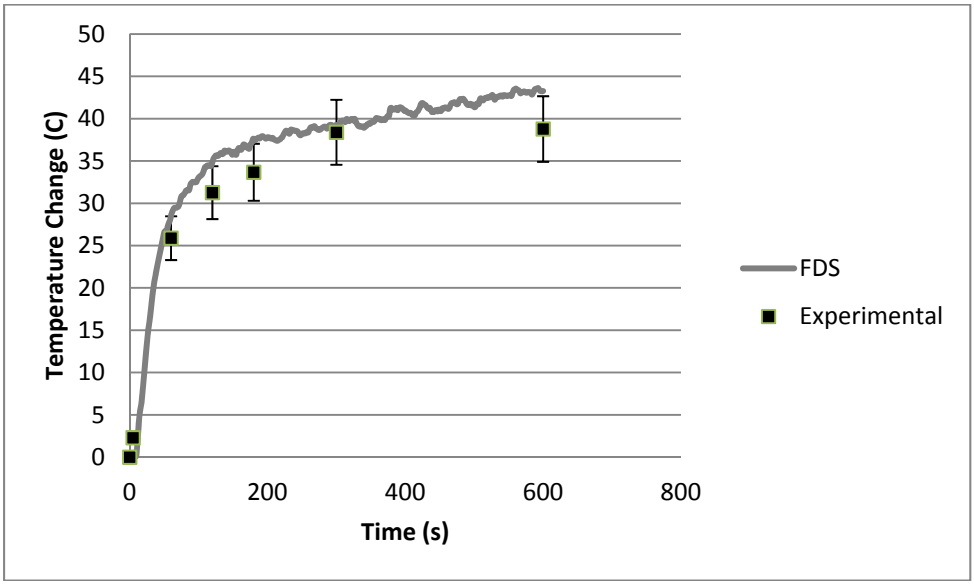

Figure 4-7: Temperature Change from Ambient at r/H=0.26, z=100 mm

It can be seen that the shape and accuracy of temperature-time curve is well represented by the FDS model prediction. Average prediction error values for z=40 mm and z=100 mm are 1.9%

and 9.4% respectively which are within the bounds of experimental uncertainty (10%) assumed here. This result indicates that temperature conditions are well represented by the model at these distances below the ceiling. The results also support the discussion above regarding the selected ceiling materials as a potential source of uncertainty for the temperature predictions at z=20 mm. The impact of heat transfer from the ceiling jet to the ceiling assembly will be most pronounced at elevations near the ceiling level. Since temperature predictions near the ceiling are high in comparison to the experiment, but are well matched at lower elevations seen here, it can be postulated that the model is under predicting heat losses through the ceiling.

In general, FDS tended to over predict compartment temperature in comparison to the experimental data. This result is in agreement with what was found in previous validation work where upper layer temperatures were generally over predicted by the model [76, 77, 82]. Based on this result, FDS has been shown to provide good agreement with experimental values for values of z between 40 mm and 100 mm. For values of z less than 40 mm, the model was found to over predict compartment temperatures by an average of approximately 20% for the data points considered here (z=20 mm at r/H=0.16 and r/H=0.75).

At all measurement locations the general trends in temperature with time are reflected in the model predictions even at measurement locations where the prediction error was more significant (z=20mm). This result should at least allow a comparative analysis and evaluation to be performed between simulations of the various ceiling recession configurations.

4.5.2 Velocity

Figure 4-8 provides a comparison of total vector velocity measurements taken by the CCV probe at r/H = 0.26 and z=20 mm with smoothed data obtained from FDS simulations. Predicted velocity values showed significant variability over time indicated by severe oscillations in the data from one second to the next. As a result, the data was smoothed by a moving average method that averaged values across 20 seconds (10 seconds preceding and 10 seconds following) for each point in time. The resulting curve is plotted in Figure 4-8.

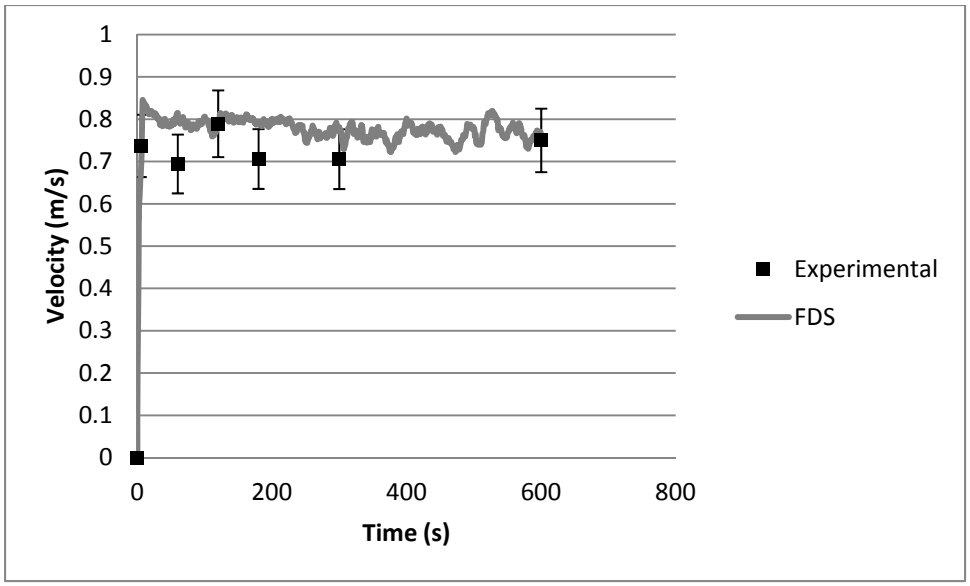

Figure 4-8: Velocity at r/H=0.26, z=20 mm

At z =20 mm and r/H=0.26, the trends and predicted values of velocity are in good agreement with the experimental data, although predicted values are consistently higher than measurements. The average prediction error at this location was 8.7%. All data points, with the exception of t=60 s, are located within the estimated bounds of experimental uncertainty.

In contrast to the good agreement at z=20 mm, a significant divergence between model predictions and experimental velocity data was observed at r/H=0.26 and z=40 mm as indicated in Figure 4-9.

In this case, velocities are consistently under predicted with an average prediction error of approximately 76%. This result is in stark contrast to model validation studies of Harrison, discussed in Section 3.3.1, where velocity profiles predicted by FDS were found to be in good agreement with experimental values measured using a pitot tube, albeit for quite different experimental conditions[33].

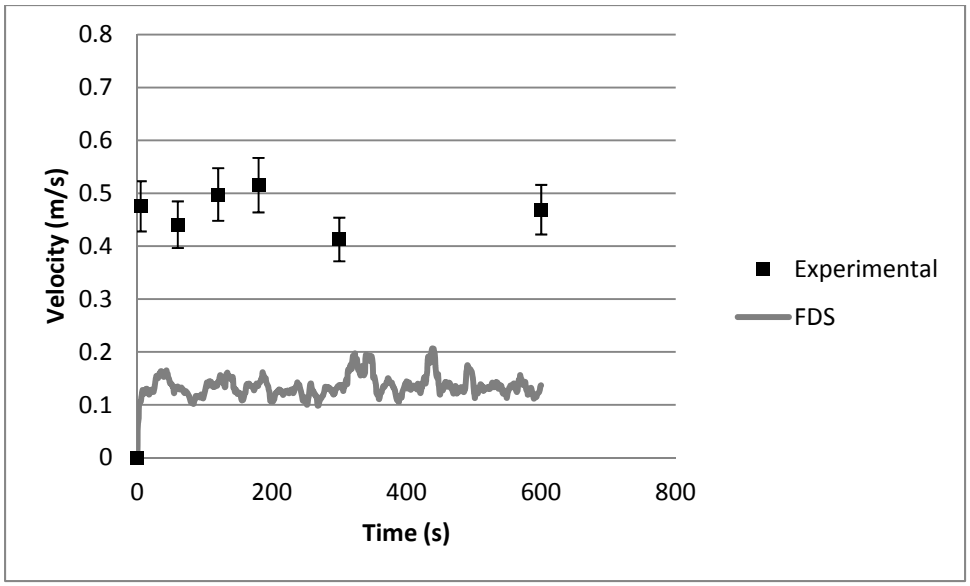

Figure 4-9: Velocity at r/H=0.26, z=40 mm

One potential cause for the high degree of error noted at z=40 mm is the location of the ceiling jet lower boundary in relation to the measurement location. A ceiling jet flow will exhibit decreasing velocity as the distance from the ceiling is increased. Therefore, if the thickness of the ceiling jet under review here was approximately equal to the selected measurement location (i.e. the bottom of the layer corresponds to the position of the velocity measurement, z=40 mm), the velocity would be highly sensitive to the simulated thickness of the ceiling jet since the probe may be in and out of the hot layer.

A correlation has been developed by Motevalli and Marks [86] to estimate the thickness of a ceiling jet (l_T) for a weak unconfined ceiling jet for a given radial distance from the source fire (r) and ceiling height (H) as follows:

$$\frac{l_T}{H} = 0.112\left[1 - \left(exp\left(-2.24\frac{r}{H}\right)\right)\right] \qquad \text{For } 0.26 \leq r/H < 2.0 \qquad [4\text{-}1]$$

Although the equation above was developed for unconfined ceiling jets, its evaluation is applied here as an order of magnitude evaluation. Application of Equation 4-1 yields an estimated ceiling jet thickness of 49 mm at r/H = 0.26, very close to the position of the measurement height. Therefore, simulated values for velocity at this location would be very sensitive to the

predicted thickness of the ceiling jet. An under prediction of the ceiling jet thickness would result in predicted velocities significantly lower than those that might be measured inside the ceiling jet. Ceiling jet thickness is not a specific (i.e. numerical) output in FDS. However, a visual estimation of the location of the lower ceiling jet boundary can be obtained based on velocity slice data by noting the grid cell at which the velocity drops to zero at r/H = 0.26 throughout the simulation. In this study, this transition occurs between z=40 mm and z=60 mm supporting the calculation of the ceiling jet thickness based on Equation 4-1 above. This suggests that velocity predictions at z=40 mm may be subject to a high degree of error as it is located near the lower boundary of the ceiling jet.

It is also possible that the velocity measurements taken by the CCV probe were subject to a greater error than originally estimated particularly at very low values of velocity (as was already indicated for the 0.75 kW heat release rate experimental measurements). However, since velocity values were not measured by any other means in the experiment this cannot be directly evaluated.

4.5.3 Grid Sensitivity

Based on the above results, a grid size of 0.02 m ($D^*/\delta = 4.14$) appears to be sufficient for prediction of ceiling jet temperatures and velocities in this scenario for values of z between 40 mm and 100 mm below the ceiling. Closer to the ceiling, the accuracy of the predicted results was reduced such that predicted values did not fall within the estimated bounds of experimental uncertainty. Consistent with all computational models, previous validation work has shown that the accuracy of FDS is highly sensitive to the selected grid size. Therefore, a grid sensitivity analysis was conducted to evaluate the impact of the grid size on predicted values of temperature and velocity. The same model setup was used with the grid size reduced to 0.01 m, resulting in a $D^*/\delta = 8.28$. This reduction in grid dimensions resulted in over three million cells and required approximately 358 hours (14.9 days) of simulation time running on an Intel i7 Quad Core Processor with 8 Mb RAM.

Figure 4-10 and Figure 4-11 contain comparisons of the predicted values of temperature with time for both grid sizes with the experimental measurements taken using CCV for a position of r/H=0.26 for z=20 mm and z=40 mm respectively.

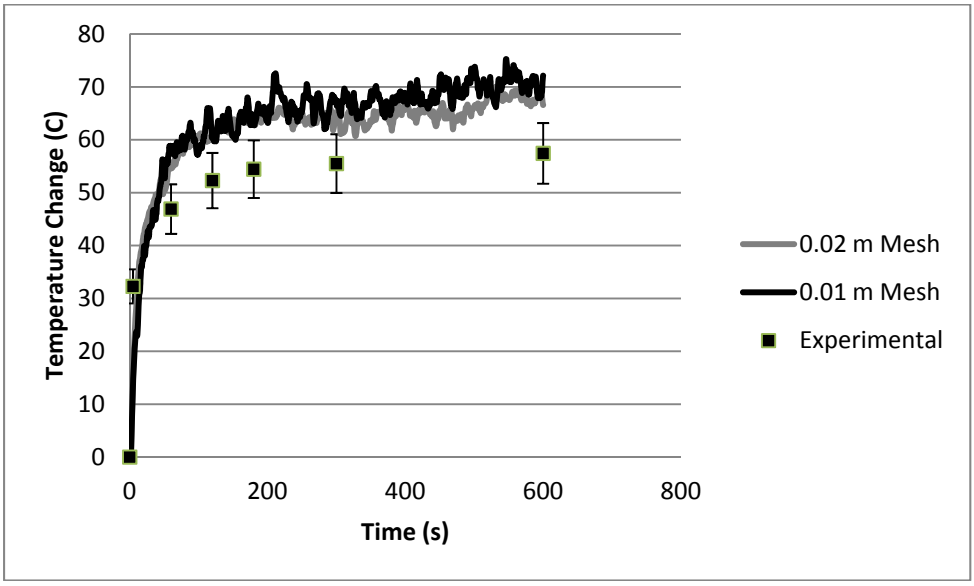

Figure 4-10: Grid size comparison for temperature at r/H=0.26 and z=20 mm

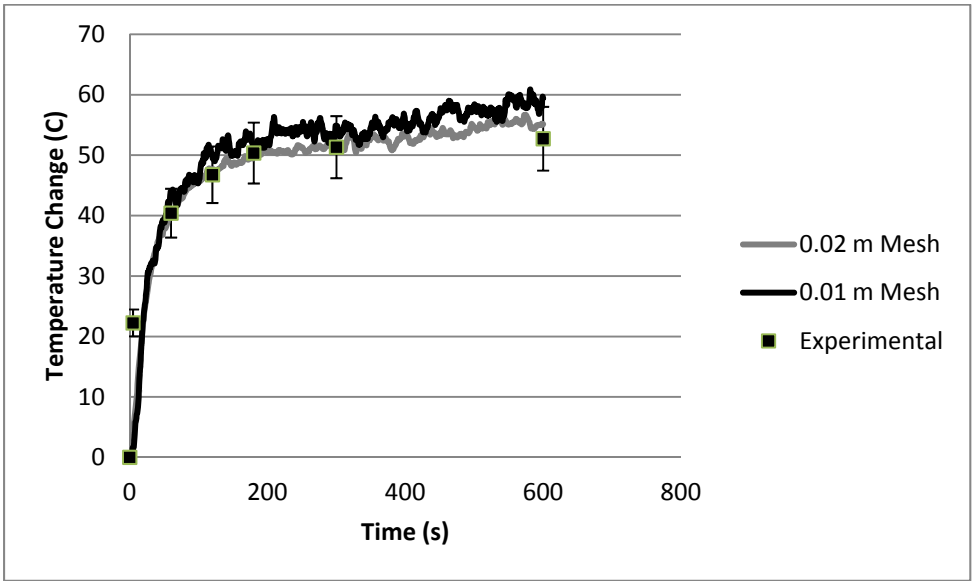

Figure 4-11: Grid size comparison for temperature at r/H=0.26 and z=40 mm

As indicated in Figure 4-10 and Figure 4-11 there does not appear to be a significant difference in the percent error between predicted and measured values of temperature for r/H=0.26 and z=

20 mm or z=40 mm. In both cases, a slight increase in the average prediction error is observed with respect to the measured data. At r/H =0.26 and z=20 mm the average predication error was increased from 16.5% to 20.4% with the decrease in grid size. Similarly, for z=40 mm at r/H = 0.26 the average prediction error increased from 1.9% to 6.8 % with the decrease in grid size. In both cases, the reduction of the grid size caused a slight increase in the predicted temperatures. Similarly, as indicated in Figure 4-12 and Figure 4-13 an increase in the predicted values of temperature was also observed at r/H=0.26 and z=100 mm, and at r/H=0.76 and z=20 mm when the grid size was reduced.

At r/H=0.26 and z=100 mm, and at r/H=0.76 and z=20 mm the increase in average prediction error with respect to the measurements for both locations was approximately 10%, a more significant result than was observed in Figure 4-10 and Figure 4-11.

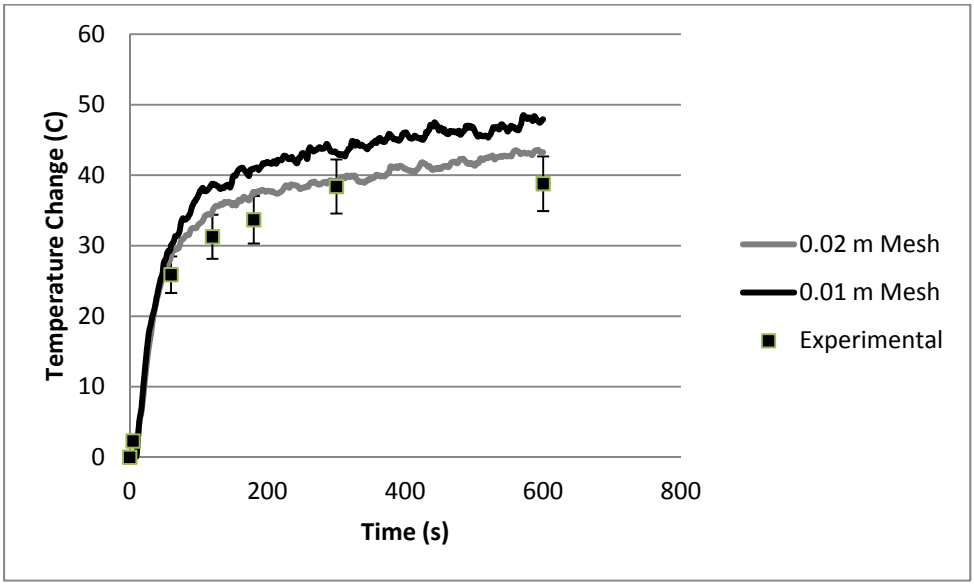

Figure 4-12: Grid size comparison for temperature at r/H=0.26 and z=100 mm

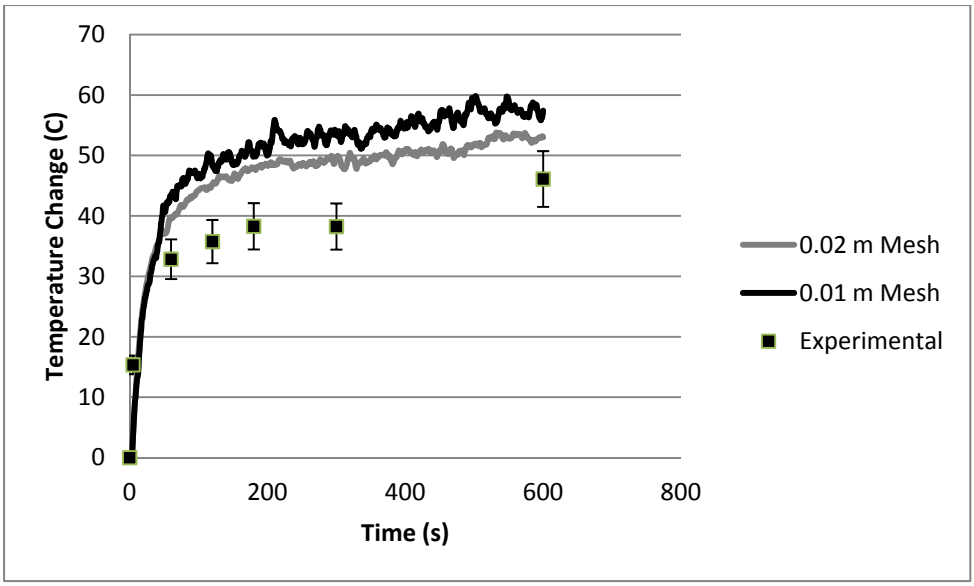

Figure 4-13: Grid size comparison for temperature at r/H=0.76 and z=20 mm

Simulated temperatures at all measurement locations increased when the grid size was reduced indicating that the coarser grid size resulted in a slight under prediction of temperature for the case considered. Although prediction error values were increased when the finer grid was applied, it is not possible to positively verify the accuracy of the experimental results. It is encouraging however to note that the simulated temperature trends were in general agreement with the trend noted in the experiments. The agreement in temperature trends suggests that, although the overall accuracy of the predictions cannot be quantified, the results may still have value on a comparative basis since the change in simulated trends could be readily evaluated relative to one another. This is of particular interest in the present research since a comparison of the performance of a series of proposed ceiling recession designs to the performance of a code compliant draft stop is sought.

Figure 4-14 and Figure 4-15 compare the predicted velocity values for both grid sizes at r/H=0.26 for z=20 mm and z=40 mm.

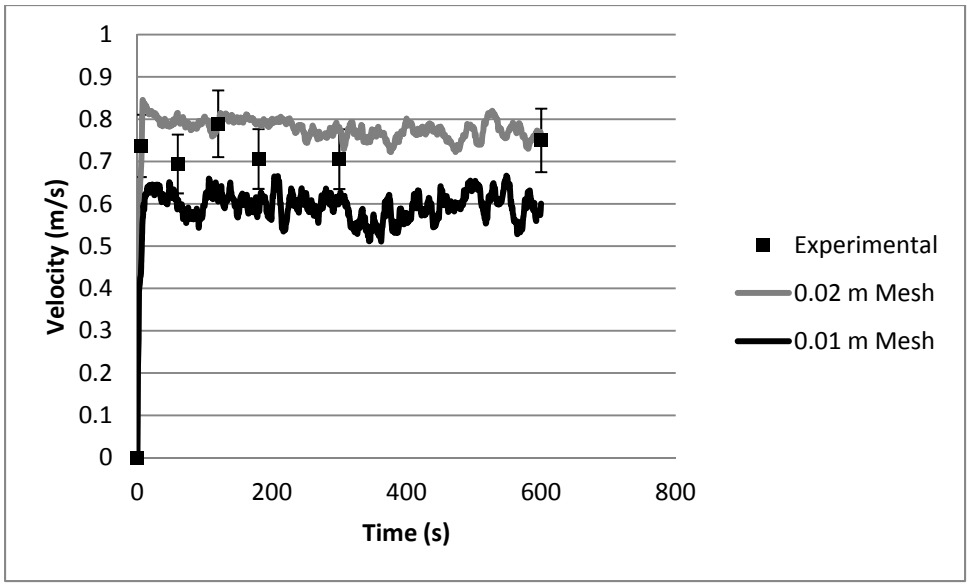

Figure 4-14: Grid size comparison for velocity at r/H=0.26 and z=20mm

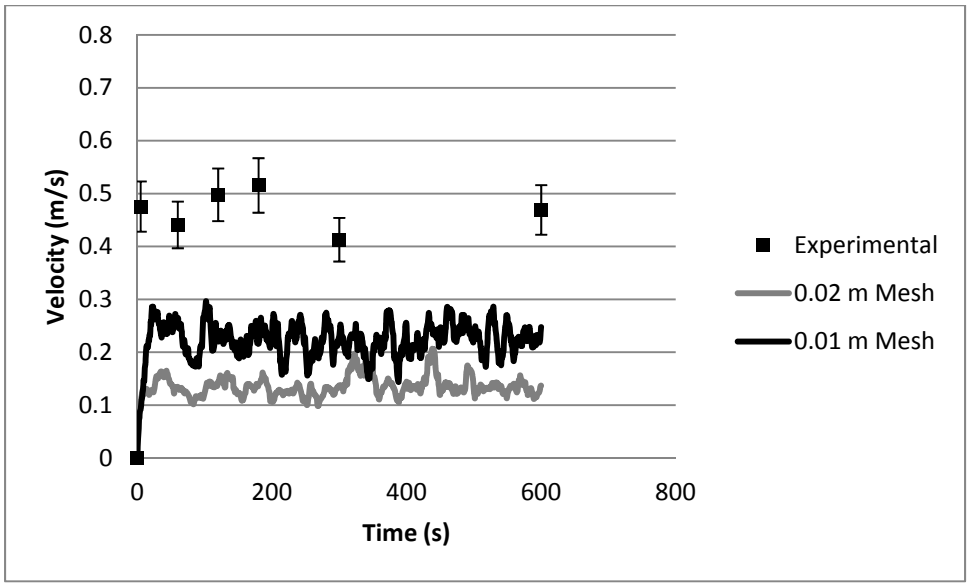

Figure 4-15: Grid size comparison for velocity at r/H=0.26 and z=40mm

At z=20 mm, the reduction in grid size resulted in an overall reduction in the predicted velocity values from an average of approximately 0.75 m/s down to 0.60 m/s. In terms of the average prediction error, this shift results in an increase in discrepancy in comparison to the experimental results. It is noted however that the velocities predicted for the finer grid at this location are close to the lower bound of estimated experimental uncertainty for all data points. This result

suggests that the coarse grid simulation slightly over predicted velocity values at this measurement location.

At z=40 mm, the opposite trend is observed as predicted velocity is increased for the fine grid size case. At z=40 mm, the average predicted velocity was increased from approximately 0.12 m/s to 0.21 m/s. Although this is a significant improvement in relation to the experimental results, the predicted velocity is still much lower than the experimental data for this measurement point. Again, this result is consistent with the notion that predicted velocities at this location are significantly impacted by the ability of the model to accurately represent the thickness of the ceiling jet. Substantially lower velocities would be predicted where the predicted thickness of the ceiling jet was less than that which occurred in the experiment, but with a finer mesh the resolution in predicted location of the interface should also increase.

Similar to the observations for the temperature results, overall velocity trends appear to be well represented by the model for both measurement locations considered here.

4.5.4 Conclusions

The validation study indicates that the model will provide reasonable representations of temperature and velocity trends for measurement locations up to z=100 mm below the ceiling for the confined ceiling jet condition evaluated here.

The overall accuracy of temperature predictions at r/H=0.26 varied depending on the measurement location under consideration. Temperature predictions were most accurate (in comparison to the experimental data available) where z was equal to 40 mm. Accuracy of the temperature predictions was reduced at values of z greater or less than 40 mm where the model tended to over predict in comparison to the experimental data. When r/H was increased to 0.75 the accuracy of the prediction was further reduced. Reduction of the selected grid size did not provide an improved result with respect to prediction error for these measurements. This result may be due to an increase in the impact of model errors, such as heat losses to the ceiling, caused by the refined mesh near the ceiling.

In terms of velocity values produced by the model, the FDS prediction at z=20 mm was shown to provide good agreement with the experimental data. A reduction in the selected grid size reduced the accuracy of the prediction of velocity at this location.

At z=40 mm the predicted velocity was significantly below the experimental data. A 50% reduction to the selected grid size was found to improve the results at this location, but at a significant cost with respect to computation time. The required simulation time of 14.9 days would render the use of this grid size, and therefore analysis methodology, impractical for evaluation of any industry alternative solutions.

The grid size reduction resulted in a value of D^*/δ of 8.28 and impacted the predicted values for temperature and velocity. The accuracy of the predicted values was not increased by the grid refinement with the exception of velocity predictions at z=40 mm and r/H =0.26. Based on these results, the ratio D^*/δ applied to the analysis of the ceiling recession configurations should be a minimum of approximately 8.3.

The accuracy of the temperature and velocity predictions using FDS cannot be verified based on the results of this study. Although encouraging results were obtained for some measurement locations, in others the predicted values were not in agreement with the experiment. This is especially true for the predicted velocities, which showed distinct differences from experimental results for z=40 mm below the ceiling. Although this discrepancy may be due to errors in the measurement, the accuracy of the experiment cannot be definitively determined. Nevertheless, the results obtained in this study do suggest that the results of the FDS model can still be of use to the evaluation of alternative solutions, the primary focus of this research.

Overall trends with respect to the shape of the time-temperature and time-velocity curves measured during the experiment are well represented by FDS. These trends were maintained with reduction in grid size and were consistent with trends expected with respect to previously observed thermal and physical characteristics of confined ceiling jet flows. This result suggests that the predictions could be used as part of a comparative analysis where predicted results are evaluated relative to one another, as well as against a benchmark situation. In this way, model

errors caused by the computational methods used, the selection of model inputs, and the selected grid size may be partially mitigated provided these elements are held constant between the various evaluations. This is of particular interest for the evaluation and possible ranking of alternative solutions since a comparison of the performance of the proposed design(s) to that provided by the prescriptive requirements of the Building Code is a mandatory element of an alternative solution.

5 ANALYSIS METHODOLGY

In this Chapter, an analysis methodology for the evaluation of the ceiling recession configuration as an alternative solution is proposed based on the findings of the preceding chapters.

An overall approach to the analysis is outlined. This approach is appropriate for an evaluation where experimental data may not be available. Following this, the proposed analysis methodology is applied to the evaluation of a ceiling recession design via a case study.

5.1 Relative Performance Evaluation

The results of Chapter 4 support the use of FDS for this analysis in terms of the ability of the model to predict ceiling jet temperature and velocity trends; however, to the knowledge of the author, no experimental data exists that relates to the ceiling recession configurations under study here. Therefore, a direct assessment of the accuracy of the FDS results relative to experimental data is not possible for the ceiling recession configuration. As was noted in Section 1.3, industry budgets and timelines often rule out the possibility of conducting experimental testing for the purposes of an alternative solution. Therefore, the method for investigating the ceiling recession configuration as an alternative solution, the primary objective of this research, cannot rely on experiments as a means of validating the FDS simulation.

Furthermore, as discussed in Chapter 2, available correlations which estimate ceiling jet temperature, velocity, and thermal detector activation do not provide the level of spatial resolution needed to evaluate various ceiling recession configurations, and therefore cannot be relied upon solely as a means of validating the FDS simulation or the ceiling recession design.

As discussed in Section 1.3, an alternative solution is required to demonstrate an equivalent (or better) level of performance than would be provided by a design based on the prescriptive requirements of the applicable code. Therefore, in any alternative solution evaluation, a comparative analysis must be conducted to assess the performance level of each new design relative to that of a corresponding code-based design.

Therefore, it is proposed that the analysis of the ceiling recession configuration be conducted using relative values to assess the level of performance, in terms of thermal detector response time.

It must be cautioned, however, that in doing such a comparison it is assumed that errors in model predictions will affect results for all designs equally, an assumption supported by the fact that the configurations under study are dimensionally similar. In taking this approach, it must be clearly understood that the results of the model predictions cannot be interpreted to represent actual values of velocity, temperature or thermal detector response times.

5.2 Proposed Analysis Methodology

Both low and high heat release rate design fires must be considered (see Sections 2.5.1.5 and 2.5.3 of this work) such that the impact of minor dimensional differences in the designs under consideration, and the impact of the ceiling jet horizontal projection at the spill edge, can be determined.

Selected model inputs, such as compartment layout, design fire location, fire growth rate, radiative fraction and ceiling thermal properties, are held constant for each set of simulations to better facilitate comparative analysis of the designs. For each input, sensitivity studies may be necessary depending on the availability of accurate input data for the scenario under consideration. For example, where the ceiling material is not known, the analysis should consider multiple material types in order to determine the impact of this input on the results.

An appropriate grid size for the simulations was selected based on the value of D^*/δ and the selected heat release rates of the design fires. Although a value of $D^*/\delta \geq 10$ is desirable, this resolution may not be necessary based on the results of validation work summarized in Chapter 3. Additionally, this degree of resolution may not be feasible for industry in terms of the required computation time in all cases. Therefore, the sensitivity of the results to the selected grid size will also be evaluated by reducing the grid size and comparing the simulated results in order to justify the selected value.

Simulated temperature and velocity results are compared to available correlations outlined in Chapter 2, as a means of assessing the simulated results. It is cautioned however that this will be an order of magnitude evaluation only since the available correlations do not provide the spatial resolution necessary to fully describe complex geometries.

Where the response time of thermal detectors in the ceiling recession configuration is determined to be less than or equal to that the prescriptive design case (i.e. draft stops), the proposed alternative design can potentially be considered reasonable with respect to this performance criteria. In the end, it is the responsibility of the designer to determine whether the relative performance is sufficient for the scenario under consideration.

6 CASE STUDY

In this Chapter the analysis methodology proposed in Chapter 5 was applied to two theoretical ceiling recession configurations in order to evaluate the use of the proposed methods as a basis for design decisions in industry. The intent of this analysis is to demonstrate and assess the proposed methodology for the evaluation of alternative solutions involving ceiling recessions for various configurations for vertical floor opening protection.

First, the two selected ceiling recession geometries are described and the FDS model setup is detailed. Temperature, velocity, and thermal detector response times were predicted using the model. The results for the two configurations were compared in order to evaluate the ability of FDS to account for small dimensional differences in the selected geometries, as this ability will be a key requirement of an industry appropriate analysis method.

Following this, an evaluation of thermal detector response time for a standard draft stop configuration is conducted and the results are compared to the two ceiling recession designs. Conclusions regarding the appropriateness of the analysis method are then drawn.

6.1 Description of Experimental Compartment

6.1.1 Geometry

For the purposes of this analysis, a compartment was modeled in FDS with dimensions based on common situations in industry for which a ceiling recession solution might be sought. Figure 6-1 and Figure 6-2 provide plan and sectional schematics of the ceiling recession and draft stop compartments selected for this analysis.

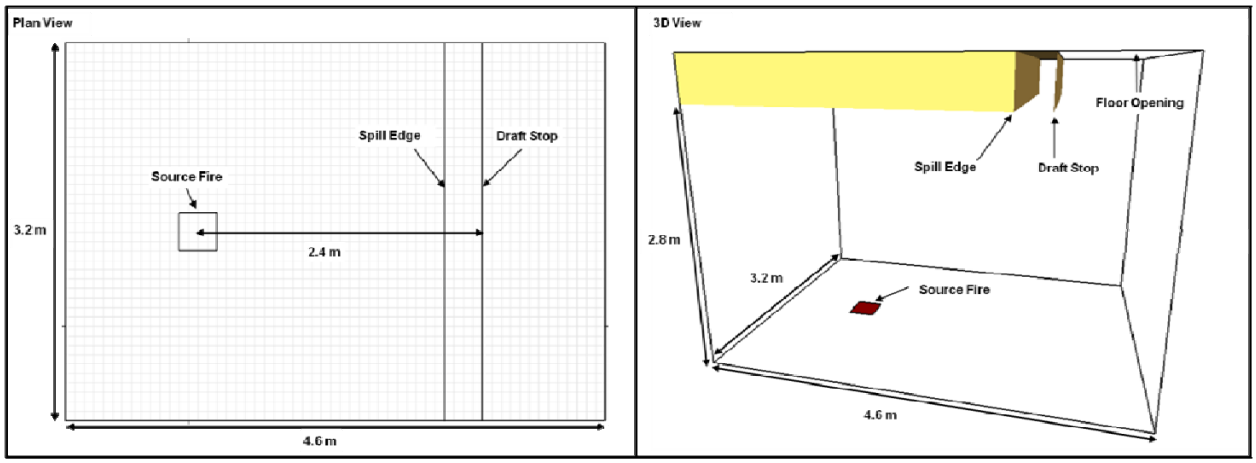

Figure 6-1: Ceiling recession compartment layout - plan and 3D views

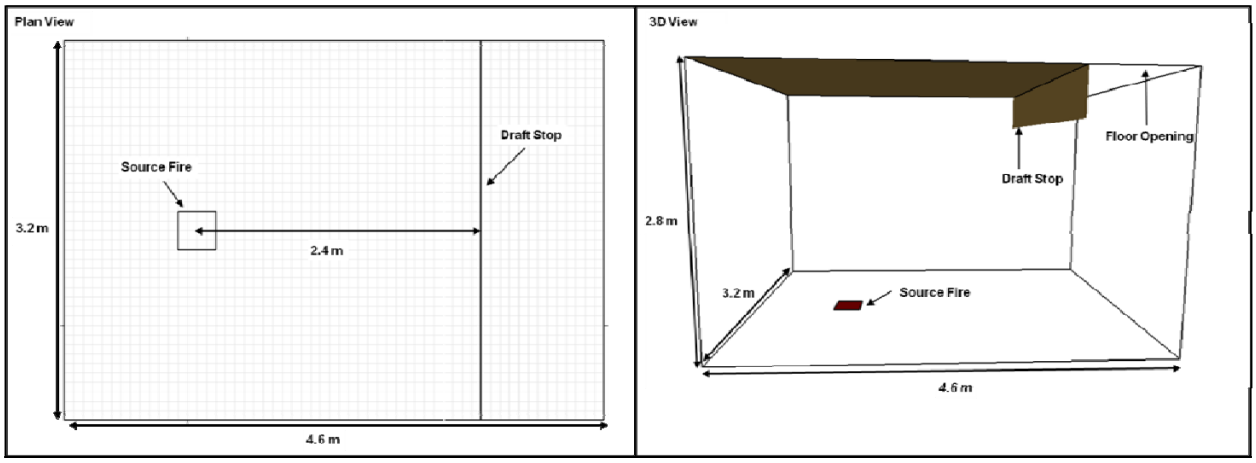

Figure 6-2: Draft stop compartment layout - plan and 3D views

For all simulations, the fire compartment was sized so as to minimize interactions between the fire plume and the compartment boundaries. The lower ceiling height for the compartment was chosen to be 2.8 m, a common ceiling height.

The length and width of the compartment were based on two factors. First, in order to minimize the impact of the compartment boundaries on the development of the ceiling jet, the compartment needed to be of sufficient size such that the source fire could be located at a distance greater than or equal to the turning radius of the fire plume. For a ceiling height of 2.8 m the resulting turning region of the plume would be equal to 0.504 m based on Alpert's definition of the turning region [12]. Second, the compartment needed to be large enough such

that the source fire could be located at a reasonable distance from the vertical floor opening and the flow characteristics at the floor opening could be observed. A distance of 2.24 m was selected as a reasonable representation of the distance which could be expected between a source fire and a sprinkler head in an NFPA 13 compliant design based on the maximum sprinkler spacing requirements of that standard [6]. A distance of 1.0 m beyond the edge of the ceiling was considered sufficient to allow for the observation of the ceiling jet flow based on the experimental observation of horizontal flow projections by Harrison [33].

Based on the above considerations and the requirement in FDS that the compartment dimensions match the selected grid size, the final dimensions of the fire compartment were chosen as 4.60 m x 3.20 m x 2.8 m.

The total height of the compartment had to be varied in order to accommodate differing depths of the ceiling recession configurations (see below). However, in all simulations the height of the lower ceiling (2.8 m) was held constant in order to facilitate comparison of the results based on consistent development of the hot ceiling jet from the fire plume.

As discussed in Chapter 2, the development of the hot layer within a fire compartment will significantly impact the actuation time for thermal detectors. Therefore, in order to remove any potential impact of hot layer formation due to the specified size of the enclosure, the side boundaries of the computational domain were modeled as open vents. This permits the ceiling jet gases to exit the domain upon reaching a side boundary, similar to a large enclosure such as a theatre or retail mall.

The floor of the compartment was modeled as an inert obstruction in order to reduce the required computational time for each simulation. This is a common modeling assumption and reasonable approximation since heat transfer to the floor will not significantly impact the formation or characteristics of the ceiling jet. The ceiling obstruction was modeled as 15.9 mm thick gypsum board such that heat transfer to the ceiling would be accounted for. For further discussion on this selection see Section 6.5 below.

6.1.2 Source Fire Definition

The source fire for all configurations was represented by a square burner with dimensions of 0.32 m x 0.32 m in order to align with the selected grid size. The source fire was located at the floor of the compartment with its center located 2.4 m horizontally from the draft stop.

Two different source fires were used in the simulations with fire heat release rates selected to represent reasonable minimum and maximum fire sizes for building fires in occupancies similar to theatres or retail malls, where vertical floor openings are common architectural features. Based on the height of the compartment (H=2.8 m), the radial distance between the source fire and the thermal detector within the ceiling recession (r=2.24 m), and the sprinkler activation temperature, a minimum fire size expected to cause sprinkler activation can be estimated from Alpert's unconfined ceiling jet correlation for values of r/H > 0.18:

$$T_g - T_\infty = 16.9 \frac{\dot{Q}^{2/3}}{H^{5/3}} \qquad [6\text{-}1]$$

Based on this calculation, the minimum heat release rate (fire size) necessary for detector activation would be approximately 334 kW.

A maximum fire size of 3000 kW was selected as a representative and reasonable fire size for a floor area containing ordinary combustible contents (i.e. furniture, merchandise, etc.). Based on fire testing of common combustible materials summarized in Section 1, Chapter 3 of the 4th edition of the SFPE Handbook [87], a 3000 kW fire is similar to the maximum heat release rate that would be produced by a 2 m by 2 m high magazine rack fully loaded with combustible products.

The selection of a specific fire growth rate was not considered to be critical to the present analysis since the performance of each ceiling configuration was evaluated relative to other scenarios. For all scenarios, then, the source fires were specified to reach the maximum heat

release rate 30 seconds after the initiation of the simulation[1]. This ensured that steady state conditions were achieved early in the simulation, such that the total required simulation times could be reduced.

All simulations were run for 500 s in order to allow steady state conditions to develop in the compartment and to ensure that the thermal detector(s) would actuate in the low heat release rate fire scenarios.

6.2 Description of Ceiling Configurations

6.2.1 Ceiling Recessions

Architecturally it is ideal for the ceiling recession to be as small as possible in order to minimize the overall ceiling space. From this standpoint, a recession that is just wide and deep enough to contain the required thermal detectors would be considered ideal. In reality, however, the dimensional limitations for the spacing of sprinklers in relation to mandated draft stops are applicable to any alternative design in order to ensure that the intended pattern of sprinkler discharge is provided. Therefore, the dimensional requirements outlined in NFPA 13 were utilized to determine the dimensions of a reference situation based on the "minimum" ceiling recession dimensions which would also permit the proper installation of sprinklers. In this respect, closely spaced sprinklers must be located not less than 152 mm from the adjacent draft stop which is further required to be not less than 457 mm deep [6]. Based on acceptable values of D^*/δ (see Section 5.6), the grid dimension was set to 0.04 m on a side and the recession dimensions were:

Recession depth	480 mm
Recession width	320 mm with detector centrally located
Draft stop depth	480 mm

Using the minimum recession configuration as a baseline, two ceiling recession configurations were developed. Table 6-1 summarizes the key dimensional properties of each configuration.

[1]This growth rate is not intended to be representative of an actual fire.

Figure 6-3 and Figure 6-4 provide two dimensional schematics of the ceiling recession layouts under study.

Table 6-1: Ceiling recession configuration dimensional parameters

Configuration #	Recession Depth (mm)	Recession Width (mm)	Draft Stop Depth (mm)	Distance from Detector to Upper Ceiling (mm)
1	480	320	480	40
2	240	320	480	40

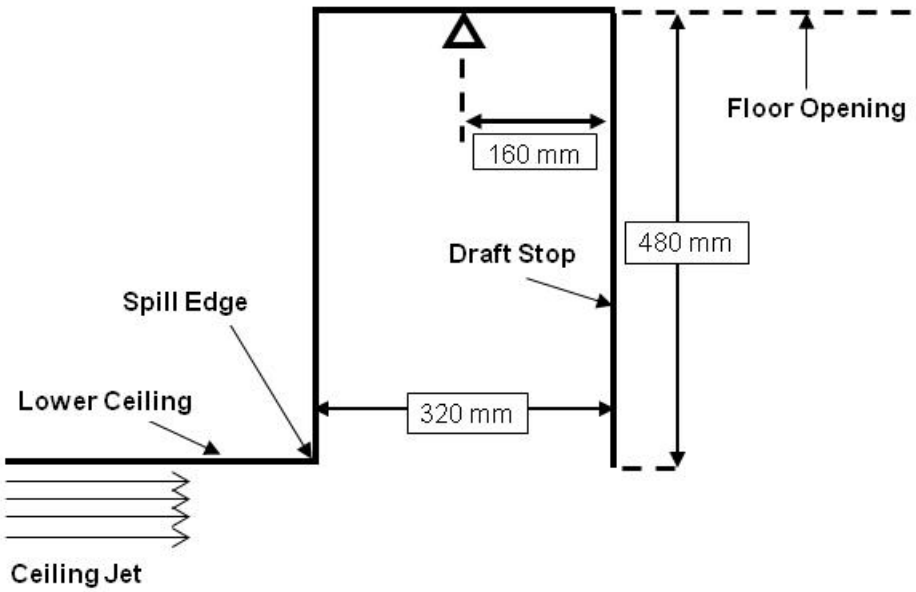

Figure 6-3: Configuration #1 - minimum ceiling recession

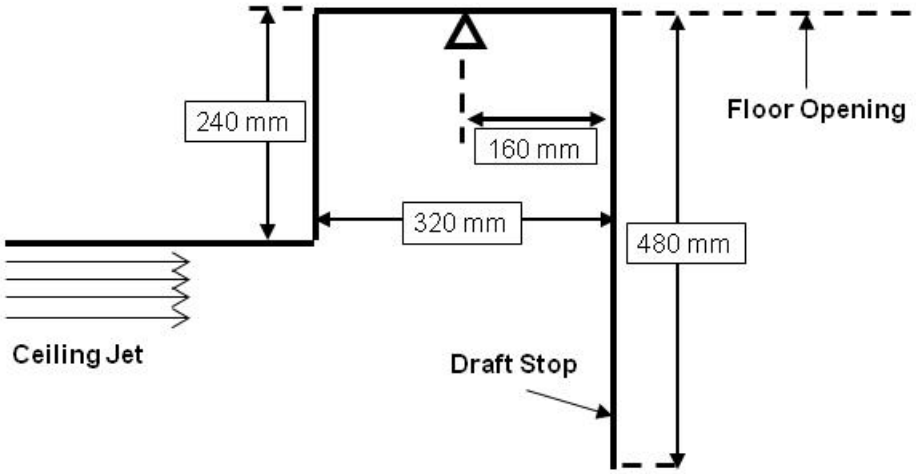

Figure 6-4: Configuration #2 - 50% recession depth decrease with full height draft stop

For each configuration, the horizontal distance between the thermal detector and the draft stop was 160 mm in order to isolate the dimensional modification and study its impact on the analysis. Similarly, the distance between the thermal detector and the ceiling level was kept constant at 40 mm such that it would be located within the volume of the cell immediately below the ceiling based on the selected grid size (see below).

6.2.2 Draft Stop

The dimensional limitations outlined in NFPA 13 for the design of draft stops were utilized to develop the standard draft stop scenario. Similar to the ceiling recession configurations, dimensional were altered slightly in order to ensure the selected design would fit the numerical grid in FDS. Figure 6-5 provides a schematic of the selected draft stop configuration.

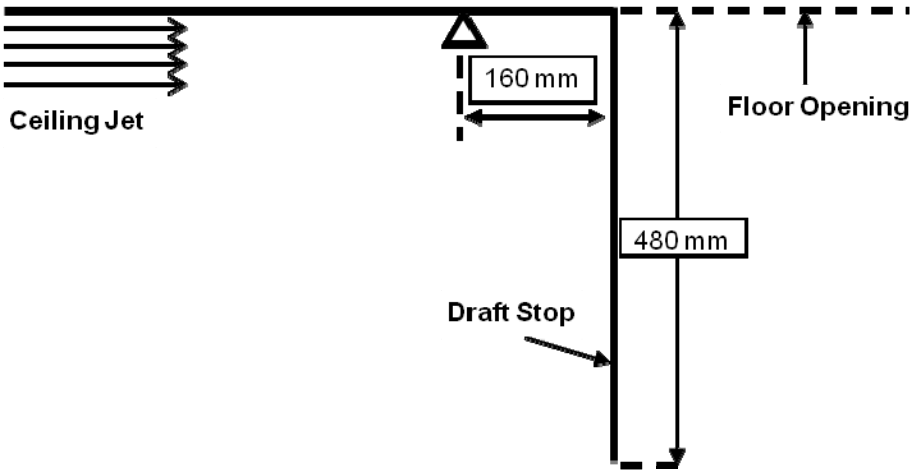

Figure 6-5: NFPA 13 compliant draft stop configuration

Further, the depth of the draft stop (480 mm), the distance between the draft stop and the detector (160 mm) and the distance between the detector and the ceiling level (40 mm) used in the draft stop configuration are the same as those applied in the recession configurations discussed above.

6.3 Simulation Measurements and Instrumentation

Predicted values of temperature and velocity at selected locations were used to compare the selected ceiling recession configurations and the draft stop configuration. Similarly, thermal detectors were simulated and their predicted response times were compared.

Temperature values were monitored within the domain utilizing simulated thermocouples implemented based on the default FDS parameters as follows:

Bead Diameter	1 mm
Bead density	8908 kg/m^3
Bead Specific Heat	0.44 kJ/kg*K
Emissivity	0.85

In order to evaluate the temperature distribution, six thermocouples were located within the recession 160 mm away from the draft stop and centered with the source fire, spaced at vertical

intervals of 80 mm from the ceiling of the recession down to the lower ceiling level (i.e. at z= 80 mm, 160 mm, 240 mm, 320 mm, 400 mm, and 480 mm). An additional thermocouple was located at the spill edge of the recession, centered on the source fire, located 80 mm below the lower ceiling level. The additional thermocouple measurement was provided in order to allow for a temperature comparison upstream of the spill edge using available ceiling jet correlations as an order of magnitude assessment of model accuracy. The measurement location of 80 mm below the lower ceiling was selected based on temperature results from Chapter 4, where temperatures were found to be well represented by the model at elevations of 40 mm to 100 mm below the ceiling.

Velocity values within the domain were monitored using simulated gas-phase detectors set to output 'Velocity' within FDS. These 'detectors' were located at the same locations as the thermocouples in the recession and at the spill edge of the recession as described above.

The thermal detectors for each analysis were modeled as heat detectors with activation temperatures of 74°C and RTI of 100 $(m*s)^{1/2}$, values which are representative of standard response sprinklers [6]. Heat detectors were used in the present analysis since the methods used by FDS for determining device actuation is identical for heat detectors and sprinklers, and evaluation of the interactions between sprinkler discharge and ceiling jet gases is outside the scope of this research. Therefore, by modeling the sprinklers as heat detectors, the flow and thermal characteristics within the compartment will not be altered during activation of the detector.

For all evaluations one heat detector was located 40 mm below the ceiling level and positioned 160 mm from the draft stop. This location for the detector was considered appropriate based on the results of the validation studies in Chapter 4, which found good agreement between experimental and simulated results at positions close to the ceiling. It is noted that the study in Chapter 4 indicated that FDS velocity predictions at this elevation (z=40 mm) were significantly less than available experimental values. One potential cause for this discrepancy was the location of the lower boundary of the ceiling jet in relation to the measurement location and the resulting prediction of velocity at that location. For the ceiling height (H=2.8 m) and radial

distance (r=2.24 m) applied here (see below), the ceiling jet thickness at the measurement point will be approximately 261 mm based on Equation 4-1[2]. Therefore, it is expected that the measurement location will be fully immersed in the ceiling jet flow (at the lower ceiling level or in the recession), precluding this source of error. Additionally, since a comparative performance evaluation is sought, it is assumed that the predicted thermal detector response times relative to one another will not be significantly impacted by the location of the lower boundary of the ceiling jet.

For configurations #1 and #2 an additional heat detector with the same thermal properties was located at the spill edge of the recession 40 mm below the lower ceiling level and centered on the source fire. The intent of these detectors was to allow for a comparison of thermal detector actuation upstream of the spill edge.

Based on the selected grid size of 0.04 m, temperature and velocity values closer to the ceiling than z=40 mm (i.e. 20 mm) will be equal to those at 40 mm, as they are located within the same cell as the specified detector location.

Figure 6-6 to Figure 6-9 provide illustrations of the selected measurement locations for the ceiling recession simulations and the draft stop simulation.

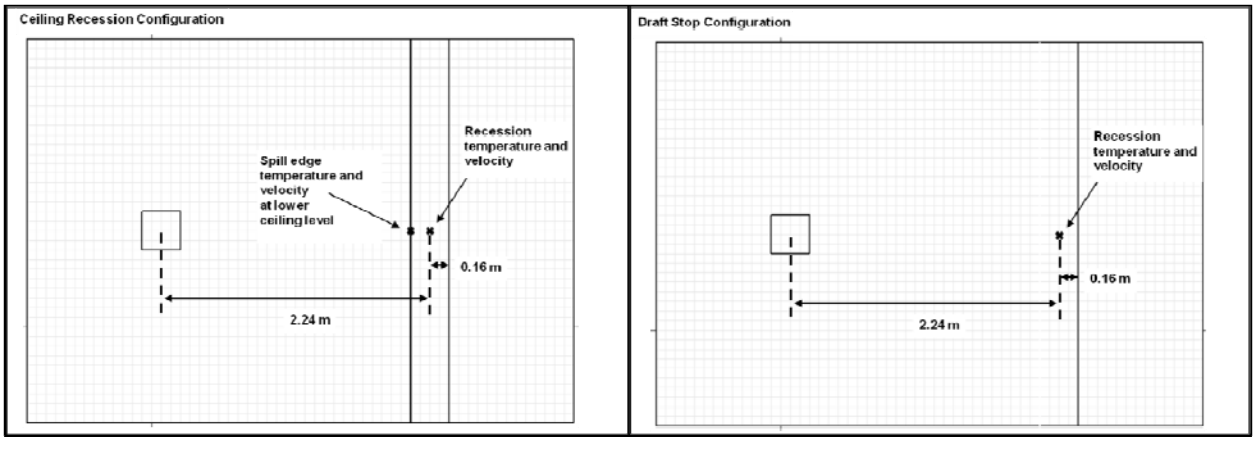

Figure 6-6: Measurement locations - plan view

[2]Order of magnitude evaluation only - Equation 4-1 was not developed for complex geometries

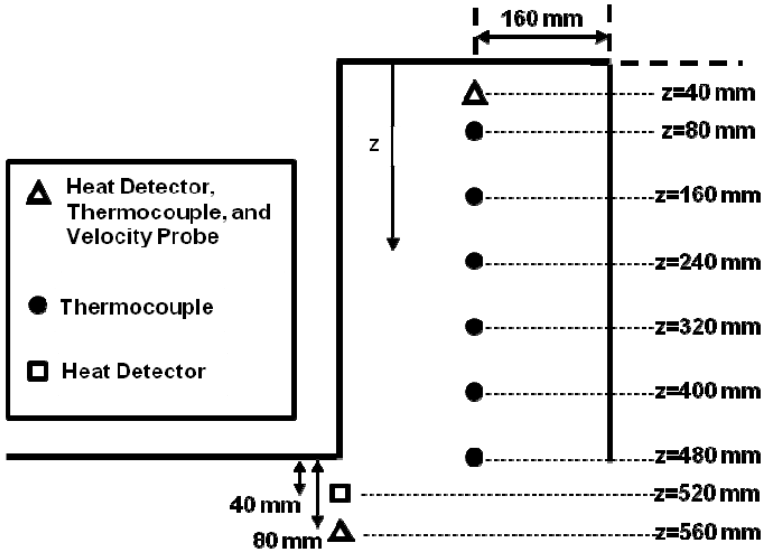

Figure 6-7: Configuration #1 measurement locations - section view

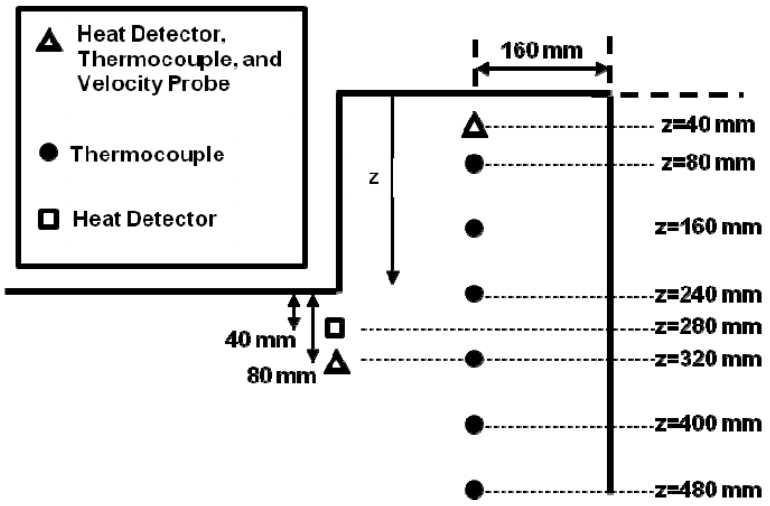

Figure 6-8: Configuration #2 measurement locations - section view

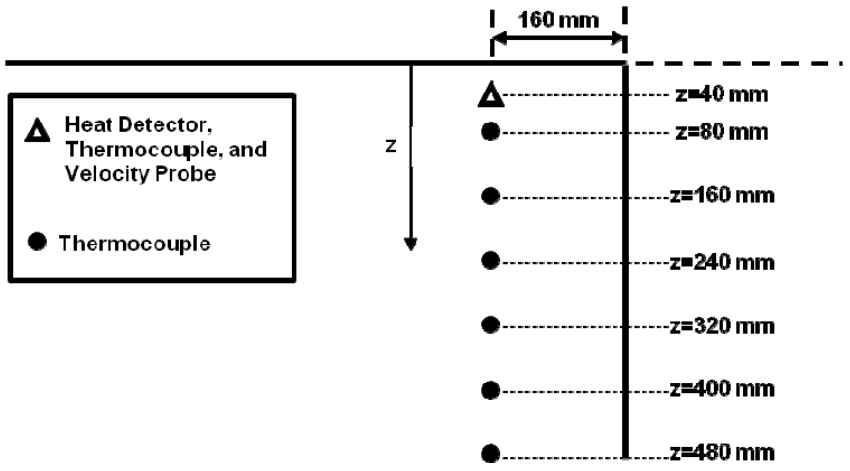

Figure 6-9: Draft stop measurement locations - section view

6.4 Grid Size and Mesh Layout

Validation work conducted in Chapter 3 for a 2 kW fire found that the model would provide reasonable estimates of temperature and velocity values close the ceiling for values of D^*/δ of approximately 4 – 8. It was also concluded that ratios of D^*/δ exceeding 8.0 may be required to achieve representative results for temperature and velocity further from the ceiling. To achieve a value of D^*/δ =8.0 for a fire heat release rate of 334 kW, a grid size of approximately 0.08 m (in all directions) would be required based on Equation 3-1. Utilizing this grid size, configuration #1 would contain 4 cells across the width, and 6 cells across the depth of the recession. Therefore, a grid size of 0.08 m^3 is considered the maximum size which would be reasonable for the present analysis.

For the LES turbulence model employed by FDS, turbulent eddies larger than the selected grid size are calculated directly, while sub-scale eddies are ignored by the model. In this context, a grid size as large as 0.08 m on a side may not be appropriate to resolve the flow within the ceiling recession, since the number of cells contained within the recession is very limited.

A grid size of 0.04 m^3 was therefore selected for the analysis, resulting in D^*/δ ratios of 16 and 38 for the 334 kW and 3000 kW fire scenarios respectively. This grid resolution results in a total of approximately 577,600 to 632,800 cells within the computational domain depending on the

configuration being analyzed. Given the results of the validation study in Chapter 3 and this number of computational cells, it was anticipated that this grid size would result in reasonable temperature and velocity predictions near the ceiling and provide a sufficient resolution for the turbulence model, whilst keeping the total computational time within reasonable limits.

To provide comparative results and evaluate the grid sensitivity for the ceiling recession configuration, an additional model run of configuration #1 with a fire heat release rate of 334 kW was conducted utilizing a grid size of 0.02 m^3. This grid size results in a D^*/δ ratio of 32 and a total 5,062,400 cells within the domain.

All simulations were conducted using a single mesh for the entire computational domain such that interfaces at mesh boundaries would not impact the predicted results.

6.5 Assumptions and Simplifications

6.5.1 Surface Materials

As discussed in Section 2.5.1.7, previous experimental work has shown that heat transfer between the ceiling jet and the ceiling primarily takes place within the turning region of the fire plume, and is not heavily dependent on the ceiling material outside of the turning region (0.18H) of the fire plume [42, 44, 45]. The theoretical turning region for the selected compartment is 0.504 m which is less than the distance between the fire plume and the selected measurement location (r=2.24 m). Therefore, the material properties specified for the ceiling and ceiling recession boundary walls are not expected to greatly influence the relative results provided that consistent values are used for all scenarios.

All compartment ceiling, ceiling recession, and draft stop obstructions were assumed to be of 15.9 mm thick gypsum with the following thermal properties:

Density	930 kg/m^3
Specific Heat	1.09 kJ/kg*K
Conductivity	0.17 W/(m*K)

Emissivity 0.9

The floor of the compartment was specified as an inert surface. The temperature of the floor was therefore maintained at a constant temperature, equal to the ambient temperature of the room, throughout the simulation. Heat transfer between the compartment gases and the floor are calculated based on this simplification. This is a reasonable approach since heat transfer to the floor is unlikely to impact thermal detector activation at the ceiling level.

6.5.2 Combustion Reaction

The source fire fuel type is not considered critical to the current analysis since comparative results are sought. Therefore, default settings were utilized in specifying the combustion parameters for the burner. Source fires for all evaluations were assumed to be propane with specified fire growth rates and maximum heat release rates as discussed in Section 6.1.2.

6.5.3 Radiation Fraction

As discussed previously, radiative heat losses from the fire to the surrounding compartment are estimated via a user-specified, fixed percentage energy loss factor. The default value in FDS is 0.35, a value considered appropriate for most sooty hydrocarbon fires [61].

The value of radiative fraction used in this analysis was not considered to be critical since only comparative results were sought between scenarios with identical source fires. Therefore, a constant value of radiative fraction of 0.35 was used for all scenarios modeled in this section.

6.5.4 Turbulence Model

The LES turbulence model was utilized for the analysis, with no alterations to the default parameters. This was considered reasonable on the basis that validation studies conducted by the author (Chapter 4.0) and others [62, 75, 77] have indicated that this model will provide temperature and velocity results which are in general agreement with experimental data close to the ceiling.

6.5.5 Ambient Temperature

Ambient temperature for all scenarios was set to 20 °C (293 K).

6.6 Grid Sensitivity

Before beginning the bulk of the calculations conducted for this research, Configuration #1 (minimum ceiling recession) was modeled for two grid sizes in order to assess whether predictions would be independent of the grid size chosen and also to verify that a grid size of 0.04 m^3 would be appropriate for the analysis. The 0.04 m^3 grid scenario consisted of 754,400 cells and took 53 hours (2.2 days) of computation time running on an Intel i7 Quad Core Processor with 8 Mb RAM. It is noted that for a single mesh simulation, FDS will only utilize a single processor for the simulation. In contrast, the 0.02 m^3 grid scenario contained 5,062,400 cells and was run on an Intel i7 Quad Core Processor with 8 Mb RAM. After 602 hours (25 days) of computation time a power outage disrupted the simulation after 419 seconds of the total 500 second model run time. An attempt to utilize the FDS restart function yielded unstable results so the available data from the initial simulation has been utilized in the following discussion for the grid sensitivity study.

During the grid sensitivity assessment, all surfaces in the computational domain were specified as "inert" in attempts to reduce the complexity of the model and thereby reduce the computation time required, especially for the 0.02 m^3 grid size case. In FDS, an inert surface is maintained at throughout the simulation at ambient temperature. However, it is important to note that this boundary condition does allow for heat transfer between the compartment gases and the surface (i.e. the surface is not adiabatic), but this heat transfer does not change the temperature of the surface. Therefore, the use of this boundary condition results in higher heat losses between the compartment gases and the surface since the rate of heat transfer is not impacted by a rise in temperature of the surface. For the same reasons, some measurement locations were also removed. This is a reasonable simplification given that the goal of this part of the evaluation was to determine the impact of grid size, and not to evaluate the response of thermal detectors.

The following measurements were monitored for each scenario:

- Heat detector at the spill edge, located 40 mm below the lower ceiling (z=520 mm)
- Heat detector centered in the recession, located at 40 mm below the recession ceiling (z=40 mm)
- Velocity and temperature at the spill edge, 40 mm (z=520 mm) and 80 mm (z=560 mm) below the lower ceiling
- Velocity centered in the recession at z=40 mm

The results of these simulations are plotted and discussed below.

6.6.1 Temperature Results

Figure 6-10 provides a comparison of predicted gas temperature results for the full scenario using a 0.04 m^3 grid and the data available for the 0.02 m^3 grid. Also plotted in Figure 6-10 is the maximum temperature expected in an unconfined ceiling jet as calculated using Equation 2-1 with the following input parameters:

Q	334 kW
r	2.08 m
H	2.8 m
ρ_∞	1.2 kg/m^3
C_p	1.0 kJ/kg K
T_∞	293 K

Equation 2-1 will be applicable at this location, right at the spill edge, since the ceiling jet has not encountered any obstructions and the flow will closely resemble that of an unconfined ceiling jet.

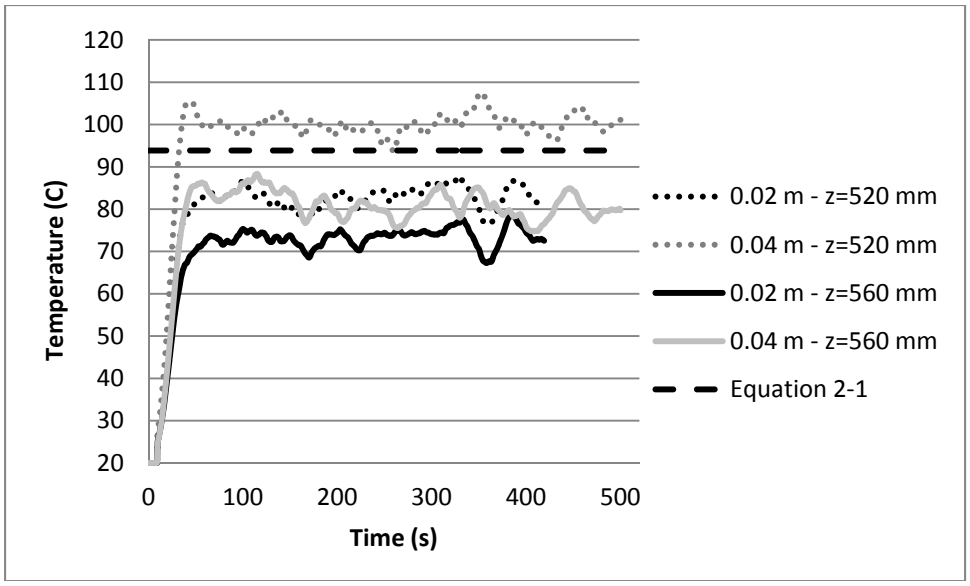

Figure 6-10: Gas temperature at recession spill edge

The reduction in grid size serves to decrease the predicted temperature with respect to the 0.04 m grid results at the spill edge by an average of 9.3% at steady-state 80 mm below the spill edge (z=560 mm). This trend was also observed at 40 mm below the spill edge (z=520 mm) but at a larger magnitude with an average reduction of 18.5% at steady-state. In most cases the simulated temperatures are less than the value predicted by Equation 2-1. This is not an unexpected result since Equation 2-1 predicts the maximum ceiling jet temperature at a given radial distance from the source fire, and does not account for the vertical location of the measurement point. Higher temperatures would be expected closer to the ceiling as is observed for the z=520 mm location where the gas temperature for the 0.04 m^2 grid size is slightly over predicted by the model in comparison to Equation 2-1. For the 0.02 m^2 grid case at z=520 mm the reduction in predicted temperature yields gas temperature results below the maximum value predicted by Equation 2-1. Based on this comparison, the model provides a reasonable approximation of the expected ceiling jet temperature. However, the importance of grid size selection is again highlighted with significant reductions in predicted temperature as a result of a reduction in grid size.

Figure 6-11 and Figure 6-12 provide a comparison of predicted heat detector temperatures at the spill edge and in the recession for the full scenario using a 0.04 m^2 grid and the first 419 s of the scenario for the 0.02 m^3 grid. Again, the result of Equation 2-1 is plotted in Figure 6-11 for reference. It must be noted however that in this case the results of the model and Equation 2-1

are not providing an estimate of the same value. Since the simulated data is the predicted temperature of the heat detector its temperature rise is impacted by the flow velocity and the thermal mass of the detector link. Therefore, agreement between Equation 2-1 and the simulated heat detector temperature would only be expected at steady state once sufficient time had elapsed to allow the heat detector link temperature to be equal to the steady-state gas temperature.

It is clear that the reduction in grid size serves to decrease the predicted temperatures for both measurement locations. Where the results for the reduced grid size are taken as the "real" results, the average prediction error for the spill edge heat detector temperature and the recession heat detector temperature are 17% and 12%, respectively. Although the change in grid size did produce a significant change in the magnitude of the predicted temperatures, the overall trends are similar, as evidenced by the similar shape of the time-temperature curves for both grid sizes.

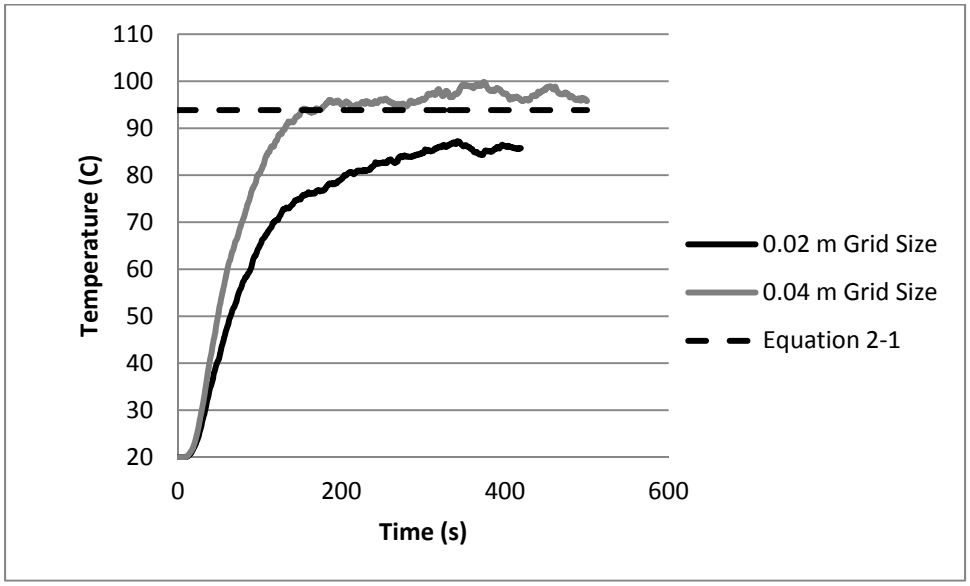

Figure 6-11: Heat detector temperature at spill edge, 40 mm below ceiling (z=520 mm)

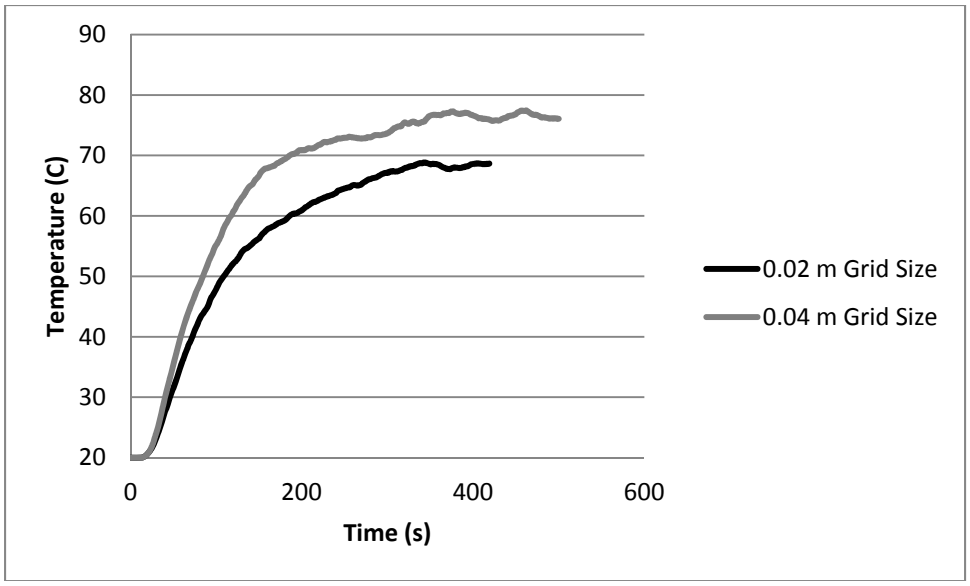

Figure 6-12: Heat detector temperature within ceiling recession at z=40 mm

The larger grid size provides better agreement with the results of Equation 2-1. However, it is important to note that the result of Equation 2-1 cannot be directly compared to the predicted results since that equation provides an estimate of the maximum ceiling jet temperature for this radial location, which may not occur 40 mm below the ceiling. Additionally, as noted above, the comparison is only valid at steady-state since Equation 2-1 does not predict heat detector link temperature. Therefore, the result of Equation 2-1 can only be viewed as an order of magnitude estimation of the expected results. In this context, the results of the model using the larger grid size provide reasonable agreement with accepted theory for unconfined ceiling jets.

It is important to note that, as discussed in Section 6.6, since inert surfaces were utilized for this analysis, predicted temperatures are expected to be lower than those predicted with material properties assigned to the ceiling and ceiling recession obstructions due to an increase in heat losses between the ceiling jet and the ceiling.

Overall, temperatures determined using the simulation on a coarser grid size of 0.04 m on a side appears to be over-predicted in comparison to those for a finer grid. Within the scope of the current research, this means that thermal detector response times predicted by the model using a grid size of 0.04 m on a side will be faster than would be produced if a more refined grid were

used. The fact that the shape of the time-temperature curves for both grid sizes are similar suggests that provided the same grid size is applied for all scenarios, the predicted thermal detector response times will not be significantly impacted relative to one another. From this standpoint, the coarser grid was considered sufficient for the purposes of evaluating temperatures in this analysis.

6.6.2 Velocity Results

Predicted velocities for both grid sizes are plotted as functions of time for comparison in Figure 6-13 and Figure 6-14. The maximum ceiling jet velocity as estimated using Equation 2-3 is also provided in Figure 6-13 as an order of magnitude comparison for the predicted velocity values.

The velocity results produced by FDS were subject to a high degree of variability, similar to that noted for the validation study (Chapter 4). The velocity values plotted in Figure 6-13 and Figure 6-14 were therefore averaged across 20 seconds, using a moving average of data for 10 sec preceding and 10 seconds following the point of interest.

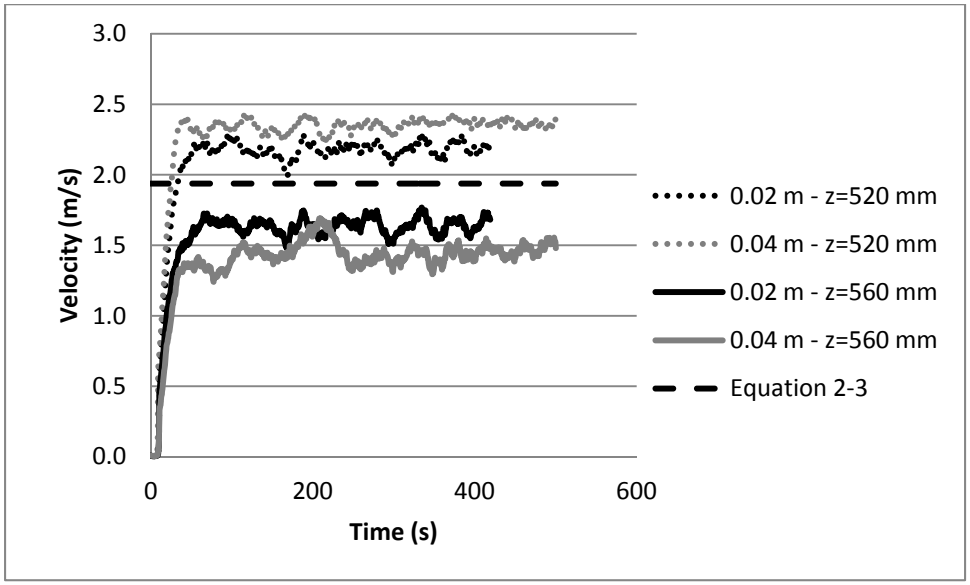

Figure 6-13: Velocity at the spill edge

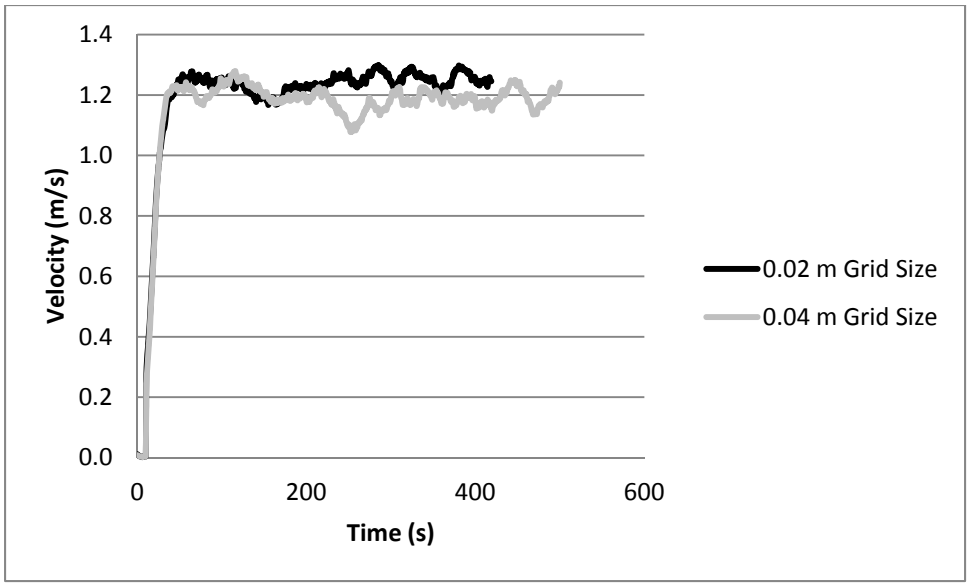

Figure 6-14: Velocity in the ceiling recession at z=40 mm

The results for both measurement locations show that the overall trends in predicted velocity with time are not significantly impacted by the reduction in the grid size. Overall, it appears that utilizing the coarser grid size 80 mm below the ceiling (z=560 mm) results in slight under prediction of the velocity at the spill edge compared to that estimated using the finer solution grid with a steady state average percent difference of 13.1%. This is also observed in the ceiling recession velocity results shown in Figure 6-14. At 40 mm below the ceiling level (z=520 mm) the trend is reversed with the courser grid size providing a slight over prediction of velocity in comparison to the finer grid case. At this measurement location, the steady state average percent difference was determined to be 7.8%. It is noted that in the course grid case, z=520 mm represents the uppermost cell below the lower ceiling. Therefore, the reversal in velocity trends at this location may be due to the requirement of FDS to apply a sub-model (Werner-Wengle wall model) for near ceiling velocity as noted in Section 2.5.4.3. However, since the magnitude of the predicted velocity is similar for both grid sizes and the small variation is unlikely to impact predicted heat detector activation times of primary importance to this work; further analysis was not conducted. For both grid sizes, reasonable agreement is provided between predicted values at the spill edge and the theoretical maximum velocity predicted by the correlation of Equation 2-3. Again, since Equation 2-3 does not necessarily provide a good estimate the velocity at a given vertical distance below the ceiling, a direct comparison of the

predicted velocity to this value is not applicable. However, the expected trend for ceiling jet velocity is well represented here, with high velocity observed closer to the ceiling.

Based on the velocity results above, grid independence appears to have been achieved even with a grid size of 0.04 m^3 for all measurement locations evaluated. Although slight changes in trend were observed between the coarse and fine grid results, the overall magnitude of the predicted velocity is not significantly altered. At 80 mm below the spill edge of the recession, the average percent velocity difference between the 0.02 m grid data and the 0.04 m data was 10.9%. A percent difference of 4.9% was determined for the location 40 mm below the ceiling recession upper surface.

6.6.3 Conclusion

Based on the results of the grid sensitivity study, the application of a grid size of 0.04 m^3 was deemed appropriate for the comparative analysis of the velocity and temperature distributions, as well as the thermal detector response time for the various ceiling recession configurations under investigation. Although temperature results were impacted by a reduction in grid size, overall trends were well represented such that relative results from the necessary simulations should not be significantly impacted.

The use of a 0.04 m grid size was also considered an appropriate tradeoff in terms of computational time, since the increase in computation time required for the more refined grid of 0.02 m was significant, in fact it increased the computational time by a factor of 10, from 2.2 days to 25 days (for the incomplete simulation). Over the longer term, since one aim of the study is to develop evaluation tools that will be used in industry, the computational time taken for use of the finer grid size would render the method impractical for the evaluation of multiple scenarios in the context of industry designs.

Therefore, a grid size of 0.04 m in all axes was applied for all simulations discussed in the following sections.

6.7 Recession Configuration Performance Analysis

In this portion of the research, the selected ceiling recession configurations were simulated in FDS, using the model formulation and geometrical parameters in Sections 6.1 to 6.6. The intent of the analysis is to compare the relative performance of each recession design with respect to thermal detector actuation and thereby to evaluate the ability of FDS to resolve small dimensional changes to the recession configuration with respect to the impact on the response times of the detectors for fires with peak heat release rates of 334 kW and 3000 kW.

6.7.1 Analysis of Recession Flow for the 334 kW Source Fire

6.7.1.1 Overall Flow and Thermal Development for Recession Configurations

Figure 6-15 provides an illustration of the developing thermal patterns seen for Configuration #1 ceiling recession at various times with a 334 kW fire source. Figure 6-15 displays the predicted results via temperature "slices" taken at the centerline of the fire plume, with the bounds of the colour contours set from 20°C to 50°C for all frames as colour filled temperature contours.

The upper left hand picture in Figure 6-15 shows that when the ceiling jet encounters the spill edge of the recession at approximately t = 9.0 s, the hot gases continue to travel horizontally past the spill edge due to their momentum. Once the flow is no longer constrained by the ceiling, buoyancy forces cause a portion of the hot gases to rise into the recession, while the lower layers of the ceiling jet continue to move horizontally toward the draft stop (far) edge of the recession. Screen captures from t=9.5 s and t=11.0 s clearly illustrate the upward movement of hot gases into the ceiling recession as well as the horizontal projection of the ceiling jet across the opening of the recession. At t=11.0 s hot gases rising into the recession still contain significant horizontal momentum and encounter the draft stop on the far side of the recession. This forces the flow to travel vertically upward along the wall, higher into the recession. The process of flow impingement and rise of hot gases into the recession is clearly shown in the frames for t=13.0 s and later, indicated by the high temperatures that form along the inner wall of the draft stop. Also at times t=13.0 s and later, the horizontal projection of the ceiling jet beyond the draft stop is clearly visible, indicating that the entire ceiling jet flow does not enter the recession.

After the initial development, ceiling jet gases continue to flow into the recession and rise, forming a recirculating flow along the walls of the recession. This is indicated by the higher temperatures near the boundaries of the recession framing a central area of lower temperature gases. Upon further flow development, the temperature conditions within the ceiling recession become more uniform as steady-state is approached.

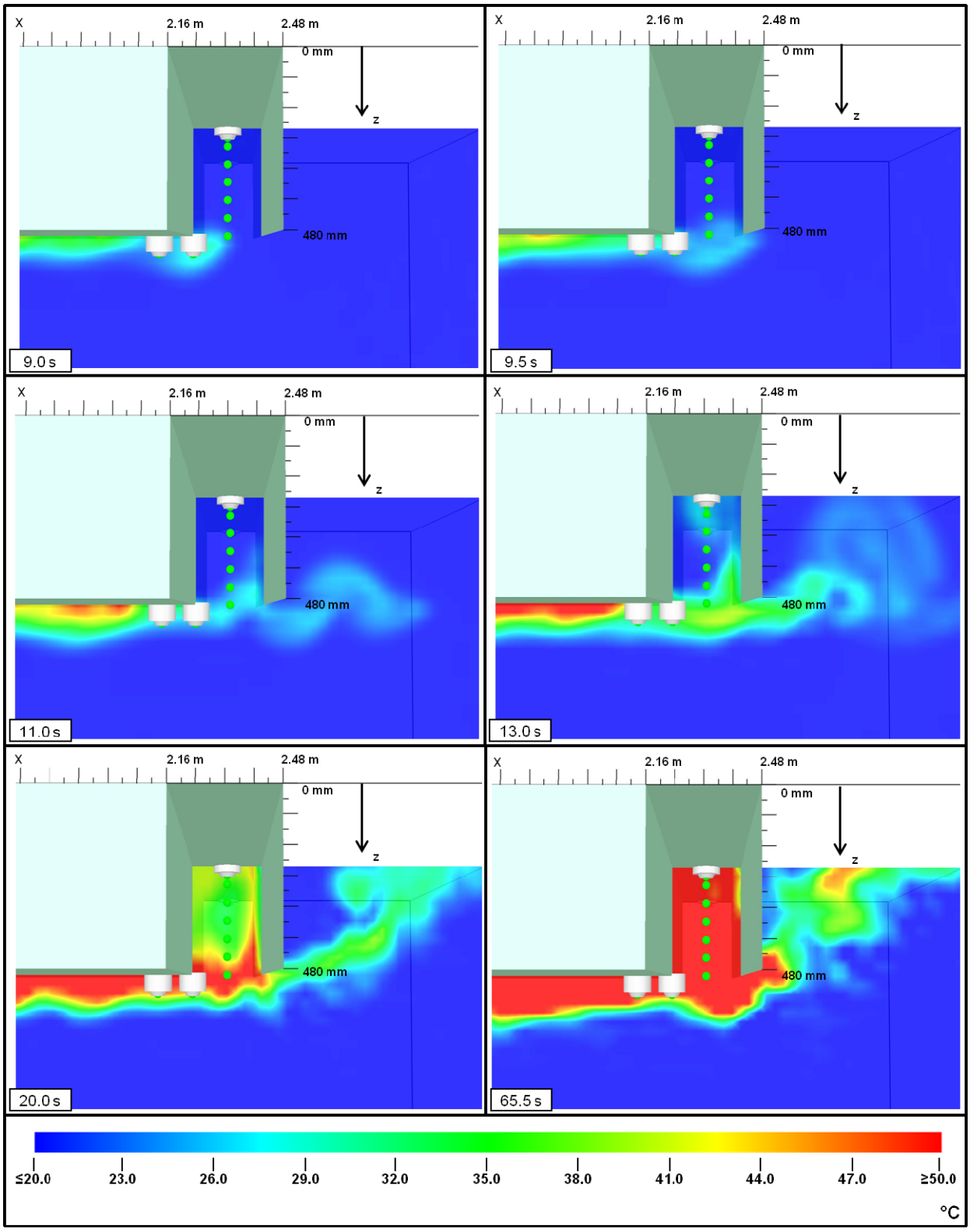

Figure 6-15: Development of recession flow - Configuration #1 – 334 kW source fire

Figure 6-16 provides an illustration of how the flow within the ceiling recession develops over time for Configuration #2 where there is a draft stop in place. The same temperature “slice" is plotted for the same time intervals as those shown in Figure 6-15 and the same bounds are used for the temperature data (20°C to 50°C) such that a direct comparison to Figure 6-15 can be made. It should be noted that the origin of "z" has been shifted for the plots in this configuration to coincide with the upper boundary of the recession.

Figure 6-16 shows that, similar to Configuration #1, when the ceiling jet encounters the spill edge of the recession the hot gases continue to travel horizontally, due to momentum, past the spill edge. Past the spill edge, portions of the ceiling jet flow begin to rise into the ceiling recession due to buoyancy. Upon impingement of the hot gases on the draft stop wall (occurring at approximately t=9.5 s) the flow moves up and down away from the impingement point along the draft stop. The upward portion of the flow moves into the recession and continues to follow along the recession boundaries forming a perimeter flow with a lower temperature core within the recession (t=13.0 s). The downward portion of the flow projects beyond the bottom of the draft stop, then begins to rise again due to buoyancy and travel up along the outside wall of the draft stop (t=20 s). As for the previous case, at later times in the flow development, hot gas temperatures within the ceiling recession become more uniform as steady-state conditions are approached.

Comparing Figure 6-15 and Figure 6-16, the impact of the draft stop on the developing flow can be clearly seen. At t=13 seconds in Configuration #1, the ceiling jet gases have started to rise into the recession but a majority of the recession is still at ambient (or near ambient) temperatures. Comparatively, at t=13 seconds for Configuration #2 a larger portion of the gases in the recession are at an elevated temperature at the bounds of the recession walls, while only a smaller volume of the flow centered in the recession is still at near ambient temperatures. The difference in flow characteristics can be attributed to the direct impingement of the ceiling jet on the draft stop causing more rapid filling of the recession, and the reduced physical size of the recession in configuration #2. These aspects of Configuration #2 result in a more rapid development of elevated temperature within the recession than is observed in Configuration #1.

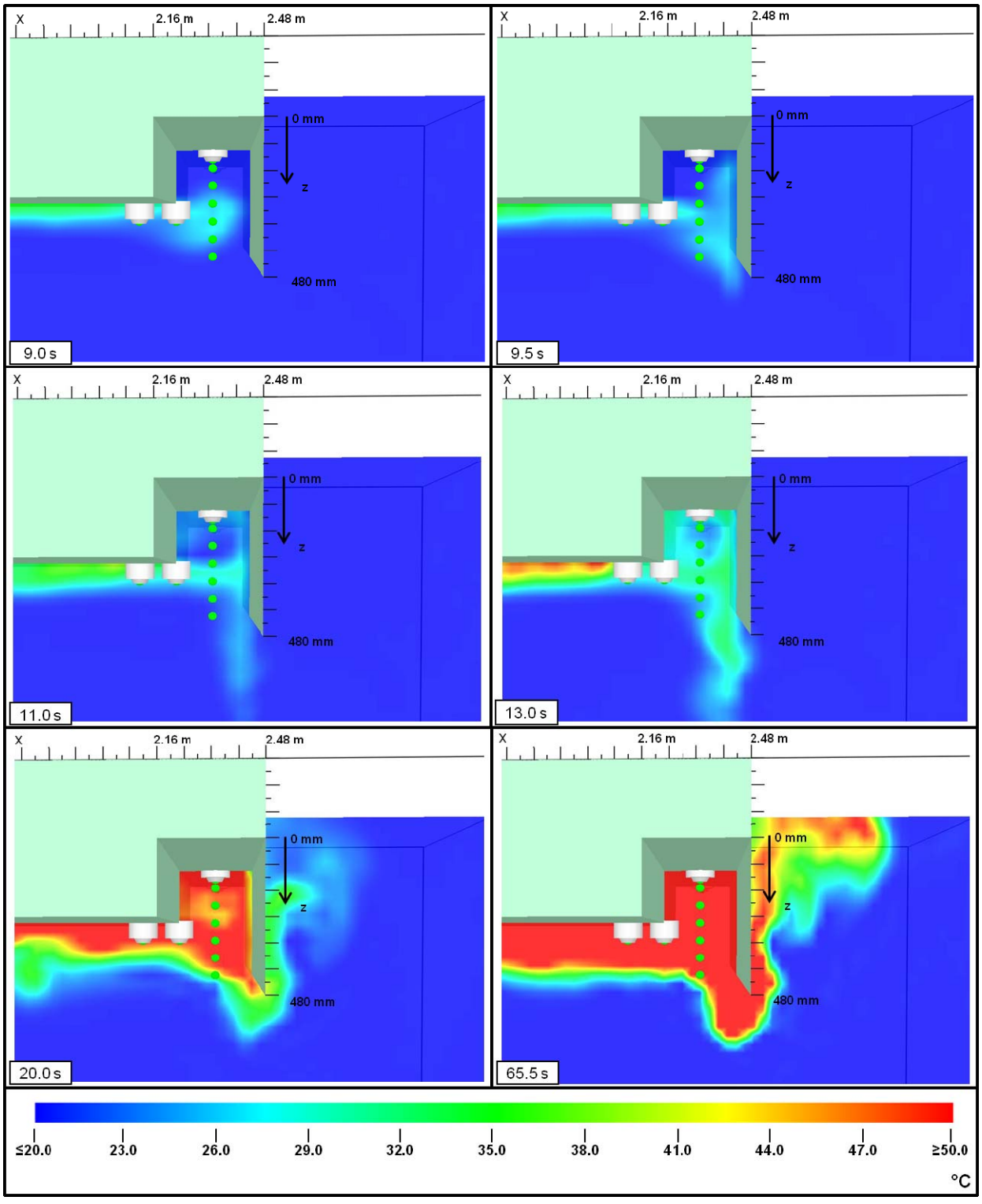

Figure 6-16: Development of recession flow - Configuration #2 – 334 kW source fire

6.7.1.2 Recession Flow Characteristics

Predicted values of temperature and velocity in the flow in the recession will govern the thermal detector actuation times predicted by the model. It is therefore of interest to compare the temperature-time and velocity-time traces predicted at the location of the detector (z = 40 mm) for each configuration. These are plotted in Figure 6-17 and Figure 6-18 and discussed in turn below.

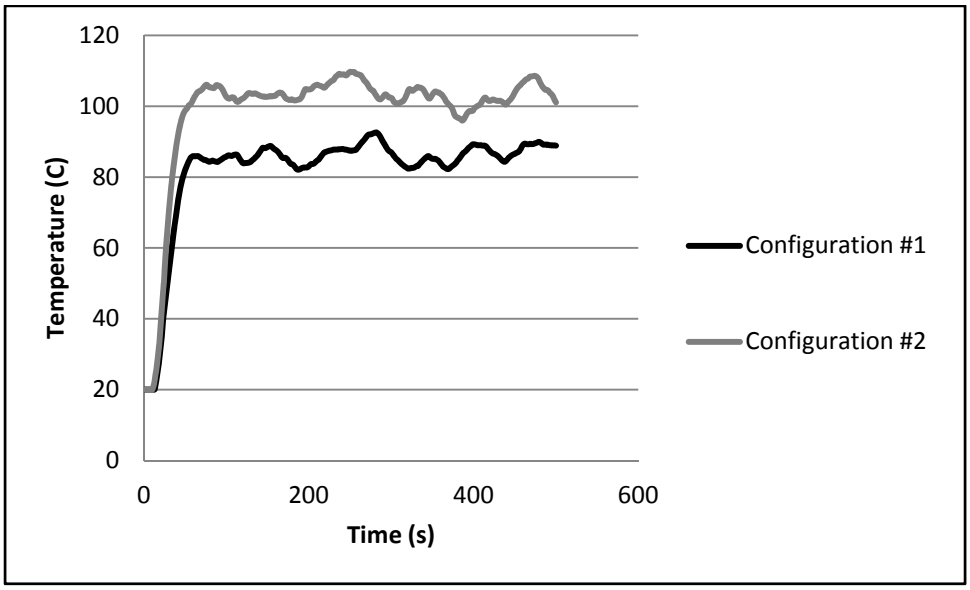

Figure 6-17: Recession temperature at z=40 mm

Figure 6-17 indicates that steady state temperature conditions are achieved in the recession in the area immediately around the thermal detector at approximately 75 seconds into each simulation. From the plot it can also be seen that the predicted temperatures are higher for Configuration 2 than for Configuration 1 at all times.

The high average steady-state temperature (i.e. the average temperature after t=75 s) of 104°C predicted at z = 40 mm for Configuration #2 is as expected since the ceiling jet directly impinges on and stagnates near the vertical midpoint of the draft stop. The draft stop effectively forms a barrier to any hot gases that, in Configuration #1, would immediately escape. From the impingement point, one portion of the gases flows upward along the wall, aided by buoyancy, and is trapped in the recession; the other flows downward along the wall acting against buoyancy

and eventually flows out around the bottom of the draft stop to ambient. The increased quantity of hot gases feeding into the confined area of the recession, as well as variations in heat transfer due to trapping of those gases, results in the faster increase and higher peak temperatures seen in Figure 6-16 for configuration 2. The temperature results alone suggest that the thermal detector should activate most quickly for this design, as long as the detector is located at (or near) the upper boundary of the recession.

In contrast, there is a significantly lower average temperature (86 °C) predicted at the detector in Configuration #1. This result may be caused by a larger portion of hot gases bypassing the recession due to the location and depth of the recession draft stop in relation to the lower ceiling level (i.e. the bottom of the draft stop is at the same elevation as the lower ceiling). Additionally, due to the decreased depth of the recession in Configuration #2, the hot gases fill the recess more quickly so that the temperature at z =40 mm also increases more quickly than for Configuration #1 as is evident in Figure 6-17.

In the case where the ceiling jet temperatures are low, values of local flow velocity will also have a significant impact on detector actuation time. Therefore, the predicted velocity time traces at z = 40 mm, the thermal detector location, for each configuration are plotted against one another in Figure 6-18.

The plots in Figure 6-18 clearly indicate that changes in the dimensions of the ceiling recession impact the flow velocities seen in the vicinity of the thermal detector. Significantly higher average steady-state velocities are predicted at the detector location for Configuration #2. If the magnitudes are comparative, velocities are approximately 0.6 m/s higher than those observed in Configuration #1, a difference of 41%. This is consistent with the flow pattern developed because of the direct impingement of the ceiling jet on the draft stop and subsequent buoyancy aided flow up the draft stop and into the recession. The overall flow development is also shown in Figure 6-19 which compares vector plots of velocity in the ceiling recession on a plane centered on the source of the fire for each configuration at 50 seconds into the simulation.

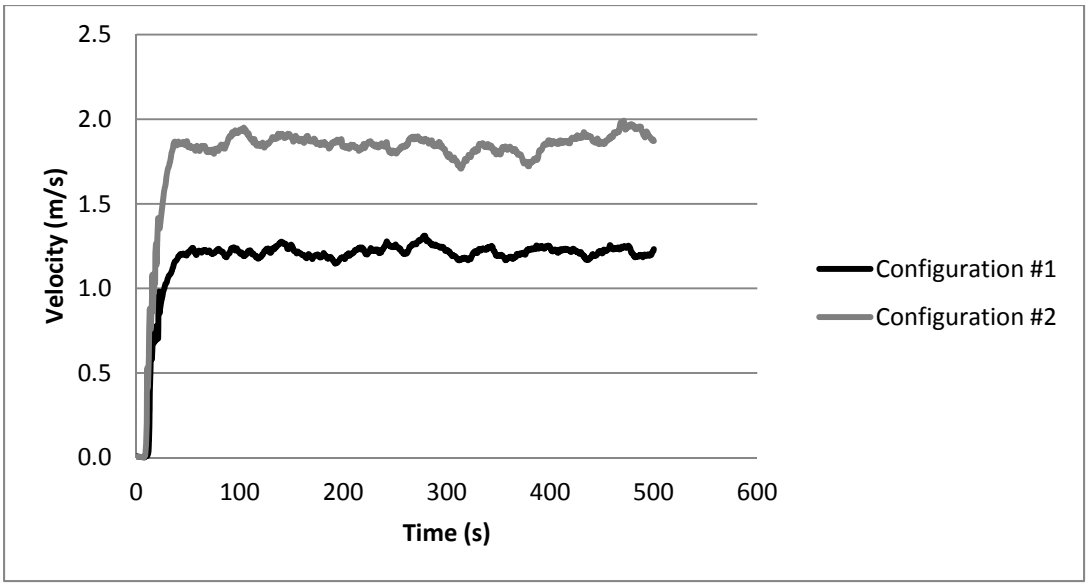

Figure 6-18: Recession velocity at z=40 mm

The expected flow patterns are observed in Figure 6-19. Flow impingement on the draft stop in Configuration #2 diverts a greater portion of the flow upward into the recession resulting in higher velocities in this configuration. In contrast, flow impingement in Configuration #1 is limited to the portion of the flow which rises above the draft stop level due to buoyancy. A large portion of the flow can be seen to bypass the recession, as evidenced by the horizontal projection of flow seen downstream (to the right) of the recession draft stop.

In both configurations, a recirculating flow pattern develops within the recession. In Configuration #2, the reduced recession depth, but similar placement of the detector below the ceiling of the recession, will result in less air entrainment, and consequently less cooling and less flow deceleration of the hot gases than would occur in Configuration #1 with a deeper recession. The velocity vector plot also highlights that the area of highest velocity is on the underside of the ceiling and therefore near the bottom of the recession in both cases. This is an expected result since at this location velocity conditions would be primarily governed by the ceiling jet flow moving horizontally away from the source fire and along the underside of the ceiling.

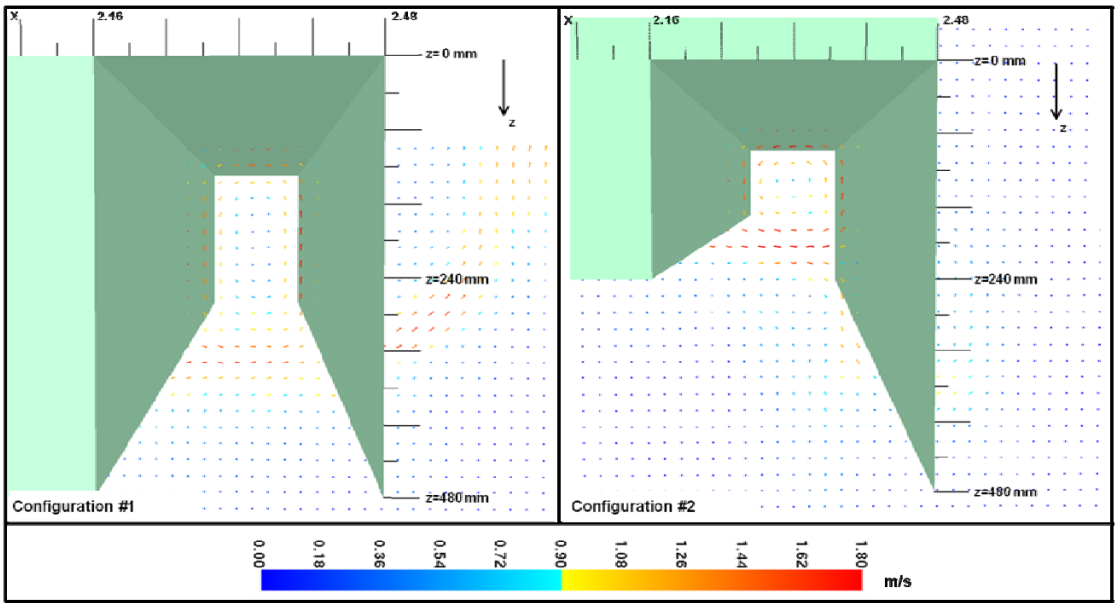

Figure 6-19: Comparison of velocity vector slices at t=50 s

Temperature distribution contours for both configurations provided in Figure 6-15 and Figure 6-16 above indicate that during the initial development of the recession flow an area of lower temperature develops at the centre of the recession since the hot gases flow mainly around the perimeter of the recession along the boundaries. This trend is of particular interest in terms of thermal detector activation since location of the detector within this lower temperature zone could result in activation delays. Figure 6-20 and Figure 6-21 plot simulated temperatures with height in the recession for both configurations at selected times during flow development. The average steady state temperature profile was determined by averaging all data points between 100 and 500 seconds and is also plotted for comparison. In Figure 6-20 and Figure 6-21, the dashed line indicated the elevation of the lower ceiling level in relation to the recession temperature measurements.

Figure 6-20 clearly displays the observed trend for Configuration #1. Temperatures near the middle of the recession height (z=240 mm) are significantly lower than temperatures at the top and bottom of the recession prior to the development of steady-state conditions in the recession. This would result in a delay in thermal detector activation during flow development if the detector was placed below the upper boundary of the recession. The impact of this flow characteristic becomes less pronounced as steady state conditions are achieved, with near

constant temperatures throughout the recession height. However, steady-state conditions are of less importance when considering thermal detector activation time since it is intended that the detector be activated as quickly as possible during the growth period of the fire.

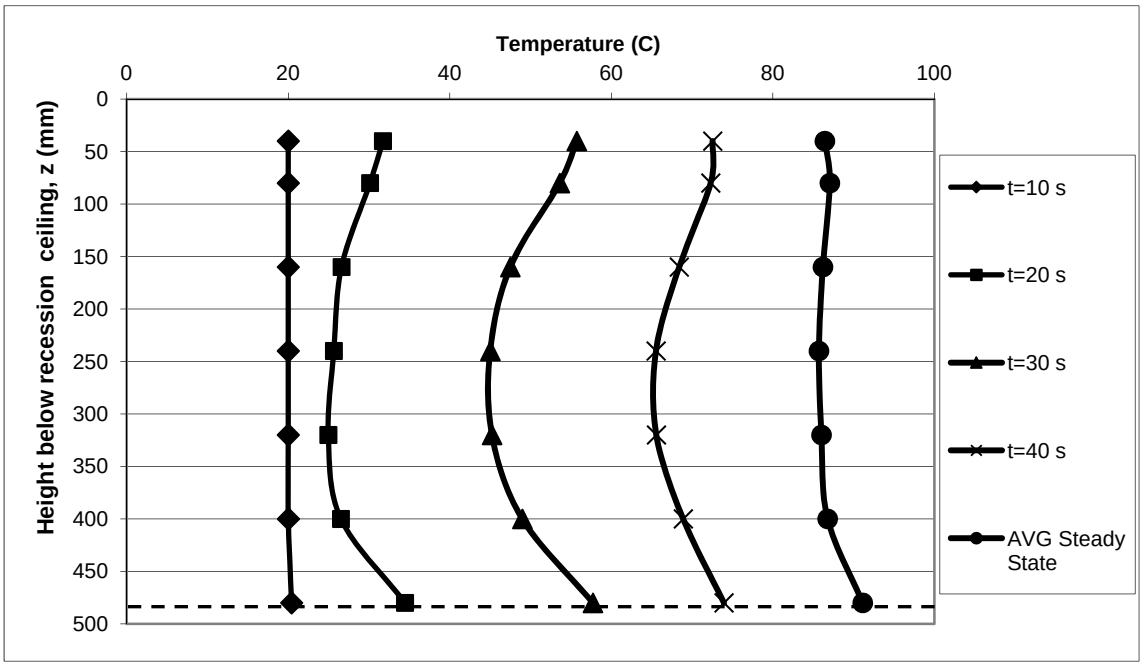

Figure 6-20: Configuration #1 - recession temperature profile development for 334 kW source

The highest temperatures for all simulation times are observed at the bottom of the recession (z=480 mm). The average steady-state temperature at z=480 mm for Configuration #1 was 91.1°C, 4.7°C higher than the average steady-state temperature observed at z=40 mm where the detector is located. This is an expected result since the measurement point at z=480 mm is located directly within the ceiling jet flow that projects horizontally past the spill edge of the recession. At this location, the flow has entrained less air and experienced less heat loss to the compartment walls. Predicted flow characteristics then suggest that for Configuration #1, the ideal location for a thermal detector, at least with respect to temperature, would be at the opening of the recession and not at the top of the recession as is normally suggested in industry.

Similar trends are observed in the developing temperature profiles for Configuration #2 plotted in Figure 6-21.

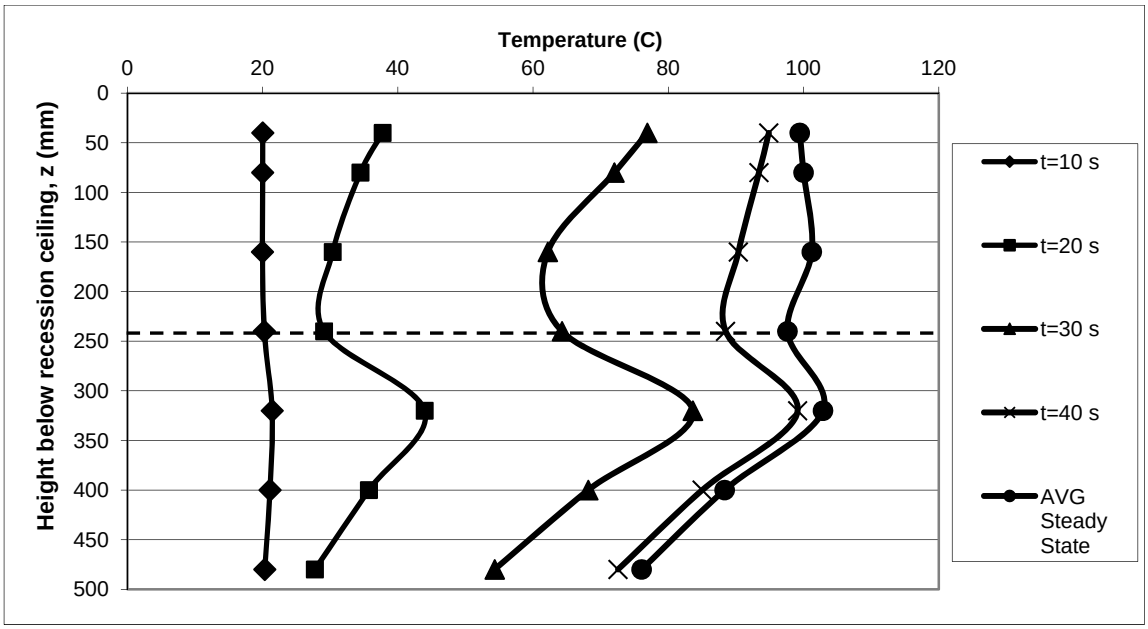

Figure 6-21: Configuration #2 - recession temperature profile development for 334 kW source

Figure 6-21 shows that a lower temperature zone develops in the recession bounded by higher temperatures at the top (z=40 mm) and bottom (z=240 mm) of the recession. It is interesting to note however that in Configuration #2 the highest temperatures were consistently observed at a point located 80 mm below the bottom of the recession. Data from the corresponding location was not obtained for the predictions for Configuration #1, so a direct comparison of this trend cannot be made here. However, in the case of Configuration #2, this trend suggests that either the ceiling jet is being directed downward due to the presence of the draft stop and the recirculating flow within the recession, or that the vertical location of maximum temperature within the ceiling jet is more than 40 mm below the lower ceiling. With respect to thermal detector response times, this result suggests that the ideal location for a detector in this recession configuration, in terms of temperature, is slightly below the lower ceiling level for Configuration #2.

The thermal detectors in the present simulations have been located near the top of the recession (z=40mm) since this is a common location proposed for such an alternative design situation. The time required for temperatures to reach the level required for thermal detector activation (assumed to be 74 °C here) at z=40 mm for Configurations #1 and #2 were 44 seconds and 30

seconds, respectively. While these values should not be interpreted as 'actual' times for detector response in a real fire situation, it is clear that detector response in Configuration #2 will occur much faster than that in Configuration #1. In addition, the predicted temperature profiles within the recession indicate that slightly faster activation times could be achieved if the detector was located at z=480 mm for Configuration #1, and at z=320 mm for Configuration #2. At these locations, the time required for the gas temperature to exceed 74 °C was 40 seconds (10% less than at z=40mm) and 28 seconds (5% less than at z = 40mm) for Configurations #1 and #2, respectively. Given that velocity values at these locations were similar to those predicted at z=40 mm, this difference should result in slightly faster thermal detector response at these locations. On a relative basis, even at these different locations, the response of the detector in Configuration #1 will still lag a similar detector for Configuration #2.

Based on the overall flow patterns seen in Figure 6-15 and Figure 6-16, as well as the more detailed temperature-time and velocity-time data shown in Figure 6-17 to Figure 6-19, the thermal detector should activate most quickly for configurations similar to Configuration #2.

Review of the developing temperature profiles within the recession, and corresponding review of the velocity vector plots indicates that the recession configuration can have a significant impact on the flow pattern of the ceiling jet resulting in areas of high and low temperature within the recession. This result could be critical in the evaluation of an alternative solution since the detector placement within the proposed recession would impact its performance. Additionally, this review has indicated that, even for low HRR fire sources, the simulations were able to distinguish (on a relative basis) differences in thermal and flow development characteristics which are important in estimating the response time of thermal detectors.

6.7.2 Comparative Analysis of Recession Flow for 3000 kW Source Fire

It is known that the strength of the fire and resulting flow characteristics are key in determining the performance of thermal detectors. Therefore, a second set of simulations was conducted using a 3000 kW fire source in order to simulate what might happen in the case of a high heat release rate fire for the ceiling recession configurations under study. In particular, it was of

interest to investigate possible changes in the horizontal projection of the ceiling jet at the spill edge and how that would influence the performance of thermal detectors in the different recession configurations. In this section, temperature, velocity, and flow development observations discussed above for the 334 kW source fire are compared to those obtained using a 3000 kW source fire.

6.7.2.1 Overall Flow and Thermal Development for Recession Configurations

Figure 6-22 and Figure 6-23 compare the developing thermal patterns for both source fire sizes for each of Configurations #1 and #2 respectively. The figures display the predicted temperature distributions within the recession for the 334 kW fire (LHS) and 3000 KW fire (RHS) via temperature slices taken on a plane through the centerline of the fire plume. The bounds of the colour contours are set from 20°C to 50°C for all frames.

It is clear from the simulated thermal patterns that, as expected, in both configurations the increase in source fire heat release rate has significantly impacted the developing flow in the recession. In both configurations, the increased heat release rate of the fire source results in a more rapid development of high temperatures within the recession. This is especially evident 13 seconds into the simulation where, in both configurations for the 3000 kW case, the ceiling recession is completely filled with gases having temperature that exceed 50 °C. Comparatively, for the 334 kW case after 13 seconds the ceiling jet flow has only started to fill the recession with steady state conditions developing later in the simulation. As was observed for the 334 kW source fire, the impact of flow impingement on the draft stop in Configuration #2 is clearly seen in Figure 6-23 for the 3000 kW fire source. It results in more rapid development of high temperatures within the recession in Configuration #2 in comparison to Configuration #1 (Figure 6-22).

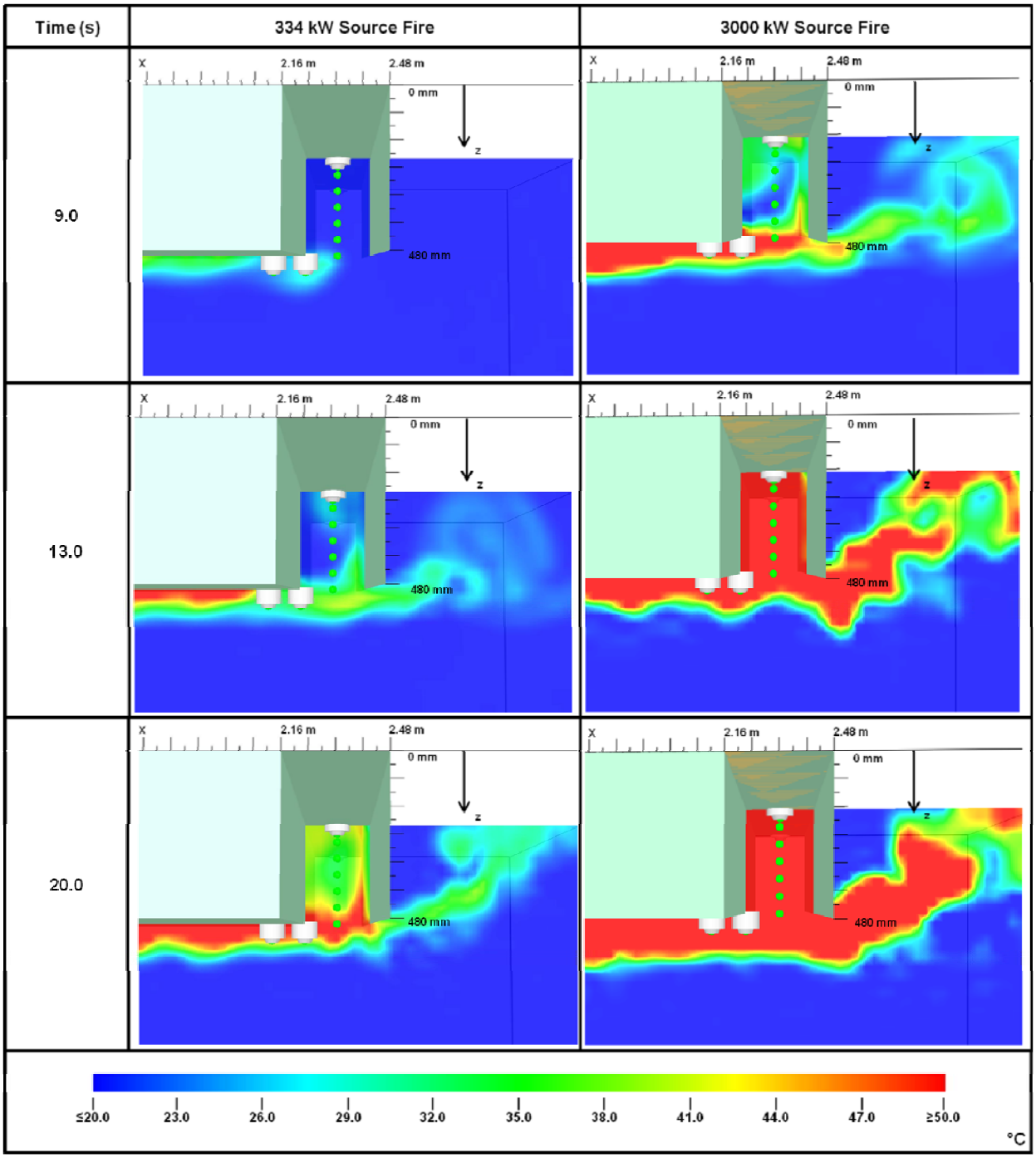

Figure 6-22: Comparison of flow development for selected heat release rates - Configuration #1

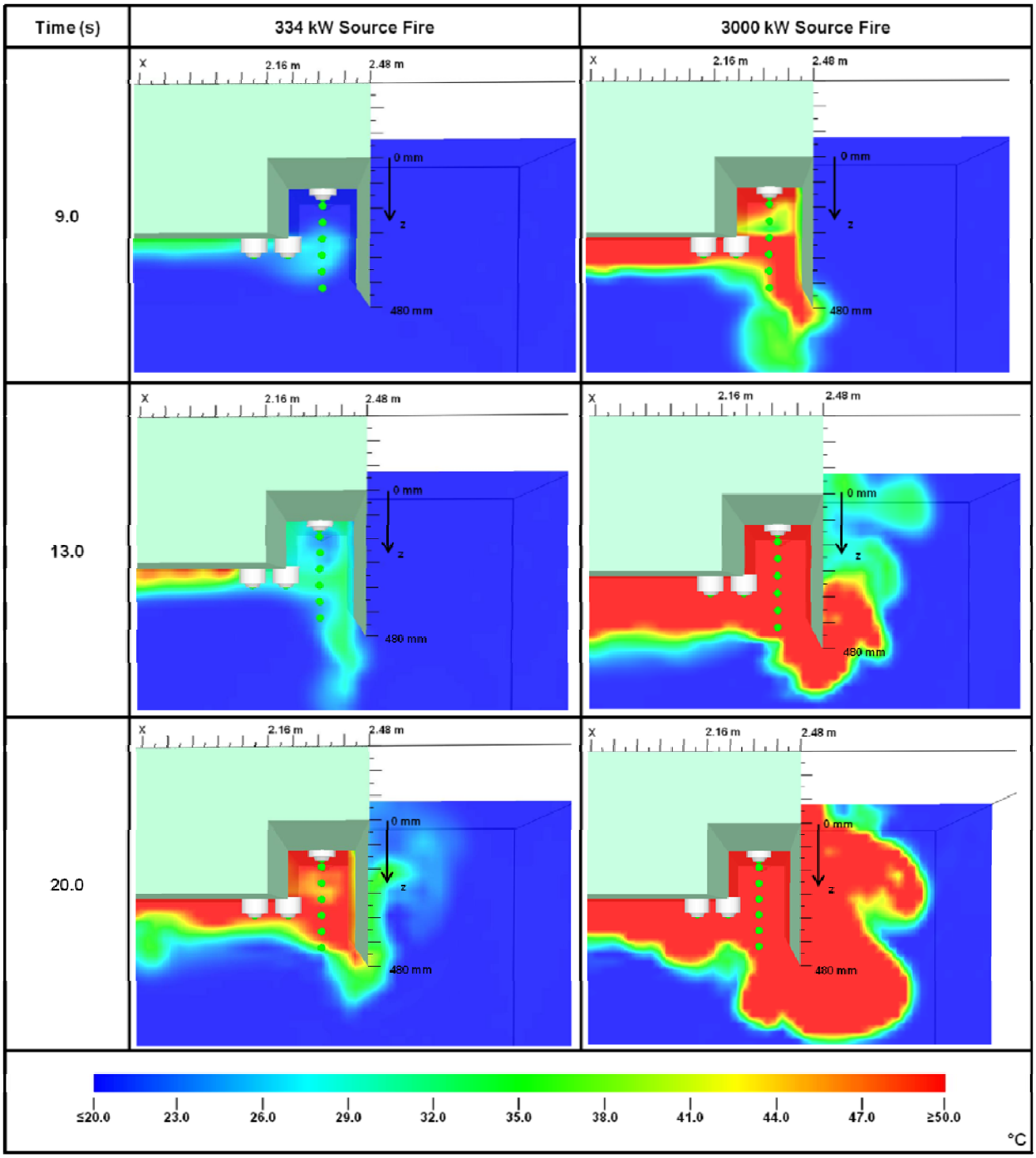

Figure 6-23: Comparison of flow development for selected heat release rates - Configuration #2

Of key interest to the evaluation of ceiling recession geometry is whether the increased horizontal velocity caused by the higher source fire heat release rate could cause the ceiling jet flow to bypass the recession. This is of particular interest for Configuration #1 where there is no direct obstruction to the ceiling jet flow via an extension downward from the elevation of the

lower ceiling. Figure 6-22 and Figure 6-23 indicate that the change in heat release rate has not significantly impacted the tendency for the ceiling jet gases to rise upward into the recession for the configurations under study here. This result supports both configurations as potentially viable alternative solutions since the recession configuration geometry itself does not appear to prevent hot gases from reaching the thermal detector.

6.7.2.2 Comparison of Recession Flow Characteristics

It is of interest to compare the temperature-time and velocity-time traces predicted at the location of the detector (z = 40 mm) for each configuration and source fire size in order to evaluate the impact of source fire heat release rate on the flow characteristics. Figure 6-24 plots the gas temperature - time curves for both configurations at z=40 mm for the 3000 kW source fire case. The required thermal detector activation temperature is also plotted (dashed line) for reference.

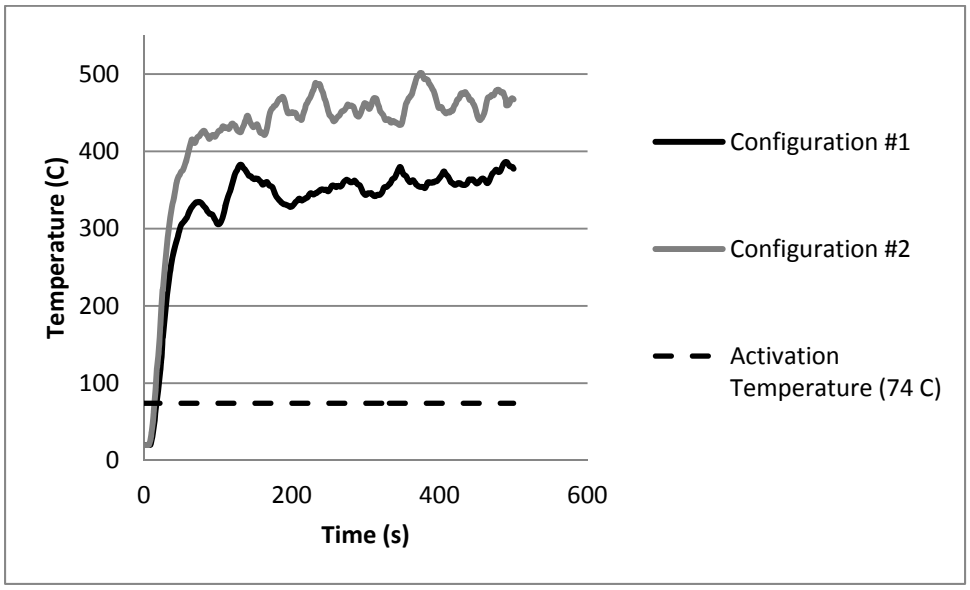

Figure 6-24: Comparison of gas temperature at z=40 mm for 3000 kW source fire

Figure 6-24 indicates that the overall trend of temperature with time is very similar to that observed for the 334 kW source fire case and that average steady state temperatures are again higher for Configuration #2 a at the top of the recession. The average steady-state temperature (taken as the average value for all data points between t=200 and t=500) for Configuration #2 was predicted to be 462 °C. In comparison, the average steady-state temperature for

Configuration #1 was 358 °C, a difference of 104 °C. This result suggests that thermal detectors in Configuration #2 should respond much more quickly than those for Configuration #1. However, since the temperature growth curves of both configurations are similar and this is the period when thermal detector activation is most likely to occur the difference in activation time for the 3000kW fire source is expected to be smaller than that observed for the 334 kW fire source.

The time required for temperatures at the thermal detector to achieve thermal activation conditions (74°C) was 17 seconds and 14 seconds for Configurations #1 and #2, respectively. These times represent a significant decrease from the 44 second and 30 second response times observed for the 334 kW fires. This is an expected result since the higher heat release rate source fire results in a significant increase in ceiling jet temperature and velocity which causes a more rapid expansion of the hot gases to the recessions and much earlier contact between hotter gases and the sensor element than for the case of a lower heat release rate source.

This result also supports the discussion presented in Chapter 2 regarding the activation time of thermal detectors and the impact of the ceiling geometry. It was suggested that low heat release rate source fires be considered in the analysis since they might be limiting cases in terms of detector activation characteristics. Considering the results from Figure 6-24 within the context of Equation 2-20 for the activation of thermal detectors, the high temperatures experienced would result in a prediction of almost equal thermal detector response times for both configurations regardless of the gas velocities since velocity plays a lesser role in detector response as gas temperature increases.

The same trends as were observed for the 334 kW case with respect to flow velocity within the recession as a function of time are observed for the case of the 3000 kW fire source. Figure 6-25 shows predicted flow velocity at z=40 mm for both configurations.

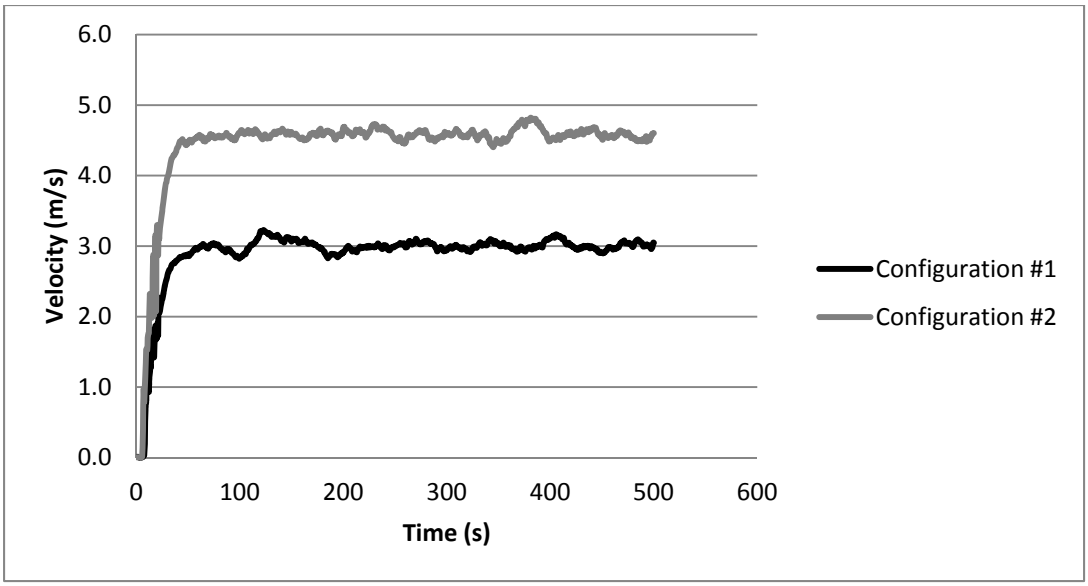

Figure 6-25: Flow velocity at z=40 mm for 3000 kW source fire

Again, the magnitude of the flow velocity increased as a result of the increased heat release rate of the source fire. For the 3000 kW fire, the average steady-state velocities for Configurations #1 and #2 were 3.0 m/s and 4.6 m/s respectively, a difference of 1.6 m/s (41.8%). The percent increase in steady-state velocity predicted for Configuration #2 versus Configuration #1 for the 3000 kW fire is comparable to the increase observed for the 334 kW case (40.7%).

Figure 6-26 and Figure 6-27 plot the development of the vertical temperature profile within both recession configurations at selected times. The location of the lower ceiling level relative to the recession is indicated in the plots by the dashed line. These can be compared with the plots shown in Figure 6-20 and Figure 6-21 for the 334kW source fire to evaluate the impact of the source fire heat release rate on the development of thermal conditions within each recession design.

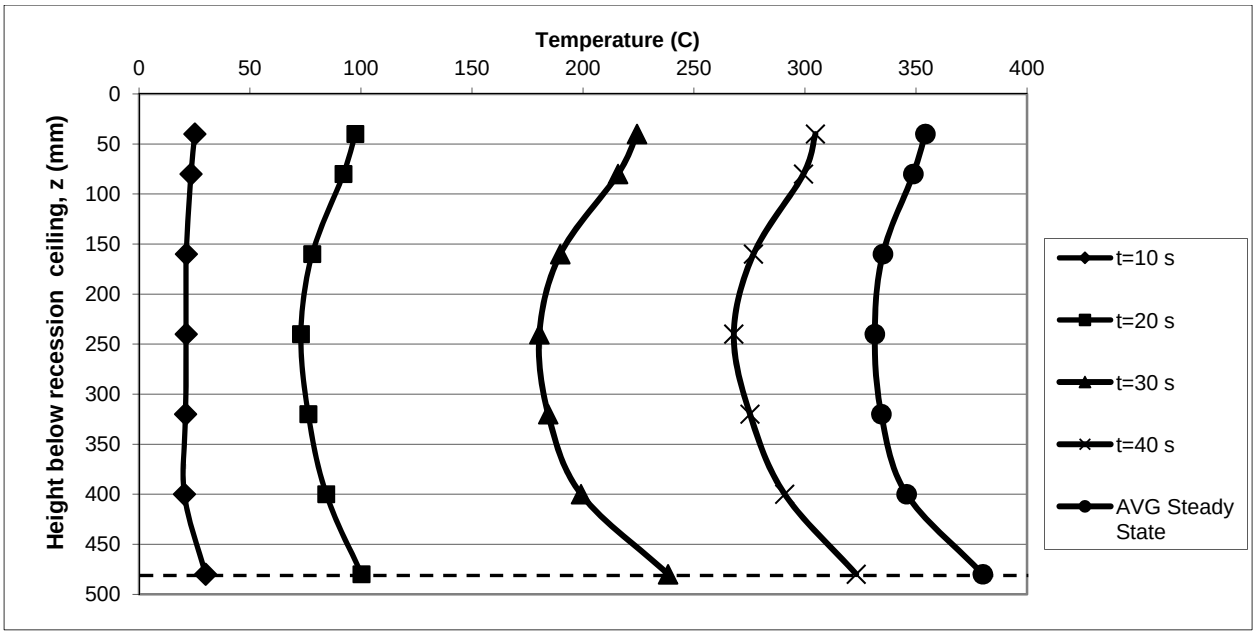

Figure 6-26: Configuration #1 - recession gas temperature profile development for 3000 kW source

The overall trends observed for the 334 kW source fire for Configuration #1 are also observed here for the 3000 kW fire. At each selected time step, the shape of the vertical profile is comparable between source fires; only the magnitude of the observed temperatures is significantly different. The largest variations in vertical temperature occur at t=30 s for both source fire sizes considered. This result indicates that the development of a vertical temperature profile within the recession is not significantly impacted by the selected source fire heat release rate. Temperature conditions required for thermal detector activation (74°C assumed) are exceeded throughout the height of the recession approximately 20 s into the simulation for the 3000 kW fire case, much faster than was observed for the 334 kW case. This is an expected result due to the significant increase in heat release rate, and therefore ceiling jet temperature and velocity. The temperature profile results indicate that thermal detector placement vertically within the recession may not be as critical for high heat release rate fires, since activation temperatures are quickly exceeded throughout the recession.

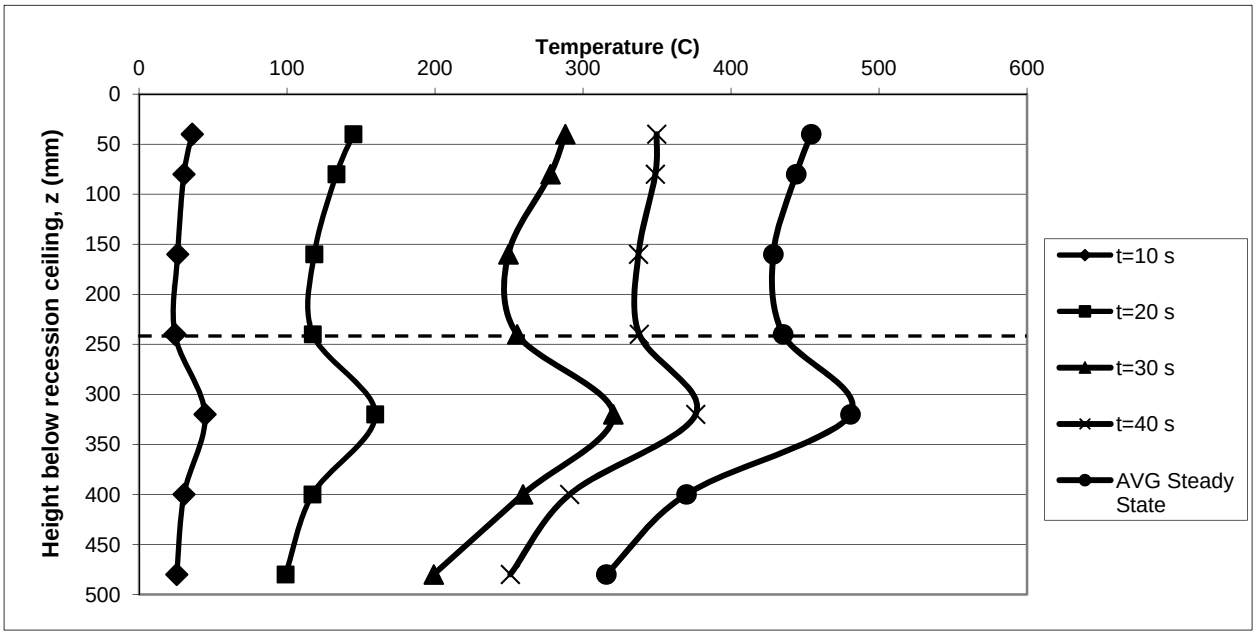

Figure 6-27: Configuration #2 - recession gas temperature profile development for 3000 kW source

Comparison of Figure 6-27 to Figure 6-21 for Configuration #2 shows that the shapes of the temperature profiles with height below the ceiling are maintained, while the magnitude of the simulated temperatures is increased. Based on the results above, temperature conditions required for thermal detector activation (74°C) are exceeded throughout the recession between 10 and 20 s into the simulation. For both source fires considered, the maximum temperature in Configuration #2 is located at z=320 mm, slightly below the lower ceiling level, supporting the above discussion regarding the importance of placement of the thermal detector in these situations. For the 3000 kW case, the steady-state temperature difference between z=40 mm (at the detector) and z=320 mm is 26.5°C (5.7%). This value is comparable to the steady state temperature difference observed between these two data points in the 334 kW cases (3.4%). The results indicate that an increase in source fire heat release rate will increase the magnitude of predicted temperatures within the recession, as expected, but will not significantly impact the trends in vertical temperature distribution for a given geometric configuration.

Comparison of temperature profiles within the recession, and corresponding review of velocity conditions in the recession, show that increases to the source fire size have significant impact on the magnitude of predicted temperature and velocity within the recession. Larger fire source size

results in a more rapid development of high temperature/velocity conditions within the recession and will yield a decrease in the simulated thermal detector activation time in comparison to the lower heat release rate fire sources.

6.7.2.3 Comparison of Thermal Detector Response Times

Based on the comparisons of overall flow development patterns seen in Figure 6-22 and Figure 6-23, as well as the more detailed temperature-time and velocity-time data shown in Figure 6-24 to Figure 6-27, the thermal detector should activate most quickly for configurations similar to Configuration #2 for the 3000 kW source fire heat release rate.

High heat release rate fires generate high temperature gases that move more quickly toward the recession mounted detector. The more rapid exposure of the thermal detector to the high temperature gases significantly increases the rate of heat transfer between the flow and the detector resulting in rapid activation.

Heat detectors positioned 40 mm below the upper boundary wall of the recession for each configuration were used to assess the activation time of thermal detectors. Table 6-2 summarizes the activation times for each configuration and source fire heat release rate.

Table 6-2: Summary of thermal detector response time for all recession configurations

Configuration #	Activation Time (s)	
	334 kW	3000 kW
1	168.5	36.0
2	100.0	29.5

It is clear that detector response times are much longer for lower heat release rate fire sources. The detector response times also show that the impact of dimensional differences of the ceiling recession configurations is more pronounced when a lower heat release rate source fire is applied. The difference in activation time was determined to be 68.5 seconds and 6.5 seconds for the 334 kW and 3000 kW source fires, respectively. This result is in agreement with the expected physics for the high heat release rate ceiling jet flow. Based on the results in Table 6-2

the highest level of performance with respect to thermal detector response time is provided by Configuration #2 for both selected source fire heat release rates.

The predictions of thermal detector response time support the proposed analysis methodology with respect to the selection of both a higher and lower value for the source fire heat release rate. Differences in thermal detector performance have been shown to be more pronounced where the heat release rate of the source fire is low, due primarily to the lower temperature of the hot gas layer and corresponding increased impact of layer cooling due to heat losses and air entrainment. The impact of dimensional differences in the chosen ceiling recession configuration is not as clear for the high heat release rate fire case, since higher ceiling jet gas temperatures dampen out the impact of differences in the development of flows in different geometries. For this reason, design evaluation using a low heat release rate fire is crucial in the assessment of thermal detector performance for a proposed ceiling recession configuration.

6.8 Performance Level Evaluation

An objective of the case study is to evaluate the performance of the ceiling recession design geometry relative to draft stops with respect to the activation time of thermal detectors as would be done in an industry evaluation of an alternative solution. In this section, the results for Configuration #2, the optimal design found above are compared to values predicted by FDS for detector activation time in the standard draft stop design configuration. Configuration #2 was also selected as the basis for the comparison since it is the most dimensionally similar to the draft stop case and will therefore further evaluate the ability of FDS to comparatively evaluate similar ceiling geometries.

As discussed in Section 6.7, the use of low heat release rate source fires allows for a clearer distinction of comparative thermal response performance of detectors. Therefore, for the purposes of this evaluation only the 334 kW source fire was reviewed. Compartment geometry and the definition of the source fire, as described in Sections 6.1 to 6.5, were applied to the draft stop configuration in this section of the analysis.

Figure 6-28 provides a comparison of the thermal development of flow around a detector for Configuration #2 and the Draft Stop Configuration for selected values of t and during the initial stages of the simulations. Figure 6-28 again includes a series of temperature slices taken on a plane through the centerline of the source fire. The color contours are based on data bounds set at between 20°C to 50°C. In addition, predicted temperatures at the thermal detectors (i.e., at z=40 mm below the upper ceiling level) are plotted for comparison in Figure 6-29.

The flow visualization in Figure 6-28 indicates that the hot ceiling jet gases flow along the ceiling and past the thermal detector until they encounter the draft stop (t=11.0 s), at which point they turn the corner and flow downward along the draft stop (t=20.0 s). Since the thermal detector is mounted directly below the ceiling before the draft stop, it is exposed to the hot ceiling jet gases earlier than is the detector in Configuration #2. As a result, the temperature of the hot gases at the heat detector is higher for the draft stop configuration earlier in the simulation, as can be observed in Figure 6-28 for the draft stop at t= 11.0 and 20.0 s and in Figure 6-29.

As the hot gases rise upward in Configuration #2, air entrainment and mixing occurs in the recession such that the gases flowing over the detector are approximately 20 C cooler at steady state than in the case of the draft stop design. It would be expected, then that the thermal detector in the draft stop configuration would activate sooner than that on the ceiling of the recession for Configuration #2 provided that the flow velocities are approximately the same.

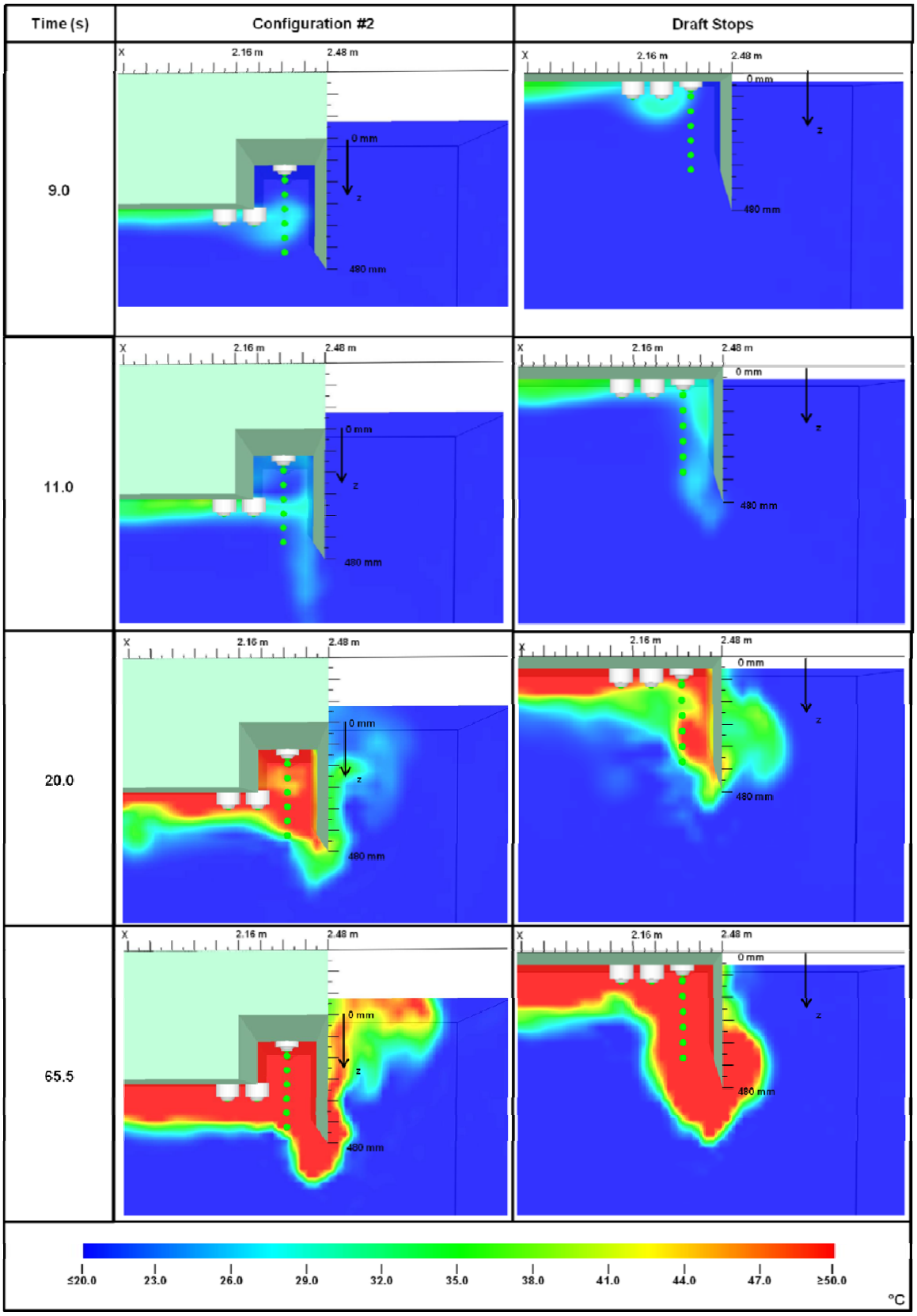

Figure 6-28: Comparison of flow development - Configuration #2 vs. Draft Stops

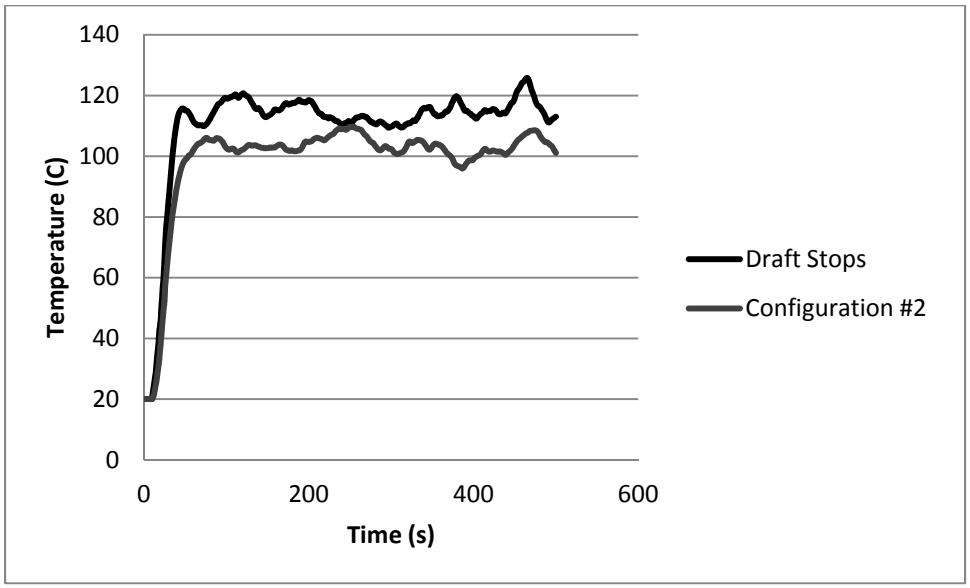

Figure 6-29: Comparison of predicted gas temperature at the thermal detector, 334 kW

As previously discussed, the velocity of the hot gases at the thermal detector can significantly impact the actuation times of thermal detectors where the temperature of the ceiling jet flow is close to the activation temperature of the detector. To investigate this aspect, predicted velocities at the thermal detector for the draft stop configuration and Configuration #2 were compared. The results are shown in Figure 6-30.

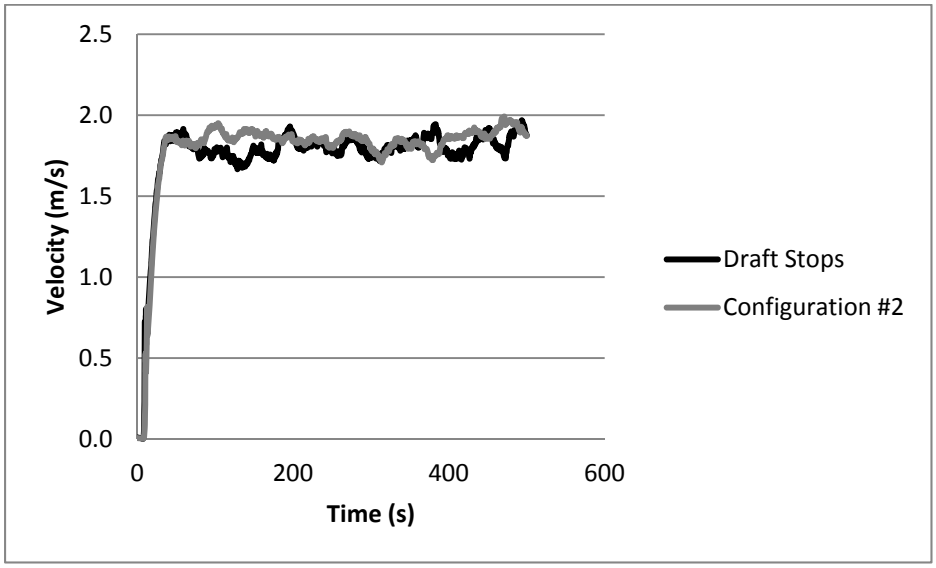

Figure 6-30: Comparison of velocity at the thermal detector 40 mm below ceiling level, 334 kW

The velocity time traces shown in Figure 6-30 indicate that predicted values of velocity are approximately equal at the thermal detector for both the draft stop and ceiling recession configurations. In combination with the temperature data discussed above, then, it is expected that the thermal detector in the draft stop configuration will activate more quickly than that in the ceiling recession design of Configuration #2.

Temperature and velocity comparisons discussed above indicate that the actuation of the thermal detector located 40 mm from the ceiling level adjacent to the draft stop will actuate more quickly than was observed in the ceiling recession configuration (Configuration #2). In Figure 6-31 are plots of the predicted thermal detector sensor temperature with time for a 334 kW fire source and for each design under evaluation.

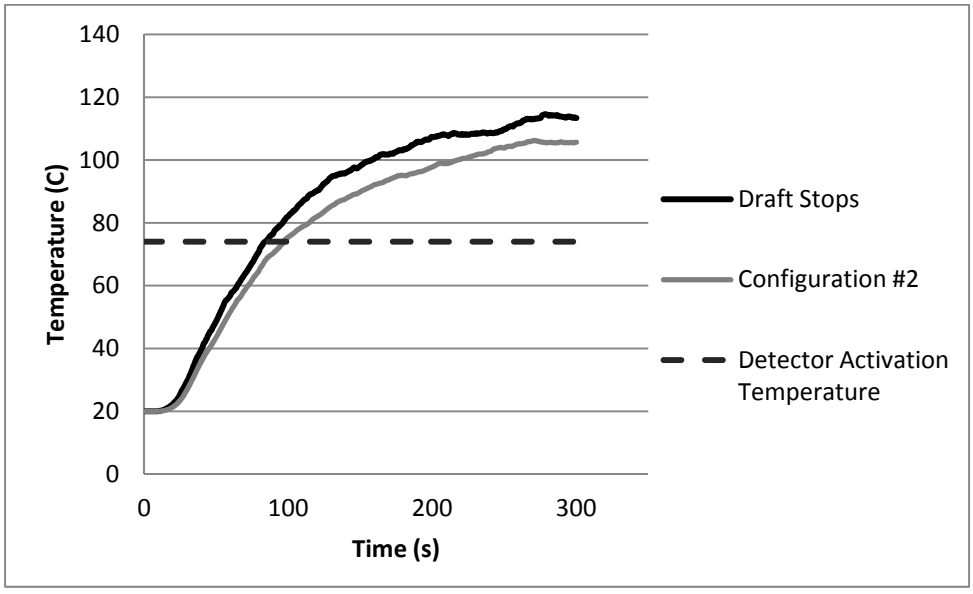

Figure 6-31: Comparison of sensor temperature in thermal detector at z=40 mm, 334 kW

These curves support the expectation that the thermal detector in the draft stop configuration increases more quickly in temperature than is predicted for the thermal detector on the ceiling of Configuration #2. As can be seen from Figure 6-31, the thermal detector response time for the draft stop configuration was 83.50 seconds, approximately 13 seconds (or 14%) faster than was predicted for Configuration #2.

For low fire heat release rates, the above analysis indicates that the performance of thermal detectors located at 40 mm below the upper ceiling in a design similar to that of Configuration #2 cannot be considered equivalent to the performance of thermal detectors located at the same position relative to the ceiling in a draft stop design. Therefore, the design under study here would not be considered viable as an alternative solution since the proposed design would result in a reduced performance level in comparison to the prescriptive requirements outlined in the Building Code with respect to thermal detector response time.

The vertical temperature profile previously discussed for Configuration #2 (Figure 6-27) revealed that the vertical placement of the thermal detector within the recession would significantly impact the thermal detector response time. Figure 6-32 compares the vertical temperature profile for the draft stop and Configuration #2 designs 80 seconds into the simulation. This plot represents the temperature profile 3.5 seconds before activation of the thermal detector at z=40 mm in the draft stop configuration.

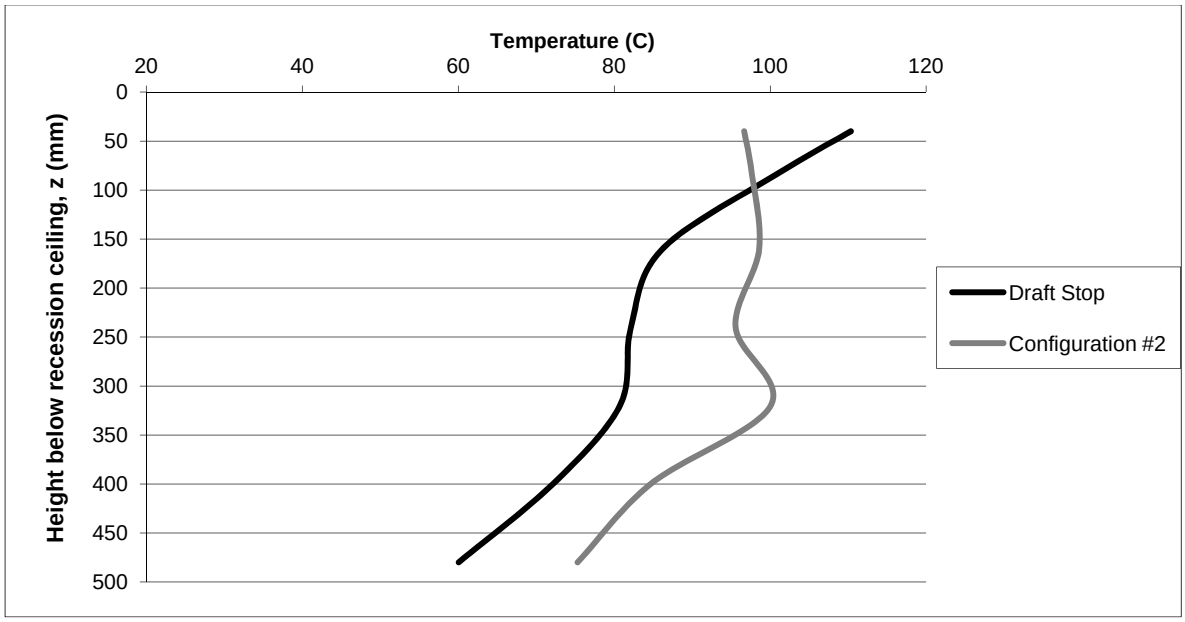

Figure 6-32: Comparison of vertical temperature profile for 334 kW fire at t=80 s

Figure 6-32 shows that, while the draft stop configuration experiences higher temperatures near the ceiling (i.e. z=40 mm) a significant reduction in temperature is observed as the distance from the ceiling is increased. This is an expected result since the recession in Configuration #2 acts to

trap the hot ceiling jet gases within the recession whereas, in the draft stop configuration, the hot gases will continue to flow down the face of the draft stop away from the detector. The point of intersection of the two curves represents the height below the ceiling where the actuation of thermal detectors would be equal in the two designs, provided velocity conditions were similar. For the configurations under study here, this point of intersection occurs at approximately z=100 mm. These results suggest that, given approximately equal velocity conditions at all locations, thermal detectors located at a distance from the ceiling exceeding 100 mm would activate more quickly in Configuration #2. Velocity data was not collected at distances below the ceiling exceeding 100 mm for either configuration studied. Therefore, a more detailed evaluation of thermal detector response for other vertical positions cannot be conducted here. Furthermore, validation work described in Chapter 4 found that velocity results at distances below the ceiling exceeding 40 mm were subject to a higher degree of error and FDS velocity results for these distances below the ceiling would require further validation work, outside the scope of this thesis. However, the temperature profiles discussed here support earlier observations regarding the importance of the vertical position of the detector with respect to response time.

The performance of detectors based in their vertical placement is of interest within the context of an alternative solution since NFPA 13, a sprinkler standard applied throughout North America, permits standard pendant and upright spray sprinkler heads to be located anywhere between 25.4 mm and 305 mm below the upper ceiling level. Therefore, in a design which complies with the requirements of NFPA 13, sprinkler heads adjacent to draft stops could be located up to 305 mm away from the ceiling level, within 152 mm of the face of the draft stop. In this sprinkler layout, the temperature results above suggest that Configuration #2 would provide a better level of performance (i.e. faster thermal detector activation) than the Code compliant design, and could be considered a viable alternative solution.

The results of the performance evaluation indicate that the proposed analysis methodology, outlined in Chapter 5, and the use of comparative FDS results for the evaluation of thermal detector performance, are appropriate for an industry evaluation of an alternative solution involving ceiling recessions. Temperature and velocity results noted above are in agreement with the expected characteristics of the heated flow for the geometries studied here. This

suggests that FDS is well suited to characterize these flows near the ceiling level, which supports its use for the analysis of these types of ceiling configurations. Temperature profile results reviewed here suggest that the performance level of a given design is significantly impacted by the vertical position of the detector.

7 CONCLUSIONS

A number of conclusions can be drawn from the results of the validation work and comparative analysis conducted in this research, particularly with respect to the applicability of the analysis methodology to evaluation of alternative solutions involving ceiling recessions.

7.1 Evaluation of Proposed Methodology

Review of available fire dynamics theory and evaluation techniques including correlations, zone models, and field models determined that FDS is suited for evaluations of the performance of ceiling recession configurations with respect to thermal detector activation.

The primary benefits of FDS over other evaluation tools were its ability to address complex geometries and the spatial resolution that could be obtained which allowed for comparison of flow and thermal characteristics outside of, but also within, each recession configuration. This attribute proved very valuable in the present work since it was found that the details of flow development within the various configurations studied had a large influence on thermal detector activation times, particularly for low heat release rate fires.

For most evaluations in industry, experimental data is not available for use in the analysis of an alternative solution. Therefore, validation of models such as FDS through a comparison of simulated data to experimental results is rarely possible. The method proposed here of comparing model results and basing the performance evaluation on relative data yields positive results while reducing model complexity and the cost associated with using FDS to fully evaluate a proposed design. In utilizing this approach, care must be taken to ensure that the simulated results are not misinterpreted to represent actual values for thermal detector response time.

Application of the proposed analysis methodology to a theoretical case study supports the use of FDS for the analysis of ceiling recession designs. However, further validation work is required where thermal detectors are located at distances greater than 40 mm from the ceiling.

7.2 Application of FDS

Literature review and independent validation work supported the use of FDS for the evaluation of ceiling jet temperature and velocity, particularly for locations close to the ceiling level (i.e. less than 40 mm below the ceiling).

As expected, the level of refinement of calculation grid used in the simulation, and consequently the ratio of D^*/δ, was found to significantly impact the prediction error observed in the model results. Based on the validation study (Chapter 4), values of D^*/δ of 8.0 or greater were required for reasonable accuracy in evaluations of ceiling recession configurations. For appropriately sized grids, prediction error was then used to provide a means of estimating expected model accuracy where experimental data was not available for comparison.

Regardless of the D^*/δ ratio applied, independent grid sensitivity analysis was required for the specific scenario being evaluated. For the purposes of the case study evaluation conducted as part of this research (Chapter 6), a grid size of 0.04 m^3 (D^*/δ ratios of 16 to 32 for the two fire sizes considered) was determined to provide a reasonable balance between model accuracy and computation time for the measurement locations of primary interest (i.e. close to the ceiling).

Two dimensionally distinct ceiling recession configurations and two source fire sizes were considered in order to evaluate the proposed analysis methodology and the ability of FDS to resolve minor dimensional changes to the ceiling recession configuration. Evaluations of developing thermal conditions and velocity of the hot gases for the selected configurations were found to agree with anticipated physics, supporting the use of FDS for the evaluation of various ceiling recession configurations.

Finally, a comparison was provided between a selected recession configuration (Configuration #2) and a Code compliant draft stop configuration. This type of comparison would be required in an alternative solution evaluation in order to assess the relative performance of the proposed design. Results indicated that a clear difference in thermal detector response could be observed based on the analysis methodology proposed. This supports the use of the analysis methodology

proposed here for the evaluation of alternative solutions involving ceiling recessions in lieu of draft stops.

7.3 Critical Parameters for Evaluations of Ceiling Recessions

Minor dimensional differences in the recession geometry were found to have the greatest impact on the characteristics of the developing flow where the heat release rate of the source fire was low. In contrast, high heat release rate fires were shown to significantly reduce the relative difference in thermal detector response times for the recession configurations studied here. This result supports the proposed analysis methodology which suggests the evaluation of low heat release rate source fires in order to better isolate the impact of dimensional differences in the proposed design.

An increase in the source fire heat release rate was found to increase the magnitude of temperature and velocity values in the recession, and to decrease the time required for activation conditions to develop at the thermal detector. The heat release rate increase did not however have a significant impact on the tendency of the ceiling jet gases to rise up into the recession for the configurations studied here. Nevertheless, the observed changes to the temperature and velocity characteristics of the flow also support the proposed analysis methodology which suggests the evaluation of high heat release rate fires in order to determine if the proposed ceiling recession configuration will prevent ceiling jet gases from reaching the thermal detectors.

Review of vertical thermal profiles within the recessions studied determined that, even at steady-state, temperature within the recession is not uniform throughout the recession height. In both configurations, areas of low temperature were observed at the mid-height of the recession bounded by areas of high temperature at the top and bottom of the recession. This result indicates that the vertical position of the thermal detector within the recession will significantly impact the resulting activation time. Therefore, the vertical position of the thermal detector is critical in the performance evaluation of any ceiling recession configuration proposed as an alternative solution.

8 RECOMMENDATIONS FOR FUTURE WORK

The results of this analysis were based on the comparison of various ceiling recession configurations simulated using FDS. Although a review of validation work and an independent validation study was conducted in order to justify the use of the model for this analysis, the results indicated that prediction errors may lead to results which differ from actual values by up to 20%. Experimental testing of one or all of the ceiling recession configurations discussed herein should be conducted to verify the predictions and refine the model as necessary.
The performance of the ceiling recession configurations was evaluated based solely on the predicted activation times for the thermal detectors. Another important function of a draft stop at the perimeter of a vertical opening is to promote cooling of the hot ceiling jet gases upon activation of the sprinkler. This, in turn, reduces the buoyancy of those gases and helps limit the vertical travel of the gases in a building. The performance of several ceiling recession configurations should therefore also be studied with respect to their impact on the cooling of ceiling jet gases and the results compared to those obtained using a draft stop. Based on such a comparison, it could be determined if any additional benefit can be realized in this regard through the use of ceiling recessions as well.

Finally, the results of the performance level evaluation determined that the ceiling recession method may provide an improved level of performance where it is also proposed that thermal detectors be installed at distances below the ceiling in excess of 80 mm. However, validation work conducted in Chapter 4 indicated that the accuracy of FDS simulations similar to that used in this research can decrease as the distance below the ceiling increases. Therefore, further work either through additional modeling or experimental testing of representative ceiling recession configurations should be conducted to confirm or refute the present results and guide refinements and improvements necessary to evolve the present model into a viable design tool.

REFERENCES

[1] National Research Council Canada, National Building Code of Canada 2010, Ottawa, 2011.

[2] Ministry of Municipal Affairs and Housing Building and Development Branch, 2006 Building Code Compendium, vol. 1, Toronto: Queen's Printer for Ontario 2006, 2006.

[3] Building Technical Council, Alberta Building Code 2006, Ottawa: National Research Council of Canada, 2006.

[4] National Fire Protection Association, NFPA 101 Life Safety Code Handbook, 11th ed., R. Cote and G. E. Harrington, Eds., Quincy, Mass.: National Fire Protection Association, 2009.

[5] International Code Council Inc., 2006 International Building Code, Country Club Hill, IL.: International Code Council Inc., 2006.

[6] National Fire Protection Association, Automatic Sprinkler Systems Handbook, 10th ed., C. Dubay, Ed., Quincy, Mass.: National Fire Protection Association, 2007.

[7] National Reserach Council of Canada, "NBC Intent Statements," National Research Council of Canada, Ottawa, 2005.

[8] American Fire Sprinkler Association, "The Impact of 18" Draft Stops on Sprinkler Activation for Vertical Opening Protection," AFSA, 2005.

[9] J. Winton, Interviewee, *Discussion regarding history of draft stop usage in Canada.* [Interview]. May 2011.

[10] R. L. Alpert, "Ceiling Jet Flows," in *The SFPE Handbook of Fire Protection Engineering*, 4th ed., Quincy, MA: National Fire Protection Association, 2008, pp. 2-21.

[11] B. McCaffrey, "Purely buoyant diffusion flames: some experimental results," National Bureau of Standards, 1979.

[12] D. Drysdale, An Introduction to Fire Dynamics, 3rd ed., Chichester, West Sussex: John Wiley & Sons Ltd., 2011.

[13] R. W. Pickard, D. Hird and P. Nash, "The Thermal Testing of Heat-Sensitive Fire Detectors," Building Research Establishment, Borehamwood, 1957.

[14] P. H. Thomas, "The Distribution of Temperature and Velocity Due to Fires Beneath Ceilings," Building Research Establishment, Borehamwood, 1955.

[15] R. Alpert, " Calculation of Response Time for Ceiling Mounted Fire Detector," *Fire Technology,* vol. 8, p. 181, 1972.

[16] R. Alpert, "Turbulent Ceiling Jet Induced by Large-Scale Fires," *Combustion Science and Technology,* vol. 11, p. 197, 1975.

[17] H. Yu, "An Investigation of Fire-Plume Impingment on a Horizontal Ceiling: 2-Impingement and Ceiling Jet Regions," *Fire and Materials,* vol. 9, p. 46, 1985.

[18] G. Heskestad and T. Hamada, "Ceiling Jets of Stong Fire Plumes," *Fire Safety Journal,* vol. 21, p. 69, 1993.

[19] G. Heskestad, "Physical Modeling of Fire," *Journal of Fire and Flammability,* vol. 6, p. 253, 1975.

[20] L. Y. Cooper, "Heat transfer from Buoyant Plume to an Unconfined Ceiling," *Journal of Heat Transfer,* vol. 104, p. 446, 1982.

[21] L. Y. Cooper and A. Woodhouse, "The Buoyant Plume-Driven Adiabatic Ceiling Temperature Revisited," *Journal of Heat Transfer,* vol. 108, p. 822, 1986.

[22] V. Motevalli and C. Ricciuti, "Characterization of the Confined Ceiling Jet in the Presence of an Upper Layer in Transient and Steady-State Conditions," National Institute of Standards and Technology, Worcester, 1992.

[23] E. E. Zukoski and T. Kubota, "An Experiemental Investigation of Heat Transfer from Buoyant Gas Plume to a Horizontal Ceiling, Part II. Effects of Ceiling Layer," National Institute of Standards and Technology, 1975.

[24] C. Beyler, "Fire Plumes and Ceiling Jets," *Fire Safety Journal,* vol. 11, pp. 53-75, 1986.

[25] R. L. Vittori, "Effect of an Obstructed Ceiling on the Activation Time of a Residential Sprinkler," National Institute of Standards and Technology, Gaithersburg, 1998.

[26] V. Babrauskas and R. B. Williamson, "Post Flashover compartment fires: basis of a theoretical model," *Fire and Materials,* vol. 2, pp. 39-53, 1978.

[27] J. A. Milke, "Smoke Management by Mechanical Exhaust or Natural Venting," in *The SFPE Handbook of Fire Protection Engineering*, 4th ed., Quincy, MA: National Fire Protection Association, 2008, pp. 4-395 - 4-396.

[28] H. P. Morgan and N. R. Marshall, "Smoke Hazards In Covered, Multi-Level Shopping Mall: an experimental-based theory of smoke production," Building Research Establishment, Borehamwood, 1975.

[29] M. Law, "Measurements of balcony smoke flow," *Fire Safety Journal,* vol. 24, no. 3, pp. 189-195, 1995.

[30] P. H. Thomas, "On the upward movement of smoke and related shopping mall problems," *Fire Safety Journal,* vol. 12, no. 3, pp. 191-203, 1987.

[31] M. Poreh, H. P. Morgan, N. R. Marshall and R. Harrison, "Entrainment by two dimensional spill plumes," *Fire Safety Journal,* vol. 30, no. 1, pp. 1-19, 1998.

[32] P. H. Thomas, H. P. Morgan and N. R. Marshall, "The spill plume in smoke control design," *Fire Safety Journal,* vol. 30, no. 1, pp. 21-46, 1998.

[33] R. Harrison, "Smoke Control in Atrium Buildings: A Study of the Thermal Spill Plume," University of Canterbury, Canterbury, 2004.

[34] L. Y. Cooper, "Heat transfer from Buoyant Plume to an Unconfined Ceiling," *Journal of Heat Transfer,* vol. 104, p. 446, 1982.

[35] V. a. M. C. Motevalli, "Transient and Steady State Study of Small-Scale Fire Induced Unconfined Ceiling Jets," *Heat and Mass Transfer in Fires,* vol. 141, pp. 49-63, 1990.

[36] D. D. Evans, "Thermal Actuation of Extinguishing Systems," *Combustion Science and Technology,* vol. 40, no. 1-4, p. 79, 1984.

[37] E. E. Zukoski, T. Kubota and B. Cetegen, "Entrainment of Fire Plumes," *Fire Safety Journal,* vol. 3, no. 3, pp. 107-121, 1981.

[38] V. Motevalli and C. H. Marks, "Transient Characteristics of Unconfined Fire-Plume-Driven Ceiling Jets," National Institute of Standards and Technology, 1990.

[39] G. Heskestad and M. A. Delichatsios, "The Initial Convective Flow in Fires," in *Seventeenth*

Symposium (International) on Combustion, 1978.

[40] L. Y. Cooper, "A Bouyant Source in the Lower of Two Homogeneous, Stably Stratified Layers," in *20th International Symposium on Combustion*, Pittsburg, 1984.

[41] G. Heskestad, "Luminous Heights of Turbulent Diffusion Flames," *Fire Safety Journal,* vol. 5, no. 2, pp. 103-108, 1983.

[42] H. Z. Yu and G. M. Faeth, "Ceiling Heat Transfer during Fire Plume and Fire Impingment," *Fire and Materials,* vol. 3, no. 3, p. 140, 1979.

[43] M. A. Kokkala, "Experimental Study of Heat Transfer to Ceiling from an Impinging Diffusion Flame," in *Fire Safety Science, Proceedings of the Third Internaional Symposium*, New York, 1991.

[44] R. L. Alpert, "Fire Induced Turbulent Ceiling-Jet," Factory Mutual Research Corporation, Norwood, 1971.

[45] C. C. Veldman, T. Kubota and E. E. Zukoski, "An Experimental Investigation of the Heat Transfer from a Buoyant Gas Plume to a Horizontal Ceiling- Part 1L Unobstructed Ceiling," National Bureau of Standards, Washington DC, 1977.

[46] NFPA 72, National Fire Alarm and Signalling Code, Quincy: National Fire Protection Association, 2013.

[47] F. P. Incropera and D. P. DeWitt, Fundamentals of Heat and Mass Transfer, 5th ed., Hoboken, NJ: John Wiley and Sons, 2002.

[48] G. Heskestad and H. F. Smith, " Investigation of a New Sprinkler Sensitivity Approval Test: The Plunge Test," Factory Mutual Research Corporation, Norwood, 1976.

[49] J. P. Hollman, Heat Transfer, 10th ed., New York: McGraw-Hill, 2009.

[50] R. L. Custer, B. J. Meacham and R. P. Schifiliti, "Design of Detection Systems," in *The SFPE Handbook of Fire Protection Engineering*, 4th ed., Quincy, MA: National Fire Protection Association, 2008, pp. 4-8.

[51] C. Beyler, "A Design Method for Flaming Fire Detection," *Fire Safety Journal,* vol. 20, no. 4, 1984.

[52] W. D. Walton, D. J. Carpenter and C. B. Wood, "Zone Computer Fire Models for Enclosures," in *The SFPE Handbook of Fire Protection Engineering*, 4th ed., Quincy, MA: National Fire Protection Association, 2008, pp. 3-222 - 3-228.

[53] W. D. Davis and L. Y. Cooper, "Estimating the Environment and the Response of Sprinkler Links in Compartment Fires With Draft Curtains and Fuisible Link-Actuated Ceiling Vents. Part 2. User Guide for the Computer Code LAVENT," National Institute of Standards and Technology, Gaithersburg, MD, 1989.

[54] D. D. Evans and D. W. And Stroup, "Methods to Calculate the Response time of Heat and Smoke Detectors Installed Below Large Unobstructed Ceilings," *Fire Technology,* vol. 22, pp. 54-65, 1986.

[55] K. A. Notarianni and W. D. Davis, " The Use of Computer Models to Predict Temperature and Smoke Movement in High Bay Spaces," National Institute of Standards and Technology, Gaithersburg, MD, 1993.

[56] K. A. Notarianni and W. D. Davis, " A Comparison of Ceiling Jet Temperatures Measured in an Aircraft Hanger Test Fire with Temepratures Predicted by the DETACT-QS and LAVENT Computer Models," National Institute of Standards and Technology,

Gaithersburg, MD, 1993.

[57] V. Motevalli and S. Riahi, "Transient Ceiling Jet Temperature and Velocity Profiles in the Presence of an Upper Layer: Comparison with Predictions by LAVENT and JET Computer Fire Models," *Journal of Fire Sciences,* vol. 26, no. 2, pp. 109-131, 2008.

[58] R. Peacock, W. W. Jones, P. A. Reneke and G. P. Forney, "CFAST – Consolidated Model of Fire Growth and Smoke Transport (Version 6)," National Institute of Standards and Technology, Gaithersburg MD, 2008.

[59] R. Peacock, K. McGrattan, B. Klein, W. W. Jones and P. A. Reneke, "CFAST – Consolidated Model of Fire Growth and Smoke Transport (Version 6) Software Development and Model Evaluation Guide," National Institute of Standards and Technology, Gaithersburg, MD, 2008.

[60] W. W. Jones, R. D. Peacock, G. P. Forney and P. A. Reneke, "CFAST – Consolidated Model of Fire Growth and Smoke Transport (Version 6) Technical Reference Guide," National Institute of Standards and Technology, Gaithersburg, MD, 2009.

[61] K. McGrattan, S. Hostikka, J. Floyd, H. Baum, R. Rehm, W. Mell and R. McDermott, "Fire Dynamics Simulator (Version 5) Technical Reference Guide Volume 1: Mathematical Model," National Institute of Standards and Technology, Gaithersburg, MD, 2011.

[62] K. McGrattan, S. Hostikka, J. Floyd and R. McDermott, "Fire Dynamics Simulator (Version 5) Technical Reference Guide Volume 3: Validation," National Institute of Standards and Technology, Gaithersburg, MD, 2011.

[63] K. B. McGrattan, H. R. Baum and R. G. Rehm, "Large Eddy Simulations of Smoke Movement," *Fire Safety Journal,* vol. 30, pp. 161-178, 1998.

[64] Fire Safety Engineering Group, "SMARTFIRE Introduction," 2012. [Online]. Available: http://fseg.gre.ac.uk/smartfire/index.html. [Accessed 15 August 2012].

[65] A. J. Grandison, E. R. Galea and M. K. Patel, "Development of Standards for Fire Models. Report on SMARTFIRE Phase 2 Simulations," Office of the Deputy Prime Minister, Fire Research Division, London, 2003.

[66] Z. Wang, F. Jia, E. R. Galea, M. K. Patel and J. Ewer, "SImulating one of the CIB W14 round robin test cases using the SMARTFIRE fire field model," *Fire Safety Journal,* vol. 36, pp. 661-677, 2001.

[67] E. R. Galea, Z. Wang, A. Veeraswamy, F. Jia, P. J. Lawrence and J. Ewer, "Coupled Fire/Evacuation Analysis of the Station Nightclub Fire," in *Fire Safety Science: Proceedings of the Ninth International Symposium*, Karlsruhe, 2008.

[68] Fire Safety Engineering Group, "SMARTFIRE Verification and Validation Report," University of Greenwich, London, 2007.

[69] FM Global, "FM Global Open Source CFD Fire Modeling Workshop," 2012. [Online]. Available: https://sites.google.com/site/firemodelingworkshop/. [Accessed 15 August 2012].

[70] Y. Wang, "FireFOAM Validation Studies: Thermal Plume," 16 April 2009. [Online]. Available: https://sites.google.com/site/firemodelingworkshop/6-presentations/05-presentations. [Accessed 2012].

[71] G. Maragkos, P. Rauwoens and B. Merci, "Application of FDS and FireFOAM in Large Eddy Simulations of a Turbulent Buoyant Helium Plume," *Combustion Science and Technology,* vol. 184, no. 7-8, pp. 1108-1120, 2012.

[72] V. Drean, P. Vanhulle and A. Coppale, "FireFoam SIMULATION OF A DIFFUSION FLAME," 17-18 May 2012. [Online]. Available: https://sites.google.com/site/firemodelingworkshop/6-presentations/2012/06_simulationDiffusionFlame.pdf. [Accessed 2012].

[73] K. McGrattan, R. McDermott, S. Hostikka and J. Floyd, "Fire Dynamics Simulator (Version 5) User's Guide," National Institute of Standards and Technology, Washington, 2010.

[74] W. D. Davis, K. A. Notarianni and K. B. McGrattan, "Comparison of Fire Model Predictions With Experiments Conducted in a Hangar with a 15 Meter Ceiling," National Institute of Standards and Technology, 1996.

[75] N. Pope and C. Bailey, "Quantitative comparison of FDS and parametric fire curves with post-flashover compartment fire test data," *Fire Safety Journal,* vol. 41, no. 2, pp. 99-110, 2006.

[76] P. Smardz and V. Novozhilov, "Validation of Fire Dynamics Simulator (FDS) for forced and natural convection flows," Ulster, 2006.

[77] M. Hurley and A. Munguia, "Analysis of Prediction Capability of FDS for Response of Thermal Detectors," *Journal of Fire Protection Engineering,* vol. 20, no. 5, pp. 77-99, May 2010.

[78] B. Husted and G. Holmstedt, "Influence of Draft Curtains on Sprinkler Activation - Comparison of Three Different Models," *Journal of Fire Protection Engineering,* vol. 18, no. 1, pp. 29-54, February 2008.

[79] A. Hamins, A. Maranghides, R. Johnsson, M. Donnelly, G. Yang, G. Mulholland and R. Anleitner, ".Report of Experimental Results for the International Fire Model Benchmarking and Validation Exercise 3.," National Institute of Standards and Technology and U.S. Nuclear Regulatory Commission, Gaithersburg, 2006.

[80] A. Tewarson, "Generation of Heat and Gaseous, Liquid, and Solid Products in Fires," in *The SFPE Handbook of Fire Protection Engineering*, 4th ed., Bethesda, Maryland: National Fire Protection Association, 2008, pp. 3-109.

[81] T. Lennon and M. D, "The natural fire safety concept-full-scale tests at Cardington," *Fire Safety Journal,* vol. 38, pp. 623-643, 2003.

[82] K. McGrattan, A. Hamis and G. Forney, "Modeling of Sprinkler, Vent and Draft Curtain Interaction," in *Fire Safety Science Proceedings. 6th International Symposium*, Poitiers, 1999.

[83] J. L. Torero and R. Carvel, "The Dalmarnock Fire Tests: Experiments and Modeling," School of Engineering and Electronics, University of Edinburgh, Edinburgh, 2007.

[84] V. Motevalli, C. Marks and B. McCaffrey, " Cross-Correlation Velocimetry for Measurement of Velocity and Temperature Profiles in Low-Speed, Turbulent, Non-Isothermal Flows," *Journal of Heat Transfer,* vol. 114, no. 2, 1992.

[85] S. R. Rockwell, "An Investigation into the use of Cross Correlation Velocimitry," Worcester, 2009.

[86] V. Motevalli and C. H. Marks, "Characterizing the Unconfined Ceiling Jet Under Steady-State Conditions: A Reassessment"," in *Fire Safety Science, Proceedings of the Third International Symposium*, New York, 1991.

[87] V. Babrauskas, "Heat Release Rates," in *The SFPE Handbook of Fire Protection Engineering*, 4th ed., P. J. DiNenno, D. Drysdale, C. L. Beyler, W. D. Walton, R. L. Custer, J. R. Hall Jr. and J. J. M. Watts, Eds., Quincy, Massachusetts: National Fire Protection Association, 2008, pp. 3-1 - 3-59.